

Rapid Antimicrobial Susceptibility Testing

Based on Bacterial Motion Tracking

by

Karan Syal

A Dissertation Presented in Partial Fulfillment  
of the Requirements for the Degree  
Doctor of Philosophy

Approved May 2017 by the  
Graduate Supervisory Committee:

Nongjian Tao, Chair  
Shaopeng Wang  
Shelley Haydel  
Kaushal Rege  
Karmella Haynes

ARIZONA STATE UNIVERSITY

August 2017

©2017 Karan Syal  
All Rights Reserved

## ABSTRACT

Antibiotic resistant bacteria are a worldwide epidemic threatening human survival. Antimicrobial susceptibility tests (ASTs) are important for confirming susceptibility to empirical antibiotics and detecting resistance in bacterial isolates. Current ASTs are based on bacterial culturing, which take 2-14 days to complete depending on the microbial growth rate. Considering the high mortality and morbidity rates for most acute infections, such long time frames are clinically impractical and pose a huge risk to a patient's life. A faster AST will reduce morbidity and mortality rates, as well as help healthcare providers, administer narrow spectrum antibiotics at the earliest possible treatment stage.

In this dissertation, I developed a nonculture-based AST using an imaging and cell tracking technology. I track individual *Escherichia coli* O157:H7 (*E. coli* O157:H7) Uropathogenic *Escherichia Coli* (UPEC) cells, widely implicated in food-poisoning outbreaks and urinary tract infections respectively. Cells tethered to a surface are tracked on the nanometer scale, and phenotypic motion is correlated with bacterial metabolism. Antibiotic action significantly slows down motion of tethered bacterial cells, which is used to perform antibiotic susceptibility testing. Using this technology, the clinical minimum bactericidal concentration of an antibiotic against UPEC pathogens was calculated within 2 hours directly in urine samples as compared to 3 days using current gold standard tools.

Such technologies can make a tremendous impact to improve the efficacy and efficiency of infectious disease treatment. This has the potential to reduce the antibiotic mis-prescription steeply, which can drastically decrease the annual 2M+ hospitalizations and 23,000+ deaths caused due to antibiotic resistance bacteria along with saving billions of dollars to payers, patients, and hospitals.

To my beloved

Grandparents..Nanu, Dadi and Nanima

*For the stories which piqued my curiosity and taught me faith*

## ACKNOWLEDGMENTS

I would hereby like to thank a few special people for the lifelong memories I made at Arizona State University. Foremost, I would like to thank my thesis advisor, Prof. Nongjian Tao for always having an open door to chat about research and his valuable lifetime experiences. I would also like to express my gratitude for the faith he kept in me while letting me explore my research in a multi-dimensional way. I owe my confidence and my passion to him.

I would also like to acknowledge Prof. Shaopeng Wang and Prof. Shelley Haydel, both of whom have played a very active role in my research. Words can't express how much I have cherished discussions with them, especially being healthily challenged and encouraged in all my endeavors. I would also like to thank my committee members, Prof. Kaushal Rege and Prof. Karmella Haynes, for their familiar support and valuable inputs over many in-person discussions. I owe my steep learning curve to them.

I would also like to acknowledge a few special people, who have helped me develop in areas beyond academics. Dr. Thomas Grys, Robert Green, Dr. Vinay Nagaraj, Arjun Sen, Kenneth Mulligan, Holly Singh, and Brent Sebold have supported me in different ways during my stay along with sharing valuable advice. I owe my motivation to them.

I would also like to acknowledge my friends and lab colleagues Yunze, Rafael, Hui, Wenwen, Yan Wang, Manni, Ali, Francis, Ashley, Wei, Xiaonan, Anasuya, Krupa and Jason, Ryan, Michelle in Haydel Lab. I thank them for valuable inputs and a good time.

Lastly, I would like to thank my family, starting with my grandparents, my parents (Mr CM Syal & Indu Syal), my uncle/aunt (Dr Umesh and Sanju Jairath), for their upbringing. A shout out to my siblings (Shivani & Sheenam) and my wife Vijeyta, for their never ending love and pampering. A thank you to my brother-in-laws (Arnab & Munish), Apar, Rene, Dr. Arnab Mukherjee, Prads, Raghu and Pankaj for innumerable discussions

which pushed me to think-out-of-box and for the perpetual guest bedroom for me. I owe my inspiration to my family and friends.

## TABLE OF CONTENTS

	Page
LIST OF TABLES.....	ix
LIST OF FIGURES.....	x
SIGNIFICANCE AND OBJECTIVE.....	1
CURRENT AND EMERGING TECHNIQUES FOR ANTIBIOTIC SUSCEPTIBILITY	
TESTS.....	4
Introduction.....	5
Current Technologies .....	8
Agar Dilution, Disk Diffusion and Antimicrobial Gradient Assays .....	8
Broth Dilution Assay .....	11
Emerging Technologies.....	12
Imaging-based AST .....	13
Non-imaging AST.....	16
Biochemical AST .....	17
Future Technologies.....	18
Microcantilevers.....	19
Flow Cytometry .....	20
Isothermal Micro Calorimetry.....	20
PLASMONIC IMAGING OF PROTEIN INTERACTIONS WITH SINGLE BACTERIAL	
CELLS.....	25
Introduction.....	26
Materials and Methods .....	28
Materials .....	28
Bacteria Purification .....	28
Surface Functionalization .....	28

	Page
Plasmonic Imaging and Flow Setup.....	29
Bacteria Immobilization .....	30
Immunofluorescence Microscopy.....	30
Image Collection and Processing .....	30
Data Analyses from Images.....	30
Results and Discussion .....	32
Imaging Single Bacterial Cells by Plasmonic Imaging .....	32
Binding Kinetics of Antibody to Single Cells.....	34
Validating Binding Kinetics by Control Experiments.....	38
Quantifying Bacterial Surface Heterogeneity.....	41
Conclusion .....	45
<b>ANTIMICROBIAL SUSCEPTIBILITY TEST WITH PLASMONIC IMAGING AND</b>	
<b>TRACKING OF SINGLE BACTERIAL MOTIONS ON NANOMETER SCALE.....</b>	
Introduction.....	47
Materials and Methods .....	48
Materials .....	48
Preparation and Growth of Bacteria .....	49
Surface Functionalization.....	49
Plasmonic Imaging and Flow Setup.....	50
Bacterial Immobilization .....	51
Image Collection and Processing .....	51
Sample Addition.....	51
Data Analyses from Images.....	52
Bacterium – Plasmon Surface Z-Distance Tracking and Z-Movement	
Calculation .....	52



	Page
Results and Discussion .....	53
Quantification of Z-Direction Motion.....	54
Correlation Between Nano-motion and Bacterial Metabolism.....	56
Changes in Nano-motion on Antibiotic Action .....	59
Power Spectral Analysis of Nano-motion.....	63
Statistics on a Bacterial Population .....	66
Testing Universality of Nano-motion AST .....	67
Conclusions.....	69
RAPID ANTIBIOTIC SUSCEPTIBILITY TESTING OF UROPATHOGENIC E. COLI IN URINE SAMPLES BY TRACKING SUB-MICRON SCALE MOTION OF SINGLE BACTERIAL CELLS .....	70
Introduction.....	71
Materials and Methods .....	72
Materials .....	72
Preparation and Growth of Bacteria .....	73
Surface Functionalization .....	74
Imaging and Flow Setups .....	74
Bacterial Immobilization .....	75
Image Collection and Processing .....	75
Data Analyses from Images .....	76
Image Segmentation and Cell Tracking Algorithm.....	76
Broth Micro-Dilution Assay .....	78
Results and Discussion .....	79
Quantification of the Bacterial Motion .....	81
Effect of Antibiotic on the Sub- $\mu\text{m}$ Motion .....	84

	Page
Population Level Bacteria Motion Changes on Antibiotic Action.....	86
Application to UPEC with Multiple Antibiotic Doses .....	86
Control Well.....	87
Bacteria Motion Responses to Clinically Relevant Antibiotic Doses .....	96
Single Cells Analysis and Cell to Cell Variations in Motion Responses to Antibiotics.....	96
Dose-curve and Defining MBC for Sub- $\mu$ m Motion .....	97
Urine Samples .....	98
Conclusion .....	102
CONCLUSION AND FUTURE WORK.....	105
Conclusions.....	105
Future Work.....	106
REFERENCES .....	110
APPENDIX	
A COPYRIGHT PERMISSIONS CHAPTER 2 .....	122
B COPYRIGHT PERMISSIONS CHAPTER 3 .....	125
C COPYRIGHT PERMISSIONS CHAPTER 4 .....	127

## LIST OF TABLES

Table	Page
1-1. Summary of AST Technologies .....	21
3-1. Kinetics of Individual Microbial cells.....	38
3-2. Correlation of Kinetics Parameters with Physical Attributes and Plasmonic Imaging Parameters .....	43
5-1. MBC of the Antibiotic at Different Concentrations of UPEC cells Spiked into Urine .....	101

## LIST OF FIGURES

Figure	Page
2-1. Evolution of Agar Dilution Methods.....	10
2-2. Rapid AST Using an Emerging Imaging Based Tool.....	15
3-1. Imaging Single Cells using Plasmonic Imaging Setup.....	33
3-2. Imaging Binding Kinetics using Plasmonic Imaging .....	36
3-3. Sensorgrams of Single Bacterial Cells Obtained by Plotting the Image Intensity Vs. Time.....	37
3-4. Using Fluorescent Imaging to Validate Binding Kinetics .....	39
3-5. Binding Kinetics of Negative Control .....	40
3-6. Distribution of Binding Constants.....	42
3-7 Distribution of the Plasmonic Image Intensity Measured at the End of Association Phase for Various Bacterial Cells.....	43
Table .....	43
4-1. Setup of Plasmonic Imaging and Tracking.....	53
4-2. Quantifying Z-direction Nano-motion of Bacterial Cells using Plasmonic Images ..	56
4-3. Z-movement in 1X PBS and LB medium.....	58
4-4. Z-movement of a Bacterial Cell in Different Mediums .....	60
.....	61
4-5 Observing Cell Death by Transmitted Images .....	61
4-6. Z-movement in 1x PBS and Different Concentrations of Antibiotic .....	62
4-7 Power Spectral Analysis and Z-movement Analysis of Different Bacterial Cells .....	65
4-8. Statistical Analysis of Amplitude Analysis Before and After Antibiotic .....	66
4-9. Z-movement Changes in Different Conditions.....	68
5-1. Image Processing of Bacterial Cells to Quantitate X and Y Displacement.....	78

Figure	Page
5-2. Schematic of the Experimental Setup to Image and Track Bacterial Cell Sub- $\mu\text{m}$ Motions .....	80
5-3. Bacterial Cells Tethered on a Surface with Sub- $\mu\text{m}$ Motion.....	82
5-4. X and Y Displacement of a Bacterial Cell Compared to a Fixed Spot .....	83
5-5. Sub- $\mu\text{m}$ Motion Before and After Adding Antibiotic for Single Cells as Well as a Population.....	85
5-6. $D_{\text{AVG}}$ of a population of cells in different wells at various time points. ....	88
5-7. Number of UPEC Cells in Different Wells over Time. ....	89
5-8. Changes in Sub- $\mu\text{m}$ Motion of a UPEC Cell Replicating on the Surface.....	90
5-9. Changes in Sub- $\mu\text{m}$ Motion of a UPEC Cell Replicating on the Surface.....	91
5-10. Decrease in Sub- $\mu\text{m}$ Motion of a UPEC Cell on the Surface in 0.25 $\mu\text{g}/\text{ml}$ of Antibiotic.....	92
5-11. Increase in Sub- $\mu\text{m}$ Motion of a UPEC cell on the Surface in a 0.25 $\mu\text{g}/\text{ml}$ of Antibiotic.....	93
5-12. Decrease in Sub- $\mu\text{m}$ Motion of a UPEC Cell on the Surface in a 2 $\mu\text{g}/\text{ml}$ of Antibiotic.....	94
5-13. Decrease in Sub- $\mu\text{m}$ Motion of a UPEC Cell on the Surface in a 2 $\mu\text{g}/\text{ml}$ of Antibiotic.....	95
5-14. Comparison with Reference Techniques .....	98
5-15. $D_{\text{AVG}}$ of a Population of Bacterial Cells Spiked in Urine to a Concentration of $5 \times 10^6$ cfu/ml.....	100

## SIGNIFICANCE AND OBJECTIVE

Discovery of antibiotics in the late 1920s led to a new era in human healthcare.<sup>1,2</sup> Antibiotics have since then been potent weapons against bacterial infections greatly improving human health outcomes.<sup>2</sup> Antibiotics are currently widely used to keep poultry healthy, post invasive surgeries to prevent bacterial infections and in everyday life to treat common infections.<sup>3</sup> However, over the last century their misuse and over prescription has led to the rapid evolution of resistance in bacteria.<sup>4</sup> Further, lack of a foreseeable pipeline of future antibiotics due to lack of antibiotic research from 1970-1990s has compounded the problem.<sup>5</sup> While multiple bacterial species continue to evolve rapidly in real-time, the world is running out of available antibiotics to treat serious infections.<sup>2,5</sup> This crisis is especially severe in developing countries in Asia such as India, China and under-developed countries in Africa, which are severely infected by bacterial diseases and also lack regulation to curtail misuse in healthcare as well as agriculture.<sup>3</sup> In the next 10 years there is a possibility of a post antibiotic era, in which house-hold minor infections can have a detrimental effect of patient morbidity, without available antibiotics for treatment.<sup>6</sup> It's imperative that to stop this crisis newer tools are developed which study these resistant bacterial cells, help the industry to make a better antibiotic pipeline and diagnose the resistant infections clinically at the earliest to enable accurate antibiotic use.

Antibiotics antibiotic susceptibility tests (ASTs) are used to clinically diagnose resistant bacteria and prescribe accurate.<sup>7,8</sup> The instruments performing AST are based on culture based technologies which have a slow turnaround time spanning 2-3 days.<sup>9</sup> This slow turnaround time is clinically unacceptable and poses a huge risk to patient's life.<sup>10</sup> I discuss the detailed impact of this slow turnaround time in Chapter 2 along with an in-depth discussion on current clinical AST devices. Further, number of emerging technologies at various stages of commercial development that are attempting to fulfill

unmet clinical needs is also discussed in Chapter 2. While these upcoming technologies have decreased the turnaround time of results to 6-14 hours, they need further work due to their dependence on culture based approaches and complex labor intensive steps (Chapter 2). Future technologies using a variety of culture-independent methodologies are geared towards providing a rapid AST results within 1-2 hours making it feasible to diagnose resistant bacteria at disease onset (Chapter 2). However, the lack of clinical application of future technologies directly to clinical samples makes their long term adaptation challenging.<sup>8</sup> This thesis attempts to meet the unmet clinical need by developing technologies that can perform rapid AST within 2 hours on clinical samples.

Bacterial cell-surfaces act as the first line of defense against antibiotics and play a crucial role in a cell's interaction with the outside world.<sup>11-15</sup> Further cell-to-cell surface diversity is critical to understand bacterial pathogenesis and resistant mechanisms.<sup>16,17</sup> Tools to study bacterial cell-surfaces interactions with external ligands rely mostly on measuring bulk bacteria, which are insufficient to study evolutionary diversity.<sup>18-20</sup> While newer imaging tools have studied single cells, they are not universal and lack quantifiable kinetics with external ligands.<sup>12,13,21,22</sup> In Chapter 3, I developed a plasmonic imaging tool (Chapter 3) to quantify the kinetic interactions of single *E. coli* O157:H7 with an antibody specific to its surface antigen.<sup>23</sup> *E. coli* O157:H7 is a highly virulent pathogen implicated in food borne outbreaks across the world.<sup>24</sup> I found out that the distribution of kinetic constants is spread over several orders of magnitude which reflects cell-to-cell heterogeneity in bacterial surfaces within a population. This validated the use of the plasmonic technique to study evolutionary diversity while developing new antimicrobials and humanized antibodies as future therapeutic drugs against bacterial surfaces.<sup>21,25</sup>

I also found out that kinetic interactions are “noisy” due to small-micromotion present in surface tethered cells.<sup>23</sup> This led us to hypothesize possible correlation between

small-micro-motion and bacterial metabolism. Traditionally, bacterial metabolism has been measured using culture-dependent approaches which results in long turnaround times for AST. In Chapter 4, using plasmonic imaging and tracking I found out that alive tethered bacterial cells move on the surface with nano-meter amplitude (nano-motion).<sup>26</sup> Further, I showed that nano-motion is correlated with bacterial metabolism and decreases on antibiotic action in real-time, enabling rapid susceptibility testing in a culture-free way. While plasmonic imaging technique is a considerable advance in the field, its long term clinical adaptation might be limited due to its complex optical setup.<sup>8</sup>

For easier clinical adaptation I set out to enable simple brightfield microscopes, present commonly in clinical labs across the healthcare world, to perform rapid AST using motion tracking. I used UPEC strain, implicated in 75% urinary tract infections in the world.<sup>27</sup> In chapter 5 I demonstrated that via an optimal combination of surface chemistry, hardware changes and automated image processing algorithms, I can perform susceptibility testing by quantitating the sub- $\mu\text{m}$  motion of bacterial cells (Chapter 5). The sub- $\mu\text{m}$  motion is dependent on surface tethering, bacterial replication cycle and nutrient conditions. I measured the clinical metric of minimum bactericidal concentration of an antibiotic against UPEC strains directly in urine samples within 2 hours enabling point-of-care use (Chapter 5). This has the potential to enable clinical microbiology lab to perform rapid AST on clinical urine samples.

In this thesis I developed a technique in Chapter 3 to aid future antibiotic research and study bacterial surface heterogeneity. In Chapter 4 and 5, I developed two imaging tools to enable rapid, point-of-care AST in the healthcare system. To achieve the promised impact, I have discussed in Chapter 6 major conclusions from study, multiple future strategies and potential pitfalls to address. Overall, this thesis aims to deliver immediate patient relief in the short term while strategizing to save antibiotics in the long run.



## CURRENT AND EMERGING TECHNIQUES FOR ANTIBIOTIC SUSCEPTIBILITY TESTS

Infectious diseases caused by bacterial pathogens are a worldwide burden. Serious bacterial infection-related complications, such as sepsis, affect over a million people every year with mortality rates ranging from 30% to 50%. Crucial clinical microbiology laboratory responsibilities associated with patient management and treatment include isolating and identifying the causative bacterium and performing antibiotic susceptibility tests (ASTs), which are labor-intensive, complex, imprecise, and slow (taking days, depending on the growth rate of the pathogen). Considering the life-threatening condition of a septic patient and the increasing prevalence of antibiotic-resistant bacteria in hospitals, rapid and automated diagnostic tools are needed. This review summarizes the existing commercial AST methods and discusses some of the promising emerging AST tools that will empower humans to win the evolutionary war between microbial genes and human wits.

## **Introduction**

Antibiotic-resistant bacterial pathogens are a global health epidemic, spreading at a rapid rate. In the US alone, these pathogens costs billions of dollars in healthcare, with 2 million hospitalizations and 23,000 deaths annually.<sup>28</sup> This epidemic is accelerated by widespread misuse of antibiotics in clinics and agriculture over the last few decades, allowing bacteria to evolve and develop means of resistance.<sup>2,3</sup> Resistant bacteria are widely found in the community and can also be acquired via nosocomial infections, post-surgery complications, and contaminated food.<sup>2,29</sup> Resistant bacterial infections can also cause sepsis, which has mortality rates ranging from 30% to 50%.<sup>30</sup> Considering the life-threatening condition of a septic patient, a key clinical task is prescribing the patient with effective antibiotics, which requires rapid diagnosis of the resistant infections and antibiotic susceptibility testing (AST).<sup>10</sup>

AST is widely used clinically to determine antibiotic resistance profiles of bacterial isolates, to guide antibiotic treatment decisions, and predict therapeutic outcome.<sup>30,31</sup> Currently, AST is usually performed in a clinical microbiology lab, which necessitates transportation of the patient samples from the healthcare provider to the lab. Susceptibility testing requires a pure culture of the offending pathogen, a process which may take several days. This delay prolongs the time to diagnosis of resistant bacteria and decisions for appropriate and effective antibiotic therapy. Delays in timely administration of appropriate therapeutics lead to increased patient mortality, poor clinical outcomes,<sup>30</sup> and use of broad-spectrum antibiotics, the latter of which promotes antibiotic resistance. To survive this evolutionary war against bacteria, humanity must pursue technologies that can rapidly perform AST to enable personalized therapies (narrow-spectrum antibiotic administration) at the earliest possible treatment stage.

After receipt of the patient sample (collected on day 0), the clinical microbiologist must isolate the potential pathogen by streaking the sample on selective culture media and incubating the inoculated media overnight (or longer) to enable growth. From a primary growth plate (day 1), isolated colonies must be obtained by subculture. Once isolated colonies from the pathogenic organism are available (day 2), the bacterial inoculum is prepared and standardized (day 2) prior to performing AST via disk diffusion<sup>31</sup> or broth dilution<sup>32</sup> methods (detailed later).

The minimum inhibitory concentration (MIC) is defined as the lowest concentration of antibiotic required to prevent bacteria growth and is used to determine if the infected pathogen is susceptible or resistant to an antibiotic.<sup>4,31,32</sup> It is important to note that the MIC does not necessarily imply bacterial death, but rather lack of growth. Thus, the MIC differs from the Minimum Bactericidal Concentration (MBC), a useful value which is seldom determined in a clinical laboratory because of the additional effort required. A breakpoint is defined as the concentration of an antibiotic that enables interpretation of AST to define isolates as susceptible, intermediate, or resistant.<sup>32,33</sup> If the determined MIC is less than or equal to the breakpoint, then the bacterial isolate is considered susceptible to the antibiotic. Clinical breakpoints for different antibiotics and bacteria are reviewed and updated annually by national organizations, such as the Clinical Laboratory Standards Institute (CLSI) in the USA and the European Committee on Antimicrobial Susceptibility Testing (EUCAST).<sup>32</sup> In addition to characterizing bacterial isolates collected from individual patients, MIC is used in epidemiological monitoring of the evolution of antibiotic-resistant bacteria. Increasing MIC values for an antibiotic over a period of time may indicate acquired antibiotic resistance for a given bacterial species.<sup>32</sup> MIC values serve as an important parameter to determine phenotypic resistance in bacterial cells, to monitor the global resistance surveillance, and to determine the

effectiveness of new antibiotics. MIC values obtained by the current AST techniques also serve as a gold standard to evaluate new AST methods. Another concept that is becoming a useful analytic modality is the Epidemiological Cutoff Value for resistance (ECOFFs).<sup>34</sup> This relates to the MIC values of a population of isolates of a particular organism against a particular drug. It can be helpful to determine intrinsic resistance that is present in some strains of a bacterial species.

The current culture-based AST tools rely on time-consuming culturing techniques, followed by disk diffusion<sup>31</sup> and broth dilution susceptibility testing<sup>32</sup>, resulting in several days before MIC values are determined and reported. Paradigm-shifting AST technologies must overcome the current bottleneck associated with the slow culturing steps. Ideally, they would be directly applicable on clinical samples without the need for selection and/or enrichment on day 1, and, preferably, be able to deliver results at the point of care (i.e., at the patient's bedside). In addition to low cost and ease of operation requirements, additional features, such as identification of bacterial strains before AST and the ability to perform AST of polymicrobial infections, will also help improve patient outcomes and reduce the selection of additional resistant organisms.

In the present mini-review, I summarize the current technologies, discuss the emerging technologies, and provide scientific opinions on future AST technologies. Given the vast number of publications in this area, I mainly focus on phenotypic AST methods. Even with this focus, I will unintentionally and inevitably exclude many exciting emerging technologies in the scientific literature due to limited page and scope. Fortunately, several reviews<sup>4,31,35,36</sup> on related topics have been published, thus enabling readers to identify topics that are inadvertently not included here.

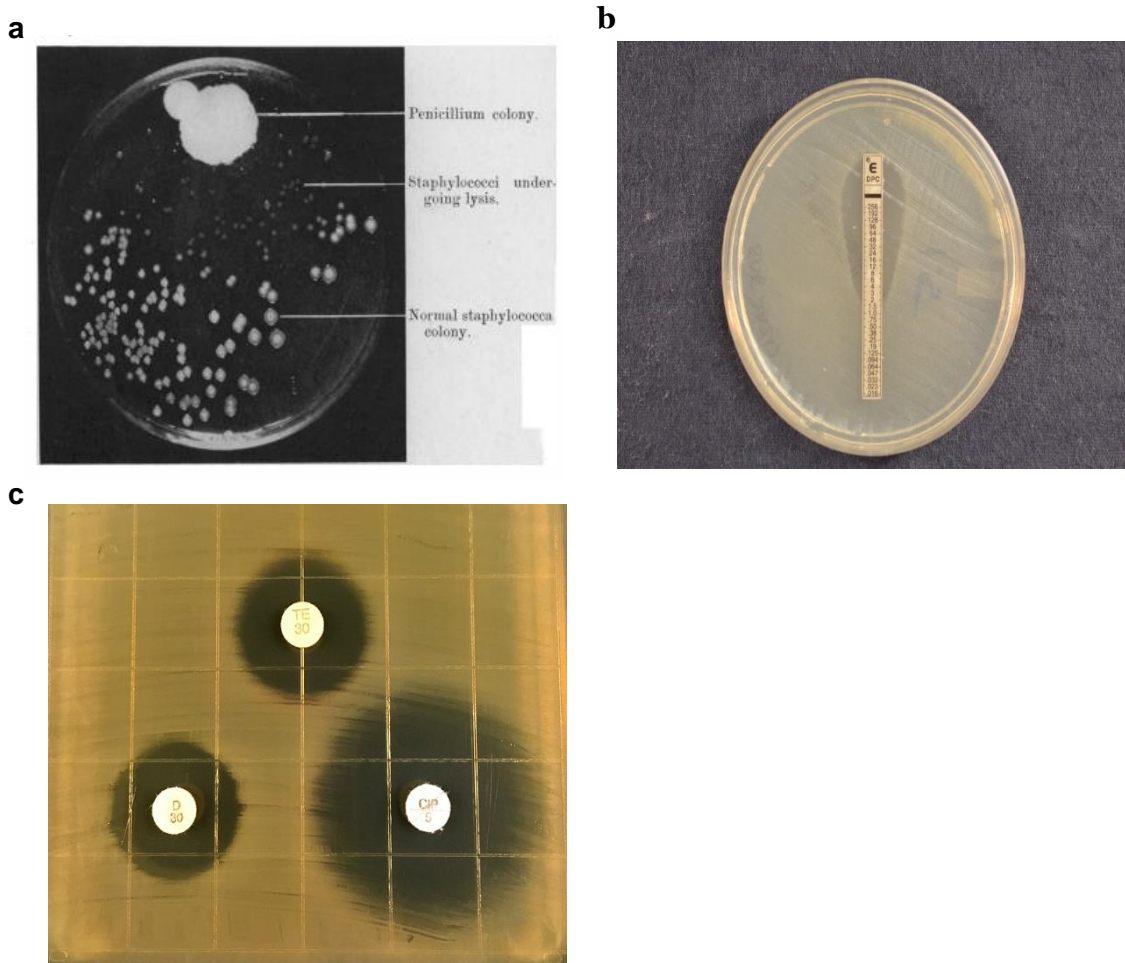
## **Current Technologies**

In 1928, Alexander Fleming discovered a mold that prevented the growth of staphylococci on an agar plate (Figure 2-1a). The mold produced an active substance, penicillin, which became the first antibiotic and ushered in the antibiotic era, a critically important milestone in modern medicine.<sup>1</sup> Antibiotics are commonly used to treat bacterial infections, to reduce the possibility of infections (e.g., during invasive surgeries) in hospitals, and to promote growth in food animals. The widespread use of antibiotics has accelerated the pace at which bacteria become resistant to antibiotics. While antibiotic-resistant bacteria are rapidly evolving, diagnostic technologies that can characterize the infection, guide treatment, minimize unnecessary use of antibiotics, and customize therapeutic strategies for specific patients have been slow. The mainstream technologies still rely on measuring bacterial growth in presence of antibiotics over a few days using methods such as agar dilution assays (E-test and disk diffusion), broth dilution assays, and automated systems from various manufacturers. These technologies rely on detecting bacterial growth, which is not conceptually different from how Fleming first discovered penicillin.

### **Agar Dilution, Disk Diffusion and Antimicrobial Gradient Assays**

In the agar dilution assay, bacteria are inoculated into an agar medium containing different antibiotic concentrations. While agar dilution testing offers reproducible results, agar dilution plates are laborious to prepare and have short shelf lives. In many clinical microbiology laboratories, an agar disk diffusion is routinely used for testing common, rapidly growing bacterial pathogens.<sup>31</sup> The disk diffusion assay involves inoculating the bacteria, enriched from clinical samples by overnight growth on selective media, onto a Mueller-Hinton agar plate, followed by placing commercially-prepared filter paper disks

impregnated with predetermined concentrations of an antibiotic onto the surface of the agar medium.<sup>35</sup> The agar plate containing the bacteria inoculum and antibiotics disks are further incubated at 35-37°C in ambient air or 5% CO<sub>2</sub> for 16-24 hours, depending on the suspected bacterium. During this incubation, the antibiotics diffuse into the agar with antibiotic concentration decreasing with increasing distance from the disk. Antibiotic susceptibility is determined by measuring the diameter of the zones of bacterial inhibition around the antibiotic disks and comparing the diameter with disk diffusion interpretive criteria updated annually by CLSI.<sup>35,37</sup> While the disk diffusion test (Figure 2-1b) is technically easy, inexpensive, and flexible, it provides only categorical results (e.g., susceptible, intermediate, resistant). Since quantitative MIC results relating the degree of susceptibility may be necessary in some cases, the gradient diffusion method offers similar flexibility and simplicity to disk diffusion and determines quantitative MICs. In the E-test, a common commercially-available gradient test, the assays are performed similarly to the disk diffusion approach except that a thin plastic strip with a continuous exponential gradient of antibiotic is used to generate diffusion of the antimicrobial agent into the agar-based medium. After overnight incubation allows bacterial growth and antibiotic diffusion, an inhibition ellipse is visible (Figure 2-1c). The quantitative MIC corresponds to the point on the strip whereby the antimicrobial concentration is no longer inhibiting bacterial growth, thus revealing the inhibitory concentration. The disk diffusion and E-test methods are commonly used in clinical microbiology labs.



Figure

## 2-1. Evolution of Agar Dilution Methods

a) Determining antibiotic susceptibility from the discovery of antibiotics currently used disk diffusion (b) and E-test (c) assays. a) Photograph showing lack of staphylococcal colonies in the vicinity of the *Penicillium* mold adapted from Alexander Fleming's original research paper on the discovery of penicillin. b) E-Test uses gradient antibiotic concentrations to determine MIC of antibiotics. c) Disk diffusion assays involve placing multiple antibiotic-impregnated disks onto an agar surface inoculated with bacteria and measuring the diameter of zones of inhibition to qualitatively determine antibiotic susceptibility. Figure 2-1a Adapted from – Alexander Fleming. On the Antibacterial Action of Cultures of a *Penicillium*, with Special Reference to their use in the isolation of *B. Influenzae*. *Br J Exp Pathol*. 1929 Jun; 10(3): 226–236 Disk diffusion assay image produced by John Popovich, Haydel Lab, ASU. E-test image produced by Rachael Liesman

## **Broth Dilution Assay**

An MIC test can also be performed using broth macrodilution, whereby broth volumes for testing each antibiotic concentration are at least 1 mL. Following incubation for 20-24 h, the MIC is the lowest concentration of antibiotic that completely inhibits bacterial growth and therefore lacks visible turbidity.<sup>32</sup> Due to the laborious nature of the broth macrodilution approach, the assay has been miniaturized and standardized by use of small, plastic, disposable microdilution trays which contain 96 wells to allow minimal volume (e.g.: 0.1 mL) and pre-determined antibiotic concentrations.<sup>31</sup> Many commercially-available systems use automatic inoculating devices, but microwells may also be inoculated with multichannel pipettes. Broth microdilution results may be determined visually or through automated instruments.

Automation of the broth microdilution assay instruments provides more precise, reliable, and quantitative AST. There are four commercially-available automated or semi-automated instruments MicroScan WalkAway, Vitek-2, BD Phoenix automated system, and Sensititre.<sup>31,33</sup> Each of these instruments consists of the following: 1) A single-use AST cassette, which can be a microdilution tray/test panel/card containing different antibiotics at different concentrations; 2) an AST instrument, which reads multiple cassettes over a period of time (usually overnight) to give AST results. These automated AST instruments require bacterial isolates obtained through routine culture from the patient samples.

Microscan Walkaway AST cassette, based on standard 96-well microdilution trays, is capable of handling 40-96 trays with automated sample-handling robotics, where the antibiotic susceptibility test uses a photometer to detect bacterial turbidity in the trays over 4.5-18 hours.<sup>31,32,38</sup> The Vitek-1/Vitek-2 AST instruments developed by bioMérieux, use a smaller AST cassette, called an AST card, in the 45-64 well plate format. Each Vitek-



2 AST instrument is capable of handling 30-240 AST cards and detects turbidity with bacterial growth over 4-10 hours to reveal AST results. The BD Phoenix is an automated microbiology system that consists of a large AST instrument capable of reading turbidity and colorimetric changes of up to 99 AST cassettes (called panels). The BD system requires an average of 6-16 hours, starting from incubating pure bacterial cultures, to obtain MIC for the bacteria. The Sensititre system by Thermo Scientific uses the standard 96-well microdilution panels (AST cassettes), which are inoculated by the Sensititre Autoinoculator, and is capable of handling 64 panels. Bacterial growth in each panel is detected from the fluorescent intensity monitored over 18-24 hours post incubation.

Automated AST instruments, representing current state of the art technologies, are extensively used in clinical microbiology labs in the US. Compared to manual methods, these instruments provide a streamlined workflow and quantitative results, thus simplifying MIC determinations for pathogenic bacteria isolated from clinical samples.<sup>39</sup> However, these automated instruments still require the use of isolated bacteria grown in pure culture, and the susceptibility tests are based on measuring bacterial growth and turbidity changes. As a result, these automated technologies remain inherently slow and are severely limited by the low sensitivity of the current detection methods. Furthermore, they are limited in the number of antibiotics and concentrations tested and lack the capability of analyzing polymicrobial samples or heterogeneous response of bacterial populations to the antibiotics.

### **Emerging Technologies**

Newer AST techniques, which are currently and actively being pursued by commercial entities for clinical translation, are considered as emerging technologies for the purpose of this review. With the increasing clinical demand for rapid AST, various new

AST techniques based on optical imaging,<sup>40-42</sup> micro-channel resonators<sup>43-45</sup> and other biosensors<sup>46,47</sup> have been pursued. For example, optical detection of bacterial growth via the cell lengths and numbers,<sup>40,42,48</sup> forward light scattering,<sup>47</sup> and measuring vibrational amplitude changes of magnetic beads,<sup>46,49</sup> have been proposed. Micro-channel resonators have also been used to detect nanoscale fluctuations associated with bacteria growth.<sup>43</sup> Quantitating molecular or biochemical markers, such as 16SrRNA,<sup>50</sup> ATP,<sup>51</sup> and luciferase,<sup>52</sup> in bacterial cells are also being used for rapid AST. These approaches can significantly improve the current commercial AST technologies, but they still rely on culturing, which is not universally applicable for anaerobes, slow-growing bacteria, and non-cultivable microorganisms. Additionally, most of these emerging technologies still require substantial sample preparation and pre-treatment steps, such as bacterial enrichment from patient samples, and cell lysis to extract biochemical markers.

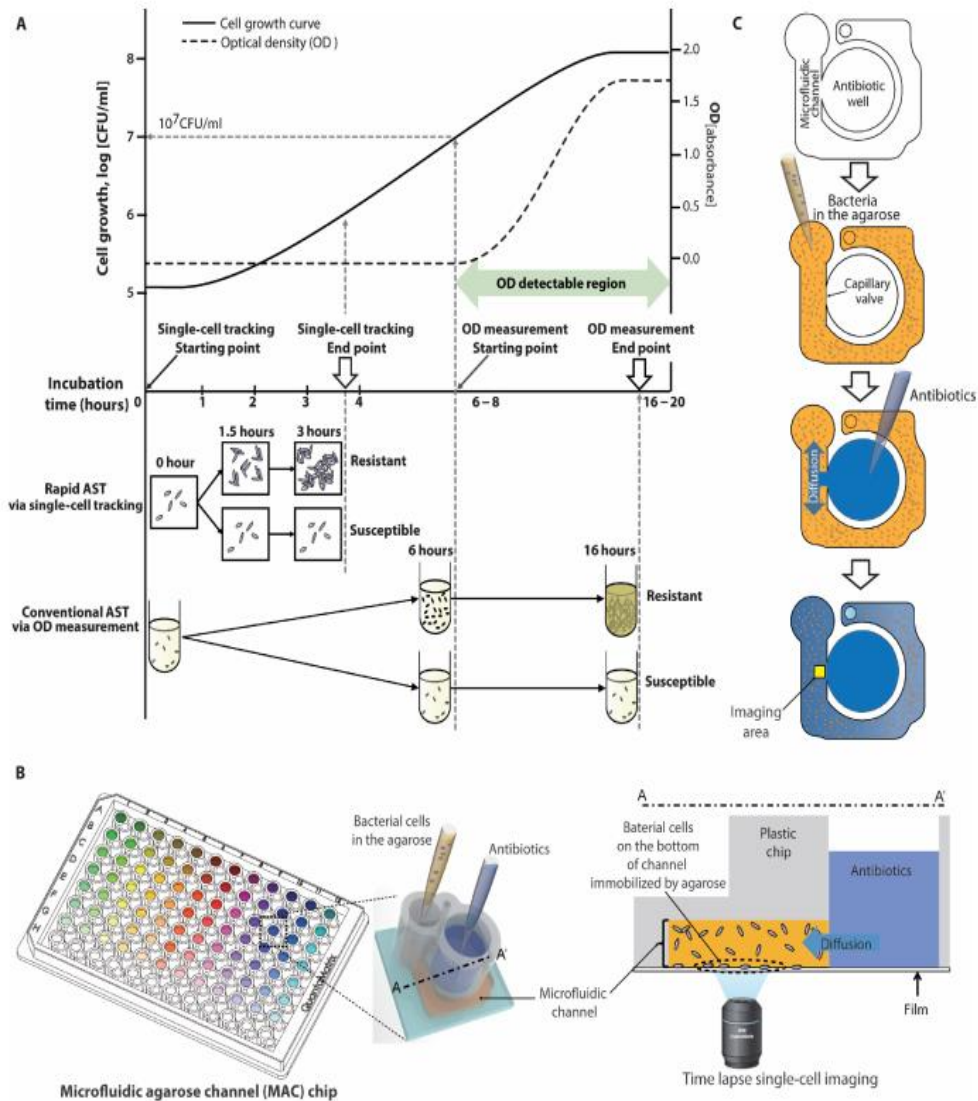
### **Imaging-based AST**

Multiplexed automated digital microscopy (MADM)<sup>41,53</sup> is an automated microscope being developed to provide rapid identification and AST of clinical samples. MADM separates bacterial cells from other substances in the clinical samples(e.g., blood or urine) using gel filters and attaches purified bacterial cells to the surface sensing surface using electro-kinetic loading.<sup>53</sup> After surface attachment, fluorescent in-situ hybridized (FISH) probes are used to identify bacterial cells within an hour, followed by AST.<sup>53</sup> To perform AST, MADM measures bacterial growth every 10 minutes as clonal aggregates multiply in Mueller-Hinton media. Since resistant cells will grow in Mueller-Hinton media with antibiotics and sensitive cells will be inhibited or killed, expansion and measurement of clonal masses over time (compared to growth controls) are used to generate growth curves and determine susceptibility. MADM also uses cell morpho-kinetic image analysis for differentiating bacterial species in polymicrobial infections, thus expanding clinical

capability and reducing of the cost of multiple assays. While the MADM imaging approach for measuring the bacteria growth rate is faster than traditional approaches and represents a significant step forward from the current commercial tools, its universality to all antibiotics remains to be addressed.<sup>40</sup>

Another imaging tool capable of rapid AST is single-cell morphological analysis (SCMA).<sup>40,54</sup> SCMA (Figure 2-2) uses bright-field microscopy to determine antibiotic-induced morphological changes in single bacterial cells and enable rapid AST. The captured images are processed using an automated image-processing algorithm to quantify the area and number of growing bacterial cells. The classification algorithm processes several morphological characteristics to produce antimicrobial susceptibility data. Another optical imaging technique is oCelloScope,<sup>55,56</sup> which is based on imaging growth of a population of bacterial cells in a fluid sample with antibiotics over a period of time. The recorded images are then processed using imaging algorithms to quantify changes in the area occupied by a growing population of cells. However, unlike other high resolution imaging methods, oCelloScope does not capture the growth of individual cells, but a population of cells in liquid fluids and thus eliminates the need to attach bacterial cells to an inert surface.

Coupling of imaging-based tools with microfluidics has been reported for rapid AST. Bacterial cells are first captured in microfluidic chambers,<sup>57</sup> micro channels,<sup>58</sup> or droplets<sup>59,60</sup> and then imaged to detect changes in the cell number,<sup>42,61</sup> size,<sup>40</sup> morphology<sup>62</sup> and viability<sup>59,63</sup> in the presence of antibiotics in order to perform AST. Novel imaging approaches, such as measuring changes in rotational frequency of magnetic beads (which is proportional to cell mass)<sup>46,49,64</sup> and electro-kinetic loading of single cells,<sup>58</sup> have been applied to AST using smartphone cameras and other imaging devices.<sup>63</sup>



Figure

## 2-2: Rapid AST Using an Emerging Imaging Based Tool

a) Schematic comparison of traditional AST using broth microdilution and imaging-based AST demonstrates how tracking single cell divisions can produce rapid results compared to traditional optical density (OD) tools which are limited by their sensitivity to measure only higher bacterial concentrations. b) Setup of a 96-well plate modified into a microfluidic agarose chip for concurrent addition of bacteria and antibiotics followed by microscopic imaging. c) Schematic of steps involved in adding bacteria and antibiotics and imaging a localized area to observe changes. Adapted from Choi J, Yoo J, Lee M, Kim E-G, Lee JS, Lee S, *et al.* A rapid antimicrobial susceptibility test based on single-cell morphological analysis. *Sci Transl Med* 2014; **6**:267ra174 Reprinted with permission from AAAS.

Although the imaging-based AST tools shorten the detection time from days to a few hours, these technologies still use replication-dependent methodologies that have a primary culture step (e.g. growth from a blood culture bottle or growth on a primary culture plate). These dependencies limit the application of imaging-based methods to slowly-growing pathogens, such as *Mycobacterium tuberculosis*. To perform AST on pathogens directly (i.e.: without a culture step) from clinical samples, it is necessary to separate bacteria from the patient sample matrix, and then measure a cellular attribute that is independent of replication.

### **Non-imaging AST**

Non-imaging methods that measure the physical or biochemical signature of bacterial cells have been proposed for AST. BacterioScan detects forward laser light scattering (FLLS) <sup>47,65</sup> analyzes the angular variation in the intensity of the scattered light, and determines the number and size of bacterial cells suspended in a solution. FLLS can measure bacterial concentrations as low as  $10^3$ cfu/ml, which is more sensitive than other optical methods and traditional automated instruments, and may enable rapid AST (within a few hours). The FLLS technology can perform AST directly on urine samples with minimal sample preparation, thus enabling point-of-care applications. Disadvantages of FLLS include the use of a replication-dependent approach to measure AST, inability to differentiate bacteria from cell sedimentation, lack of single cell resolution, and inability to differentiate bacterial species for polymicrobial analysis.

LifeScale develops microchannel resonators for rapid AST, where the microchannel resonators are individual microcantilevers. The technology measures the mass of the bacterial cells upon passage through the microfluidics channels inside of the micro-cantilevers.<sup>45</sup> Microchannel resonators permit quantitation of bacterial cells and

measure mass changes of the individual cells to assess antibiotic activity.<sup>43,45,66</sup> The advantages of microchannel resonator AST are the ability to perform sensitive mass and morphology measurements on single bacterial cells and the promise of AST within ~3 hours. However, the applicability of the approach to clinical samples remains to be fully established.

### **Biochemical AST**

While the AST technologies described above detect physical and morphological features of bacteria, tools that measure molecular and biochemical signatures, such as changes in 16s RNA,<sup>50,67</sup> DNA<sup>68,69</sup> and ATP,<sup>51</sup> of growing bacterial cells have also been studied. A biosensor-based AST (b-AST) assay being developed by Genefluidics measures bacterial growth via quantitating 16s rRNA molecules, which are specific for each bacterial species.<sup>50,67</sup> After DNA probes hybridize specifically to 16S rRNA molecules, an electrochemical signal permits amplification and quantitative detection. This approach allowed for AST as short as ~4 hours using clinical urine samples from patients experiencing a urinary tract infection. Smarticles technology in development by Roche Diagnostics<sup>52</sup> introduces recombinant bacteriophages with DNA probes, such that a specific binding of DNA probes inside the bacterial cells leads to luciferase expression. Luciferase expression produces light, which is used to quantify the number of bacterial cells and perform rapid AST. Real-time PCR is another molecular approach, which quantifies copies of bacterial DNA and correlates this value with bacterial growth in a sample. This technique targets highly conserved regions of bacterial chromosomal DNA to ensure species specificity and has been applied to various combinations of antibiotics and bacterial species. Another approach detects bacterial genetic fingerprints that are detected upon exposure to antibiotics rather than relying on a single specific gene or DNA sequence in the other approaches described above.

While the nucleic acid-based biochemical assays, such as real-time PCR, can give faster results than the current techniques, it has several disadvantages such as relying on high bacterial concentrations to extract sufficient DNA, manual sample handling steps such as lysing bacterial cells to extract nucleic acids.<sup>70</sup> These manual steps make clinical adaptation of these technologies difficult, where the need of the hour is rapid automated testing. Further the extracted DNA contains DNA from both alive/dead cells leading to a higher false positive rate for these techniques.<sup>71</sup> Other disadvantages include the need of previously known sequences, micro-heterogeneity in the 16s RNA within a species,<sup>72</sup> lack of correlations between genotypic and phenotypic resistance,<sup>73</sup> and inability of performing tests on clinical samples.

Other biochemical signatures, such as ATP and NADH, have been studied as AST biomarkers with electrochemical amplification.<sup>51,74-76</sup> These biochemical signatures are indicators of the metabolic activities of bacteria, thus providing critical information on bacterial viability. While some of these techniques are capable of providing rapid AST within a few hours, these techniques currently lack sensitivity to perform AST at lower antibiotic concentrations and dilution ranges. Further, the universal application of the probe molecules to multiple strains and antibiotics is also questionable. While promising, these emerging approaches require further studies and evaluations.

### **Future Technologies**

The emerging technologies, being actively pursued by commercial entities discussed above, promise rapid AST within a few hours. Furthermore, some of the technologies can be directly applied to patient samples without any sample pretreatment. However, further shortening the test time and applying them to slowly growing organisms

will require innovative approaches. I discuss future technologies that can meet these requirements below.

### **Microcantilevers**

Microcantilevers have been recently used to perform rapid AST,<sup>44,77,78</sup> whereby bacterial cells are attached to a microcantilever and deflection of the microcantilever associated with the micromotions of the bacterial cells, is detected as the signature of bacterial metabolism. This approach has led to AST within two hours for *Escherichia coli* and *Staphylococcus aureus* strains for different antibiotics<sup>44,77</sup>. The correlation between the micromotions and viability (metabolism) has been studied for both prokaryotic and eukaryotic cells<sup>79</sup>. While sensitive, the micromotion of bacterial cells producing microcantilever deflections is affected by flowing liquids, and recent reports have also indicated inefficient transfer of antibiotics to immobilized bacterial cells under laminar flow conditions<sup>45</sup>. Furthermore, the sensitive cantilever deflections are caused by bacterial cells attached to the tip, so the small area of the tip limits the number of bacterial cells which are adsorbed to the surface, potentially preventing the application of the technique to lower bacterial concentrations present in clinical samples<sup>45</sup>. It is unclear how this approach can be applied directly to complex matrix of clinical samples and polymicrobial systems. Given that eukaryotic cells can also cause cantilever fluctuations,<sup>79</sup> sample preparation for this technique might need extraction of bacterial cells from complex matrix along with a longer incubation of bacterial cells to attach the sensor surface, especially for low bacterial load patient samples.



## **Flow Cytometry**

Flow cytometry (FC) measures changes in morphology, cellular numbers, and viability via labeling to perform AST<sup>80-82</sup>. After a dye is used to stain viable cells, individual cells flow through a channel into a reader zone, where light scattering is used to measure morphology and excitation/emission spectra of cells is used to assess cell counts and viability. Multiple research studies have shown the application of this technology using various dyes<sup>81,82</sup> applied to multiple bacterial species and antibiotic combinations. Although flow cytometry can produce rapid AST with 2-3 hours, it is not a widely used technique yet. Possible disadvantages are lack of use in complex patient samples, staining inefficiency of dyes, presence of auto-fluorescence, inability to differentiate cellular damage caused by bactericidal or bacteriostatic antibiotics, and lack of clinical databases for validation<sup>83</sup>.

## **Isothermal Micro Calorimetry**

Isothermal micro calorimetry (IMC) is a novel technique that measures cumulative heat and generates heat curves of growing bacterial cells<sup>84</sup>. Heat curves of growing bacteria are similar to the growth curve measured by standard turbidity detection instruments. Since the lower limit of detection for IMC is  $\sim 10^4$ cfu/ml, the approach enables a faster AST<sup>84</sup>. IMC produces AST results within 3 hours using patient urine samples<sup>85</sup> and has been effective with various bacterial species, including *Mycobacterium tuberculosis*<sup>86</sup>, *E. coli*, and *S. aureus*<sup>84</sup>. Although this new analytical tool uses a new signature of bacterial metabolism to perform AST, heat curves do not correlate with current standard techniques and do not shorten the time to generate MIC considerably due to dependence on culturing tools. Other discrepancies such as delays in onset of detectable heat due to insufficient bacterial numbers and lack of cellular level metabolic

understanding of heat curves limit its current clinical use. While novel, sample preparation might involve purification of bacterial samples by overnight culturing to enable translation of this technique to complex clinical samples such as blood and sputum. This novel tool needs to be advanced further and studied in more to meet the expectations of current rapid AST.

Table  
1-1. Summary of AST Technologies

<u>AST Technologies</u>	<u>Summary of Method</u>	<u>Time of AST</u>	<u>Direct on patient sample</u>	<u>Real MIC</u>	<u>FDA Approval</u>	<u>Reference</u>
<b>Current Technologies</b>						
<b><i>Solid Media Cultures</i></b>						
1. Agar Dilution Assay	Bacteria inoculated on agar plates with antibiotic discs of different concentrations	16-24 Hours	No	Yes/No	Yes	31
2. Disk Diffusion	Bacteria inoculated on agar plates with a single antibiotic disk	16-24 Hours	No	Yes/No	Yes	31,35
3. E-test	Bacteria inoculated on agar plates with a graded antibiotic concentration strips	16-24 Hours	No	Yes	Yes	31,35
<b>Liquid Media Cultures</b>						
1. Broth Dilution Assay	Bacteria inoculated in liquid media with different antibiotics to monitor growth	12-24 Hours	No	Yes	Yes	31,33
<b>2. Automated Instruments</b>						
a) MicroScan WalkAway	Measure bacterial growth in the presence of antibiotics by recording bacterial turbidity using a photometer	4.5-18 Hours	No	Yes	Yes	32,38
b) Vitek-1/Vitek-2	Measure bacterial growth in the presence of antibiotics by recording bacterial turbidity using a photometer	6-11 Hours	No	Yes	Yes	39,87
c) BD Phoenix	Record bacterial growth in the presence of antibiotics by recording bacterial turbidity and colorimetric changes	9-15 Hours	No	Yes	Yes	88
d) Sensititre	Record bacterial growth with antibiotics by measuring fluorescence	18-24 Hours	No	Yes	Yes	31
<b>Emerging Technologies</b>						
<b><i>Imaging Based Tools</i></b>						
1. Multiplexed automated digital	Image single bacteria growing into colonies with antibiotics and quantify growth rates	3-5 Hours	Yes (Urine, Blood)	Yes	Yes	53,89,90

microscopy (MADM)						
2. Single-cell morphological analysis (SCMA)	Image single bacterial cell's morphology changes on antibiotic action	3-4 Hours	Yes (Urine)	Yes	No	54.91
3. oCelloscope	Measure growth of bacterial cells using low resolution optical system	1-4 Hours	Yes (Urine)	Yes	No	55
<b>Non-Imaging Based Tools</b>						
1. BacterioScan FLLS	Measures bacterial numbers and sizes on antibiotic action	3-10 Hours	Yes (Urine)	Yes	No	47.65
2. LifeScale Micochannel Resonator	Count bacterial cells and morphology changes on single cells post antibiotic action	> 3 Hours	No	Yes	No	66
3. Genefluidics	Count 16s RNA increase as a proxy to bacterial growth	4 Hours	Yes (Urine)	Yes/No	No	67.92
4. Smarticles	Bacteriophages which express luciferase on growing cells	-	-	-	No	52
<b>Future Technologies</b>						
1. AFM Cantilever	Measure cantilever fluctuations originating from bacterial motion as a proxy for metabolism	< 2 Hours	No	Yes	No	44
2. PIT	Image and Quantify sub-nanometer motion of bacterial cells	< 2 Hours	Yes	Unkno wn	No	26
3. Flow Cytometry	Count viable bacterial cells using dyes	2-3 hours	No	Yes	No	80
4. IMC	Heat signature of growing cells	3-14 Hours	Yes	Yes	No	85

## **Conclusions**

Current manual and automated AST technologies are the backbone of today's clinical microbiology labs. Given their ease-of-use, relatively low cost to perform AST and prevalence across the globe, they will be indispensable in the immediate future. In the near future, I anticipate that the emerging and future innovative technologies, such as MADM, AFM and IMC, will lead the next wave of more powerful AST tools for rapid clinical diagnostics. Future tools to measure bacterial metabolic activity in real-time without culturing will be a quantum leap forward from the existing commercial AST technologies. These tools will enable a one-hour AST, within the time span of an outpatient clinical visit. Such rapid and real-time AST tools will not only help save lives,<sup>10</sup> but also have the potential to enable accurate antibiotic treatment at disease onset, potentially slowing the evolution of antibiotic resistance and improving antibiotic stewardship. Given the ever-increasing spread of antibiotic resistance, we must develop innovative technologies which permit rapid AST within an hour, can be applied to fluids collected directly from the patient, and are applicable to slow-growing and non-cultivable microbes.

## PLASMONIC IMAGING OF PROTEIN INTERACTIONS WITH SINGLE BACTERIAL CELLS

Quantifying the interactions of bacteria with external ligands is fundamental to the understanding of pathogenesis, antibiotic resistance, immune evasion, and mechanism of antimicrobial action. Due to inherent cell-to-cell heterogeneity in a microbial population, each bacterium interacts differently with its environment. This large variability is washed out in bulk assays, and there is a need of techniques that can quantify interactions of bacteria with ligands at the single bacterium level. In this work, we present a label-free and real-time plasmonic imaging technique to measure the binding kinetics of ligand interactions with single bacteria, and perform statistical analysis of the heterogeneity. Using the technique, we have studied interactions of antibodies with single *Escherichia Coli* (*E. coli*) O157:H7 cells and demonstrated a capability of determining the binding kinetic constants of single live bacteria with ligands, and quantify heterogeneity in a microbial population.

## Introduction

Bacteria interact with environment through their surface constituents, such as lipid bilayers, peptidoglycan layers, lipopolysaccharides (LPS), pili, flagella and outer membrane proteins. The surfaces of bacteria act as the first line of defense against harmful external stimuli, including antibiotics<sup>11</sup> and antimicrobial peptides,<sup>12,13</sup> and also play crucial roles in interacting with other surfaces, including host tissues<sup>14</sup> and medical plastics,<sup>15</sup> to help bacterial cells attach and colonize. In order to survive in a changing environment, bacteria replicate and evolve quickly,<sup>16,17</sup> leading to diversity of different bacteria species, and variability within the same species<sup>17,93</sup>. It is thus important to study and quantify the interactions of bacteria with external ligands at the single bacterium level.

The interactions of external ligands and bacteria have been studied using *ex situ* and *in situ* approaches, such as fluorescence assay,<sup>21</sup> quartz crystal microbalance (QCM)<sup>94</sup>, surface plasmon resonance (SPR)<sup>19,20</sup>, microcantilevers<sup>44</sup> and atomic force microscope (AFM).<sup>12,15</sup> The *ex situ* approaches include the study of reconstituted artificial membranes<sup>95,96</sup>, membrane protein embedded liposomes<sup>97</sup>, and extracted surface constituents (e.g., membrane proteins<sup>98</sup> and sugars<sup>99</sup> from bacteria. Given the complexity of the bacteria, *in situ* study of intact bacterial cells in their native environments are more attractive<sup>100</sup>.

Traditional studies of intact bacteria cells are largely based on bulk assays and susceptibility testing assays, using techniques such as SPR<sup>18–20</sup> and disk-diffusion<sup>31</sup>. The data generated with these bulk assays are averaged over many bacteria, which wash out important variability or heterogeneity of different bacterial cells. Various imaging techniques, such as fluorescence<sup>13,21</sup>, AFM<sup>12,15</sup> and transmission electron microscopy (TEM)<sup>21</sup>, and non-imaging microfluidics techniques, such as flow cytometry<sup>101</sup> and micro electrophoresis<sup>17</sup>, have been used to study bacterial surfaces. These techniques have contributed to the understanding of bacteria, but each has disadvantages. For example,

the fluorescence method requires labeling, which limits its application to only certain probe molecules and cultivable strains, and gram negative bacteria with sugars cannot be easily labeled by engineering cells<sup>22</sup>. In addition, the fluorescence method is an end-point assay, which is not suitable for quantifying the kinetics of molecular binding to bacteria. TEM requires extensive sample preparations and is unsuitable for live cell analysis in aqueous solutions. AFM can operate in aqueous solutions, but it is usually too slow to follow fast binding of ligands with bacteria, and the scanning AFM probe may perturb the binding process. In this study, we present a plasmonic imaging technique<sup>102–104</sup> (Figure. 3-1a) to study and quantify the interactions of a single *E. Coli O157:H7* cell with an antibody, and perform statistical analysis of the bacterial heterogeneity.

*E. Coli O157:H7* is a highly virulent food borne pathogen that causes diseases, such as diarrhea, hemorrhagic colitis and hemolytic uremic syndrome<sup>24</sup>. Many groups have tried detecting this pathogen by several culture assays as well biosensing approaches. Several groups have used conventional SPR to detect *E. Coli O157:H7* by direct detection of bacterial cells binding to surface (Tawil et al., 2012; Torun et al., 2012), indirect detection of surface immobilized cells using complementary probes<sup>19,20</sup> or coupling SPR with other techniques.<sup>108</sup> In this study, we focus on the binding kinetics of goat *anti-E Coli O157:H7* IgG polyclonal antibody(Ab157)<sup>19,20</sup> onto single *E. Coli O157:H7* cells. Commercial humanized antibodies are increasingly used as an alternate therapy for immune clearance of pathogens,<sup>21,109</sup> hence the study of antibody binding kinetics with single bacterial cells is important to elucidate their efficacy and potential as future drugs.



## **Materials and Methods**

### **Materials**

Lyophilized Bacterial pellets of *E. Coli O157:H7* (ATCC43888) were purchased from Fisher Scientific. Affinity purified goat *anti-E. coli O157:H7* IgG and *anti-E. coli O145:H7* polyclonal antibodies were purchased from Kirkegaard and Perry Laboratory Inc. (Gaithersburg, MD) and suspended in 1ml PBS (1x). Secondary antibody Alexa Fluor 555 rabbit anti-goat IgG (H+L) was purchased from Life Technologies (Carsbad, CA). (1-Mercapto-11-undecyl) hexa(ethylene glycol) (PEG) and Carboxyl-terminated hexa(ethylene glycol) undecane thiol (PEG-COOH) was purchased from Nanoscience Instruments (Phoenix). Other reagents were purchased from Sigma-Aldrich.

### **Bacteria Purification**

The lyophilized bacteria was suspended in 1ml PBS (1x) and cleaned by centrifugation at the speed of 50g for 1 minute to remove charcoal and collecting the supernatant containing bacteria. The supernatant was collected and washed further by pelleting bacteria in the centrifuge at the speed of 2000g for 15 minutes. The pelleted bacteria was suspended in 1ml PBS and mixed thoroughly. Further, the above washing step was repeated three times. The final 1ml of bacteria in PBS solution, after 3 rounds of purification, was saved in small aliquots of 20  $\mu$ l and frozen at -80 °C.

### **Surface Functionalization**

Clean BK7 glass cover slips were coated with 1.5 nm chromium and 47 nm gold to prepare SPR chips. The chips were cleaned with deionized water and ethanol multiple times and blown dry with nitrogen gas and then cleaned by hydrogen flame. The cleaned chips were submerged in 1 mM PEG/PEG-COOH ethanol solution and left overnight in dark for 24 hrs. The overnight incubated chips were taken out and cleaned with deionized

water, ethanol solution multiple times and blown dry with nitrogen gas. PEG/PEG-COOH self-assembled monolayer (SAM) was deposited on each chip with this protocol.

Next, the SAM coated chip was activated with 0.5 ml of freshly prepared mixture (1:1) of 0.1 M NHS and 0.4M EDC to produce NHS ester receptors capable of binding with amino group of antibodies via an amide bond. The chip was cleaned with deionized water and blown dry with nitrogen gas. Polyclonal anti-*E.Coli O157:H7* antibody suspended in 20mM sodium acetate (NaOAc) pH 5.5 at the concentration (30 µg/ml) optimized for maximum bacteria immobilization was immediately applied to NHS/EDC activated surfaces above and kept for about 60-90 mins.<sup>20</sup> The chip was again cleaned by deionized water and blown dry with nitrogen gas. This antibodies conjugated sensor chips are ready for bacteria capture on SPRM setup later.

### **Plasmonic Imaging and Flow Setup**

The plasmonic imaging setup is based on the Kretschmann configuration with a high numerical aperture objective (NA 1.49) and an inverted microscope (Olympus IX81) (Figure 3-1). The sensor chip was placed on the objective lens with refractive index matching immersion oil. A 680nm super luminescence diode (Qphotonics, Ann Arbor, MI) was used to excite the SPR images and a CCD camera (Pike-032B, Allied Vision Technologies, Newburyport, MA) was used to record SPRM images. A FlexiPerm sample well was mounted on top of the antibody functionalized gold chip and filled with PBS (1x) buffer. The assembled gold chip was then mounted on top of the plasmonic imaging setup. The incident angle of the light beam was adjusted to the surface plasmon resonance angle, showing minimal image intensity. Sample delivery was based on a multichannel gravity based drug perfusion system, which flew sample solutions over the immobilized bacterial cells. The flow rate was 330 µl/min and the transition time between different flow solutions was in the range of 1-2 seconds.

## **Bacteria Immobilization**

An aliquot of frozen purified bacteria was thawed for 2 minutes, and then 20  $\mu\text{l}$  of bacteria were added to the sensor chip. The bacteria started to attach and immobilize onto the sensor surface via antibody binding. After about 15-20 minutes of incubation, sufficient amount of bacteria were attached onto the gold chip. 1x PBS buffer was flowed over the chip to wash out unattached bacteria from the solution, then 5 mg/mL BSA were added to the chip and incubated for 1 hour to completely block the surface and prevent non-specific adsorption of antibody.

## **Immunofluorescence Microscopy**

Following kinetics of Ab157 binding to *E. Coli O157:H7* cells, fluorescence labeled secondary antibody at a concentration of 10  $\mu\text{g/ml}$  was introduced for 5 minutes and washed with PBS to remove unbound secondary antibody.

## **Image Collection and Processing**

All plasmonic imaging videos were collected at 3.3 fps at a pixel resolution of 640x480. We chose an appropriate exposure time to maximize image intensity at the same time avoiding over exposure. Images were subtracted from the first recorded image to remove background noises and interference patterns. Further, images were plotted in 2D frequency domain using Fast Fourier Transform (FFT) conversion, and cleaned up with a spatial band pass filter. The cleaned images were converted back from frequency domain using inverse FFT. For better visualization, images were converted to scaled color images.

## **Data Analyses from Images**

As mentioned in text, the plasmonic imaging intensity in each of the selected regions, including regions of the bacteria and bare gold chip regions, was analyzed with a MATLAB program. The plasmonic image intensity from each bacterium was reference corrected with the background bare gold regions to analyze the binding kinetics. The

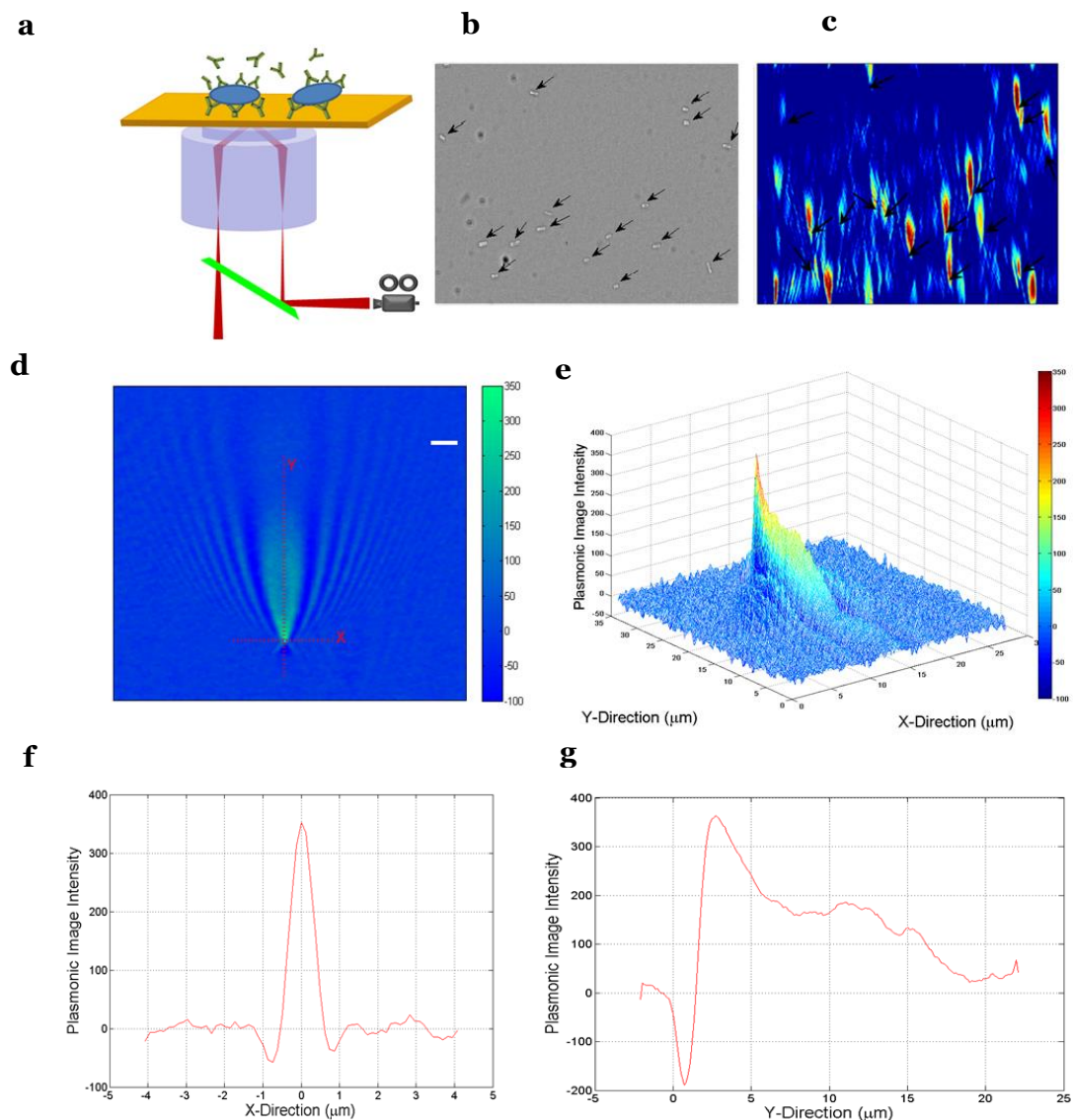
binding kinetics was determined with the first order kinetic equation, and  $k_a$ ,  $k_d$  and  $K_D$  ( $=k_a/k_d$ ) were obtained from the fitting.

## **Results and Discussion**

*E. Coli* O157:H7 bacteria were immobilized on the sensor chip using an *anti-EColi* O157 (antibody Ab157), which were imaged with a plasmonic imaging setup (Figure 3-1a) described in detail elsewhere.<sup>102–104,110,111</sup> Briefly, the setup is based on an inverted optical microscope (Olympus IX81) with high numerical aperture oil immersion objectives (N.A. 1.49). Light from a super-luminescence diode (Qphotonics, Ann Arbor, MI) with wavelength of 680 nm is directed onto the sensor chip, made of glass coverslip coated with a 47 nm thick gold film. The incident angle of light is tuned to excite surface plasmons, and the reflected light is imaged with the same objective together with other components, including a CCD imager.

### **Imaging Single Bacterial Cells by Plasmonic Imaging**

The individual bacteria were imaged as distinct V-shaped patterns (Figure 3-1c), which match well with the positions of the bacteria in the Bright-field optical image (Figure 3-1b). These V-shaped patterns are caused by the scattering of surface plasmonic waves by the bacteria immobilized on the surface.<sup>104</sup> The distinct patterns in the plasmonic image are helpful to distinguish bacterial cells from interference patterns originated from the optical setup, and other spatial background noises on the image.



Figure

### 3-1. Imaging Single Cells using Plasmonic Imaging Setup

a) Schematic of the plasmonic imaging setup using a high numerical objective and the immobilization of bacterial cells on top of gold chip by covalently attached antibodies. b) Bright-field optical image of immobilized bacteria. c) Plasmonic image of bacteria shown as V-shaped diffraction patterns at positions of bacteria on bright field image. d) Magnified plasmonic image of a single bacterium showing clearly the V-shape diffraction pattern. e) 3D histogram of the bacteria in Figure 3-1d. f) Profile of the V-shaped pattern along the basin of V in Figure 3-1d. g) Profile of the V-shaped pattern along the middle axis in Figure 3-1d. Scale bar:  $2\mu\text{m}$ . Reprinted from *Biosensors and Bioelectronics*, Vol 63, Karan Syal, Wei Wang, Xiaonan Shan, Shaopeng Wang, Hong-Yuan Chen, Nongjian Tao. Plasmonic imaging of protein interactions with single bacterial cells. Pages 131–137, Copyright 2017, with permission from Elsevier.

Figures 3-1d and 3-1e show more clearly one of the V-shaped patterns, and also reveal that the region of maximum intensity in each V-shaped pattern overlays one immobilized bacterial cell. The intensity profile along the basin of the V shaped diffraction pattern (X-direction) of bacterial cells show a full-width at half maximum (FWHM) of about 0.5  $\mu\text{m}$  (Figure 3-1f). This FWHM is due to the optical diffraction limit of our setup.<sup>104</sup> The intensity profile along the plasmonic wave propagation direction (Y-direction) reveals that the intensity decays with a FWHM of about  $\sim 4 \mu\text{m}$  (Figure 3-1g). The intensity decay is due to the finite propagation length of surface plasmonic waves, which depends on the type of the metal film, and the wavelength of incident light<sup>104</sup>. We observe similar V-shaped patterns for all immobilized bacterial cells with no major differences in the decay length and FWHM for different cells.

### **Binding Kinetics of Antibody to Single Cells**

Using the plasmonic imaging setup, we next imaged the binding process of Ab157 antibody to the *E. Coli* O157:H7 cells immobilized on the surface. Figure 3-2a shows a bright-field image of 4 immobilized bacterial cells. We started the binding study by initially flowing 1xPBS at 330  $\mu\text{l}/\text{min}$  continuously over the bacterial cells for about 2 minutes. We then switched the flow to 1x PBS containing 10  $\mu\text{g}/\text{mL}$  Ab157 to study the association of the antibody to the individual bacterial cells. After 3 minutes, we switched the flow back to 1x PBS in order to follow the dissociation process.

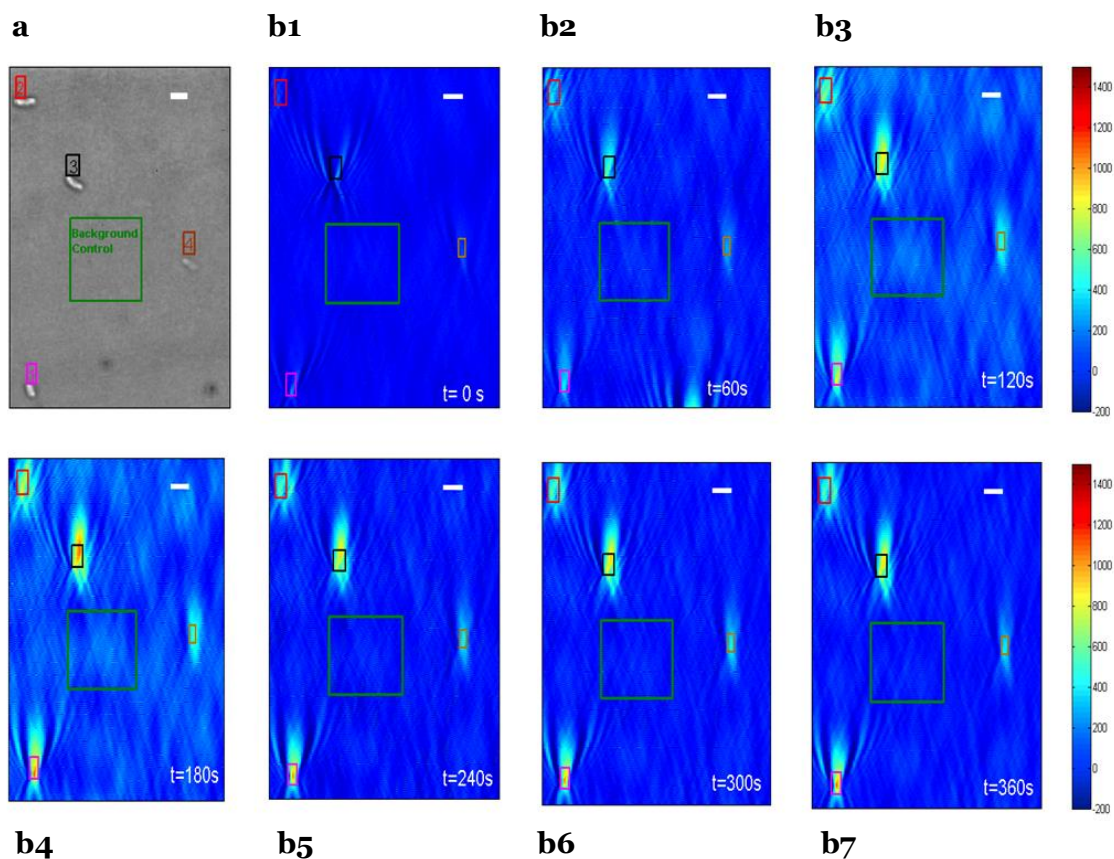
Since we are interested in the association and dissociation processes of antibody onto the bacteria, time-differential images were obtained by subtracting the first frame from the subsequent frames to show changes in the image over time. Figure 3-2b1 is a time-differential image captured before the introduction of solution containing antibody, which shows weak contrast of the bacteria. If the bacteria were static, then there should be no contrast in the time-differential image before antibody binding taking place. The

observation of the small contrast is due to micro-motions of the live bacterial cells. We will return to this later.

Upon exposure to the PBS containing the antibody, binding of the antibody to the bacteria, primarily via the O-antigen<sup>112</sup> on the outer membrane surfaces of the bacteria, takes place, which is revealed as an increase in the image contrast of the individual bacterial cells. Figures 3-2b (2-4) show several time-differential plasmonic images of the association process from which detailed information of the association process can be obtained. For example, the images show the contrast increases for different cells are different, demonstrating the cell-to-cell heterogeneity that is washed out in the bulk assay. The images also show the increase in the intensity in the regions between the bacterial cells, which, as we will discuss later, is mainly due to the increase in the bulk refractive index as we switch the solution.

Snapshots of the time-differential plasmonic images during the dissociation process are shown in Figures 3-2b (5-7), which were captured after switching the antibody-containing solution back to PBS. During the dissociation phase, the image intensity of each bacterial cell decreases at a slow rate compared to the association process, which is expected as the antibodies dissociate from the bacterial cell. Like the association process, the dissociation also varies across different cells. Note also that the image intensity in the regions without bacteria returns to the baseline level quickly, which further supports the interpretation of bulk refractive index change as the origin of the intensity change in these regions.





Figure

### 3-2. Imaging Binding Kinetics using Plasmonic Imaging

a) Bright-field optical image of immobilized *E. Coli O157:H7* cells. The region chosen to analyze the plasmonic image intensity of each bacterium is marked as a colored box in the bright-field image. Also shown is the background control region as a green box near the center of the image. b) Time-differential plasmonic images captured during different stages of association (b1-b4) and dissociation (b4-b7) processes. A complete plasmonic video of the binding kinetics is given in the supporting information. Scale bar: 2 $\mu$ m. Reprinted from Biosensors and Bioelectronics, Vol 63, Karan Syal, Wei Wang, Xiaonan Shan, Shaopeng Wang, Hong-Yuan Chen, Nongjian Tao. Plasmonic imaging of protein interactions with single bacterial cells. Pages 131–137, Copyright 2017, with permission from Elsevier.

The image intensity vs. time profiles obtained from the recorded image sequence provides detailed kinetic information of the antibody binding to the bacterial cells (Figure 3-3). This type of plots has been widely referred to as sensorgrams, but Figure 3-3

represents the first sensorgrams on single bacterial cells. The sensorgrams are “noisy”, which is mainly due to micromotions of the bacteria. The bacterial cells in the present work were alive and attached to the sensor surface via relatively weak non-covalent bonds, so we observed frequent movement of the bacterial cells in the plasmonic images. Despite the micro-motions, the sensorgrams can be fit with the first order kinetics model, from which kinetic constants, including  $k_a$ ,  $k_d$  and  $K_D$ , for each of the bacteria cells are obtained (see Table 3-1). Figure 3-3 also plots the image intensity vs. time profile of a region between the bacteria cells, which shows only a bulk index change with no binding kinetics curve as observed over bacterial cells. This observation indicates that non-specific binding of the antibody to the sensor surface is insignificant.

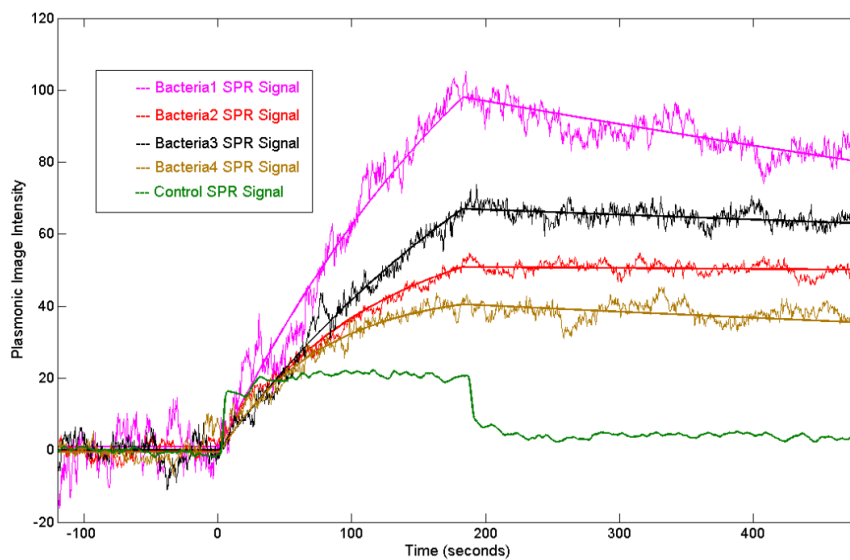


Figure 3-3. Sensorgrams of Single Bacterial Cells Obtained by Plotting the Image Intensity Vs. Time

Smooth solid lines are fits to the first order kinetics for different cells, allowing the determination of kinetic constants,  $k_a$ ,  $k_d$  and  $K_D$  for each of the bacteria cells. The green line plots the sensorgram of a region without bacteria cells, showing a sudden increase and decrease as the flow is switched from PBS buffer solution to sample solution, and then back to PBS buffer, respectively. Reprinted from Biosensors and Bioelectronics, Vol 63, Karan Syal,

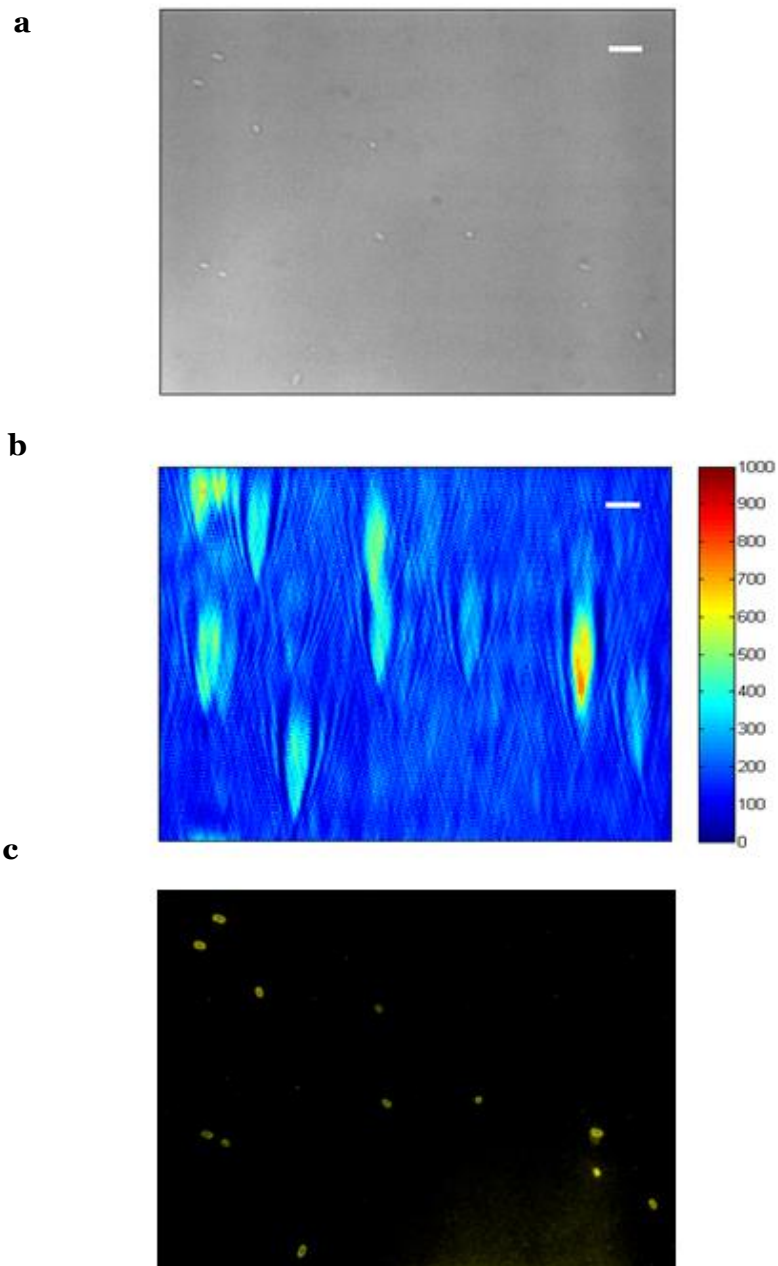
Table

3-1. Kinetics of Individual Microbial cells

<b>Bacteria</b>	<b>Association rate (<math>k_a</math>) (<math>M^{-1} s^{-1}</math>)</b>	<b>Dissociation rate (<math>k_d</math>) (<math>s^{-1}</math>)</b>	<b>Dissociation Constant (<math>K_D</math>) (M)</b>	<b>Peak Plasmonic Image intensity</b>
Bacteria 1	$5.1 \times 10^4$	$6.9 \times 10^{-4}$	$1.3 \times 10^{-8}$	97.5
Bacteria 2	$1.3 \times 10^5$	$5.1 \times 10^{-5}$	$4.0 \times 10^{-10}$	50.8
Bacteria 3	$5.1 \times 10^4$	$2.1 \times 10^{-4}$	$4.1 \times 10^{-9}$	67.0
Bacteria 4	$2.0 \times 10^5$	$4.4 \times 10^{-4}$	$2.3 \times 10^{-9}$	40.1

### Validating Binding Kinetics by Control Experiments

To further validate the plasmonic imaging of the antibody binding to bacterial cells, we used AlexaFluor555 labeled secondary antibody to bind to the attached primary antibody. Figure 3-4 shows the conventional bright field optical, time-differential plasmonic and fluorescence images of a sensor surface covered with multiple bacteria cells. The fluorescence image (Figure 3-4c) confirms that the increase in the plasmonic image intensity is due to the binding of the primary antibody to the bacterial cells. As an additional validation experiment, we used a goat *anti-E. coli O145* IgG polyclonal antibody (Ab145) as a negative control. The exposure of *E. Coli* cells to Ab145 did not change the plasmonic image intensity (Figure 3-5), indicating that the binding kinetics of Ab157 with *E. Coli* cells were specific.

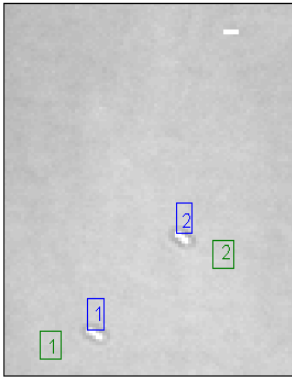


Figure

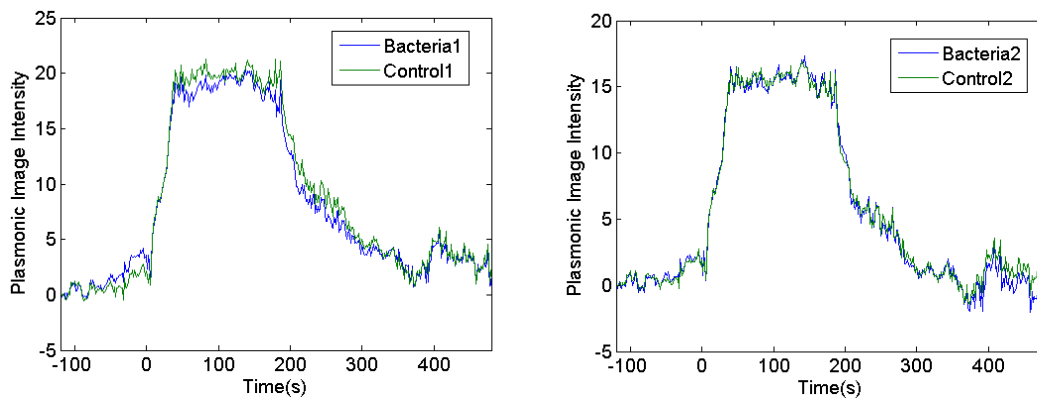
### 3-4. Using Fluorescent Imaging to Validate Binding Kinetics

a) Bright-field optical image of bacteria immobilized on a gold chip. b) Time-differential plasmonic image showing V-shape diffraction patterns corresponding to the individual bacterial cells in Fig. 4a. c) Fluorescence image after adding secondary antibody labelled with AlexaFluor555. Scale bar: 5  $\mu\text{m}$ . Reprinted from Biosensors and Bioelectronics, Vol 63, Karan Syal, Wei Wang, Xiaonan Shan, Shaopeng Wang, Hong-Yuan Chen, Nongjian Tao. Plasmonic imaging of protein interactions with single bacterial cells. Pages 131–137, Copyright 2017, with permission from Elsevier.

**a**



**b**



Figure

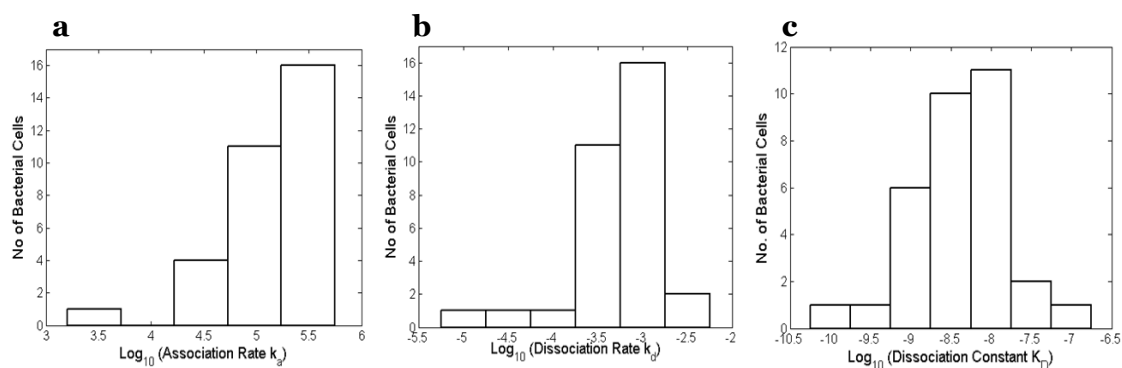
### 3-5. Binding Kinetics of Negative Control

a) Bright-field optical image of immobilized *E. Coli* O157:H7 cells. Scale bar: 2  $\mu\text{m}$ . b) Sensorgrams of single bacterial cells on flowing the negative control antibody Ab145. There is no increased plasmonic image intensity observed for bacterial cells compared to the background signal. The data shows that the binding of the bacteria with the antibody Ab157 was specific. Reprinted from *Biosensors and Bioelectronics*, Vol 63, Karan Syal, Wei Wang, Xiaonan Shan, Shaopeng Wang, Hong-Yuan Chen, Nongjian Tao. Plasmonic imaging of protein interactions with single bacterial cells. Pages 131–137, Copyright 2017, with permission from Elsevier.

The results discussed above demonstrate a new capability for studying the binding kinetics of single bacteria. Compared to the conventional SPR approach which studies a layer of many bacterial cells immobilized on a sensor surface,<sup>19,20</sup> the single bacteria binding kinetics analysis capability can discriminate non-specific binding taking place on the regions of the sensor surface without bacteria cells. More importantly, it opens up the possibility of detecting individual microbes in mixed communities, biofilms as well as microbe-infected patient samples. We demonstrate below kinetics analysis of multiple bacterial cells and cell-to-cell heterogeneity.

### **Quantifying Bacterial Surface Heterogeneity**

Figure 3-6a and 3-6b show the distributions of  $k_a$  and  $k_d$  values, respectively. The data were obtained by fitting the sensorgram of each bacterial cell (33 bacteria cells) with the first order binding kinetics model. Although the number of bacterial cells was limited, the data shows 2 orders of magnitude variability in  $k_a$  and  $k_d$ .  $K_D$  was obtained from the  $k_a$  and  $k_d$  values with the relation,  $K_D = k_d / k_a$  (Figure 3-5c). Unlike the distributions of  $k_a$  and  $k_d$ , the distribution of  $K_D$  has a center, which is near 3.9 nM. This  $K_D$  value is close to the previously reported values in literature.<sup>19</sup> However, the presence of 4 orders of magnitude in  $K_D$  conveys the heterogeneity in how an antibody might interact with individual cells.



Figure

### 3-6. Distribution of Binding Constants.

(a) Distributions of association rate,  $k_a$  (a), dissociation rate,  $k_d$  (b), dissociation constant,  $K_D$ , (c) observed on various bacteria. The large variability in the observed kinetics conveying cell-cell heterogeneity in Ab157 interacting with bacterial cells. Reprinted from Biosensors and Bioelectronics, Vol 63, Karan Syal, Wei Wang, Xiaonan Shan, Shaopeng Wang, Hong-Yuan Chen, Nongjian Tao. Plasmonic imaging of protein interactions with single bacterial cells. Pages 131–137, Copyright 2017, with permission from Elsevier.

We also obtained distribution (Figure 3-7) of the plasmonic image intensity measured at the end of association phase from various bacterial cells. Since the plasmonic intensity is proportional to the mass density change of the sensor surface, the data reflects the distribution in the expression levels of O-antigen on the outer membranes of the bacterial cells. We performed statistical analysis and found no obvious correlations between the measured O-antigen expression levels,  $k_a$ ,  $k_d$  and  $K_D$  and the physical parameters, including length and size, of the bacteria (Table 3-2).

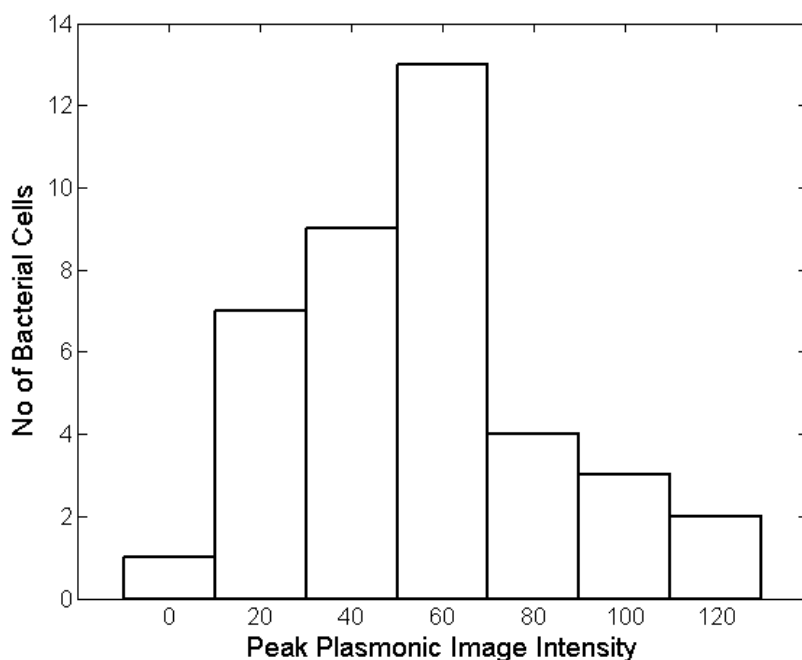


Figure  
3-7 Distribution of the Plasmonic Image Intensity Measured at the End of Association Phase for Various Bacterial Cells.

Reprinted from Biosensors and Bioelectronics, Vol 63, Karan Syal, Wei Wang, Xiaonan Shan, Shaopeng Wang, Hong-Yuan Chen, Nongjian Tao. Plasmonic imaging of protein interactions with single bacterial cells. Pages 131–137, Copyright 2017, with permission from Elsevier.

Table  
3-2. Correlation of Kinetics Parameters with Physical Attributes and Plasmonic Imaging Parameters

All Bacteria	$k_a$	$k_d$	$K_D$	Plasmonic Intensity	Length	Breadth	Area	Peak V-shape Intensity
$k_a$	1.00	0.17	0.47	0.27	0.04	0.34	0.21	-0.10
$k_d$	0.17	1.00	0.24	0.01	-0.32	-0.31	-0.29	-0.42
$K_D$	0.47	0.24	1.00	-0.29	-0.38	-0.70	-0.37	-0.32
Plasmonic Intensity	0.27	0.01	0.29	1.00	0.52	0.06	0.36	-0.02



We believe that the reason for the observed cell-to-cell variability is the O-antigen on the surfaces of the bacteria,<sup>112</sup> which is the target for the antibody. Studies have shown large variations in the chain length of O-antigen, which give E. Coli distinct surface morphologies (smooth, semi-rough and rough).<sup>113</sup> This variation in chain length exists owing to Wzz and Wzy proteins, which are responsible for modulating the O-antigen chain lengths. Wzz assembles the O-antigen around a specific modal length whereas Wzy assembles O-antigen to a stochastic length.<sup>114,115</sup> These variations in O-antigen may be the primary reason for the observed cell-to-cell variability in the antibody binding kinetics.

The wide distributions in kinetic constants indicate the natural phenotypic diversity in a bacterial population. Capturing this diversity is important, especially because microbial sub-populations with variable phenotypic characteristics are known to play an important role in microbial evolution and antibiotic resistance.<sup>116</sup> The traditional bulk assays that measure average  $K_D$  of a large number of bacteria cells could be misleading, especially when a species evolves and sub-populations emerge. In contrast, the present plasmonic imaging method can provide quantitative analysis of ligand interactions with individual live bacteria, which represents an unprecedented capability for studying the role of physiological heterogeneity in microbial population behaviors and providing new insights into microbial diversity arising from the rapid replication of bacteria.

## **Conclusion**

We have described a plasmonic imaging method for studying the interaction kinetics between biomolecules and individual bacterial cells. The method is label-free, quantitative and in real time. Using the method, we have measured the kinetics of an antibody binding to single *E. Coli* O157:H7 bacterial cells. The mean values of the measured kinetic constants (e.g.,  $K_D$ ) are consistent with the reported literature values obtained from bulk assays. However, the present method revealed large cell-to-cell variations in binding kinetics with kinetic constants distributed over several orders of magnitude. These results are direct evidence that large heterogeneity in the binding capability of bacteria with external ligands naturally exists in a bacterial population. Such heterogeneity has been hypothesized as an important mechanism for evolution and fitness in microbes. We anticipate that this method will improve the understanding of bacterial behaviors, such as pathogenesis and immune escape of virulent microbes, action and efficacy of antimicrobial peptides in acting on a microbial population and binding affinities of humanized antibodies against microbes for future drug therapies.

## ANTIMICROBIAL SUSCEPTIBILITY TEST WITH PLASMONIC IMAGING AND TRACKING OF SINGLE BACTERIAL MOTIONS ON NANOMETER SCALE

Antimicrobial susceptibility tests (ASTs) are important for confirming susceptibility to empirical antibiotics and detecting resistance in bacterial isolates. Currently, most ASTs performed in clinical microbiology laboratories are based on bacterial culturing, which take days to complete for slowly growing microorganisms. A faster AST will reduce morbidity and mortality rates and help healthcare providers administer narrow spectrum antibiotics at the earliest possible treatment stage. We report the development of a non-culture-based AST using a plasmonic imaging and tracking (PIT) technology. We track the motion of individual bacterial cells tethered to a surface with nanometer (nm) precision and correlate the phenotypic motion with bacterial metabolism and antibiotic action. We show that antibiotic action significantly slows down bacterial motion, which can be quantified for development of a rapid phenotypic-based AST.

## Introduction

Acute infections, such as sepsis, affect over a million people every year, leading to mortality rates of 30-50%.<sup>30,117</sup> For septic and other day-to-day patients infected with bacterial pathogens, antimicrobial susceptibility testing (AST) is used to predict the *in vivo* success or failure of the chosen antibiotic therapy along with diagnosing antibiotic resistant bacteria. Current culture-dependent AST technologies are slow with a turnaround of 1-3 days (Chapter 2), thus posing a risk on the patient's life.<sup>118</sup> A rapid AST will help generate antibiotic susceptibility profiles at the earliest possible stages of infection, identify antibiotic-resistant bacterial isolates, and allow narrow-spectrum or personalized administration of antibiotics.

Antimicrobial susceptibility testing methods currently used in clinical microbiology and commercial diagnostic labs include culture-dependent disk diffusion and broth dilution tests (Chapter 2) which may take up to two days to complete.<sup>9,32,119</sup> Many emerging technologies (Chapter 2) efforts have been devoted to develop faster AST technologies in recent years, several of which are based on characterizing the physical features of bacterial growth, such as the number, size, and length of bacterial cells.<sup>42,46,49,54,55,58,89</sup> Another approach is to use imaging technologies to analyze the changes in imaging area<sup>54,55,58,89</sup> or fluorescent signal<sup>42,120</sup> associated with the growth of the bacterial cells. This imaging approach has achieved some success, especially in susceptibility testing of single cells present within polymicrobial mixtures of complex clinical samples, including broncho alveolar lavage specimens collected from patients with ventilator-assisted pneumonia<sup>41</sup> and urine samples spiked with bacterial cells.<sup>55</sup> However, the accuracy of these imaging approaches requires further improvement.<sup>40</sup> Moreover, most of these approaches still rely on culturing, which is not universally applicable, especially for slow-growing, difficult-to-culture, or uncultivable bacteria.<sup>121</sup>

More recently, future technologies such as Atomic Force Microscope (AFM) cantilevers (Chapter 2) have been used to detect bacterial cell metabolism and perform rapid antimicrobial susceptibility testing.<sup>44,77,78</sup> The method immobilizes several hundred bacterial cells on a cantilever and detects cantilever deflections associated with the micro-motions of the bacterial cells immobilized on the cantilever. The correlation between the micro-motions and the viability (life or death) has been studied for both prokaryotic and eukaryotic cells recently.<sup>44,77,79,122,123</sup> The AFM cantilever approach does not resolve the micro-motions of each individual cell which might be useful for poly-microbial samples and finding resistant sub-populations of bacteria.

Here we report a plasmonic imaging<sup>23,111</sup> and tracking (PIT) method to quantify the motions of single bacterial cells with nanometer resolution and correlate the nano-motion with bacterial metabolism and antibiotic action. To demonstrate the plasmonic tracking approach, we study *Escherichia coli* O157:H7, a bacterial pathogen implicated in food-borne illness outbreaks, as a model strain.<sup>24</sup> For these proof-of-concept studies, we use polymyxin B, a bactericidal antibiotic which permeabilizes the outer membrane of Gram-negative bacilli.<sup>124</sup> We also show the feasibility of this approach to a clinical relevant strain Uropathogenic *Escherichia coli* CFT073 (UPEC), which is implicated in 65%-75% of urinary tract infections (UTIs).<sup>27</sup> We have imaged the individual bacterial cells, tracked their nano-motion, analyzed the correlation between their viability and the nano-motion, and examined the PIT technique as a rapid antimicrobial susceptibility testing method.

## **Materials and Methods**

### **Materials**

Lyophilized bacterial pellets of *E. coli* O157:H7 (ATCC 43888) were purchased from Fisher Scientific. UPEC *E. coli* strain CFT073 was purchased from ATCC. Affinity-purified goat anti-*E. coli* O157:H7 IgG polyclonal antibodies were purchased from

Kirkegaard and Perry Laboratory Inc. (Gaithersburg, MD), suspended in 1 ml PBS (1X), and stored in aliquots at -20°C. Polymyxin B (PMB) was purchased from Sigma-Aldrich and dissolved in 1X PBS at a stock concentration of 10 mg/ml. PMB was stored in dark at 2-8°C according to manufacturer's instruction. 1-Mercapto-11-undecyl hexa(ethylene glycol) (PEG) and carboxyl-terminated hexa(ethylene glycol) undecane thiol (PEG-COOH) were purchased from Nanoscience Instruments (Phoenix, AZ). Other reagents were purchased from Sigma-Aldrich.

### **Preparation and Growth of Bacteria**

The lyophilized bacteria were suspended in PBS centrifuged at the speed of 50 x g for 1 min to pellet the charcoal. The supernatant containing bacteria was collected and centrifuged at 2000 x g for 15 min to pellet the bacteria. The bacterial pellet was re-suspended in 1 ml 1X PBS and mixed thoroughly. The final 1 ml of bacteria in PBS solution, after 3 rounds of purification, was collected in small aliquots of 20 µl and frozen at -80°C adding 5% glycerol. Similarly, *E. coli* strain CFT073 strain was mixed 5% glycerol and frozen in smaller aliquots at -80°C.

An aliquot of frozen *E. coli* O157:H7 or *E. coli* CFT073 strain was thawed and used to inoculate 10 ml of LB medium. *E. coli* O157:H7 cultures were prepared by diluting the overnight culture (grown at 37°C) into fresh LB medium to a concentration of 10<sup>7</sup> colony forming units (CFU)/ml and continuing growth at 37°C with gentle rotary mixing until the cultures reached mid-logarithmic phase of growth. Bacterial cells were collected by centrifugation at 2000 x g for 15 min and re-suspended in 1 ml PBS (1X).

### **Surface Functionalization**

Clean BK7 glass cover slips were coated with 1.5 nm chromium and 47 nm gold and used as SPR sensing chips. The chips were cleaned with deionized water and ethanol for a few times, dried with nitrogen gas, and then cleaned by hydrogen flame. For antibody

surface, the cleaned chips were submerged in 1 mM PEG/PEG-COOH ethanol solution and left in the dark for 24 h to coat a PEG/PEG-COOH self-assembled monolayer (SAM) on each chip. For APTES surface, the cleaned chips were submerged in 1 mM PEG solution and left in the dark for 24 h to coat a PEG SAM on the chips. The coated chips were then cleaned again with washes in deionized water and ethanol and subsequently dried with nitrogen gas.

To attach antibodies next, the PEG/PEG-COOH SAM-coated chips were activated with 500  $\mu$ l of a freshly prepared mixture of 0.1 M NHS and 0.4M EDC in 1:1 ratio to produce NHS ester receptors, which react with the primary amine groups on the antibodies *via* an amide bond. Chips with activated PEG/PEG-COOH SAM were cleaned with deionized water and blown dry with nitrogen gas. Polyclonal anti-*E. coli* O157:H7 IgG antibodies dissolved in 20 mM sodium acetate (NaOAc), pH 5.5 (30  $\mu$ g/ml) were immediately applied to the NHS/EDC-activated surfaces and incubated for 60-90 min. The antibody-coated chips were again cleaned with deionized water and dried with nitrogen gas prior bacterial cell capture on the PIT setup.

To attach the APTES linker to the sensor surface, the PEG SAM-coated sensors were activated with 100  $\mu$ l of a freshly prepared 1% APTES in ethanol (with 5% water) for 2 minutes. The APTES linked sensor chips were again cleaned with deionized water and dried with nitrogen gas prior bacterial cell capture on the PIT setup.

### **Plasmonic Imaging and Flow Setup**

The plasmonic imaging setup is based on the Kretschmann configuration with a high numerical aperture objective (NA 1.49) and an inverted microscope (Olympus IX-81) (Fig. 1).<sup>103,104,110</sup> The sensor chip was placed on the objective lens with refractive index matching immersion oil. A 680 nm super luminescent diode (Qphotonics, Ann Arbor, MI)

was used to excite the SPR images, and a CCD camera (Pike-032B, Allied Vision Technologies, Newburyport, MA) was used to record PIT images.

A FlexiPerm reusable well (SARSTEDT) was mounted on top of the antibody-functionalized gold chip and filled with 500  $\mu$ l PBS (1X) buffer. The assembled gold chip was then mounted on top of the plasmonic imaging setup. The incident angle of the light beam was adjusted to the surface plasmon resonance angle, revealing minimal image intensity.

### **Bacterial Immobilization**

Bacterial cells (20  $\mu$ l) were added to the sensor chip and tethered onto the sensor surface *via* non-covalent antibody binding. After 10-15 min incubation at room temperature, bacterial cells were sufficiently attached to the gold chip. PBS buffer was subsequently flowed over the chip to remove unattached bacterial cells.

### **Image Collection and Processing**

All plasmonic imaging sequences were collected at 106 fps at a pixel resolution of 640x480. We chose an appropriate exposure time to maximize image intensity and avoid over exposure. Images were recorded in either transmitted or plasmonic imaging mode for various time durations.

### **Sample Addition**

Multiple sample solutions, including LB medium or PBS, were added to the bacterial cells *via* a gravity-based multichannel drug perfusion system (Warner Instrument, Hamden, CT). The drug perfusion system flew sample solutions over the immobilized bacterial cells at a flow rate of 330  $\mu$ l/min with the transition time between different flow solutions in the range of 1-2 sec. The flow system was stopped and stabilized for 5 min before adding PMB, streptomycin or glucose. To deliver antibiotics, we pipetted small volumes of antibiotics into the Flexiperme well mounted on the microscope.



## **Data Analyses from Images**

We chose small time durations of about 20 sec from the videos to analyze our data and to avoid the influence of focus drift on nano-motion analysis. The images were processed using custom-written MATLAB programs and Image J scripts.

### **Bacterium – Plasmon Surface Z-Distance Tracking and Z-Movement**

#### **Calculation**

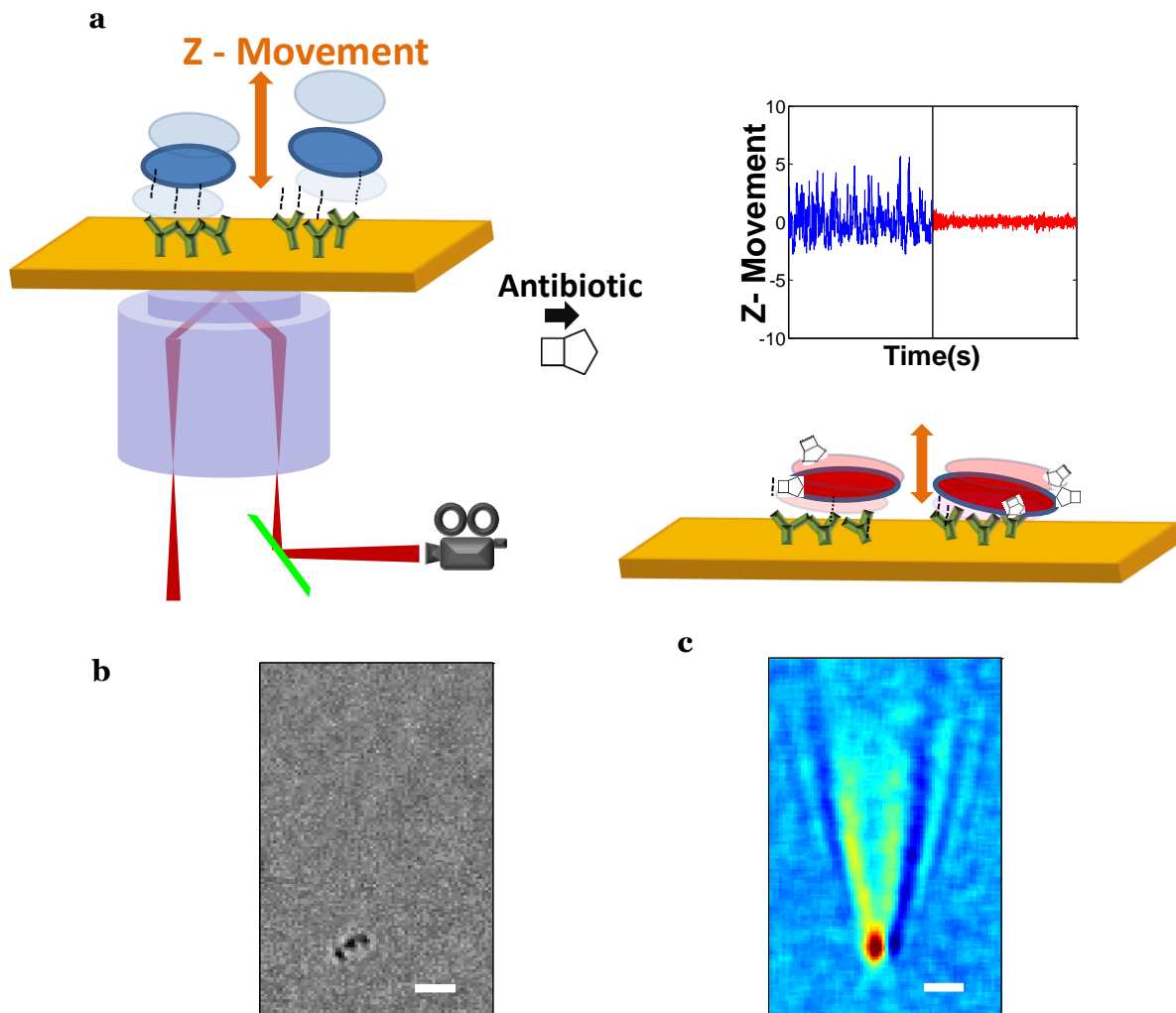
The plasmonic image intensity was calculated by obtaining averaged intensity within a fixed area around the bacterial cell using the bare gold chip regions as reference. The z-distance of the bacterial cell above the sensor surface was then calculated from the plasmonic image intensity ( $I_z$ ) with a calibrated curve, given by

$$I_z = I_0 \exp\left(-\frac{\Delta z}{L}\right), \quad (\text{Eq. S1})$$

Where  $I_0$  is a constant,  $\Delta z$  is the z displacement of a bacterial cell, and L is the decay constant. The decay constant was determined to be  $\sim 95.8$  nm.<sup>125</sup> Using the above calibration, we calculated the error in the z-displacement to be about 0.1 nm.

We define “z-movement” as the relative z-distance, where the mean bacterium-plasmon surface z-distance in a given time duration is subtracted from the z-distance at a given moment. Further “amplitude” is defined as the standard deviation of the z-movement for a given period of time.

## Results and Discussion



Figure

### 4-1. Setup of Plasmonic Imaging and Tracking

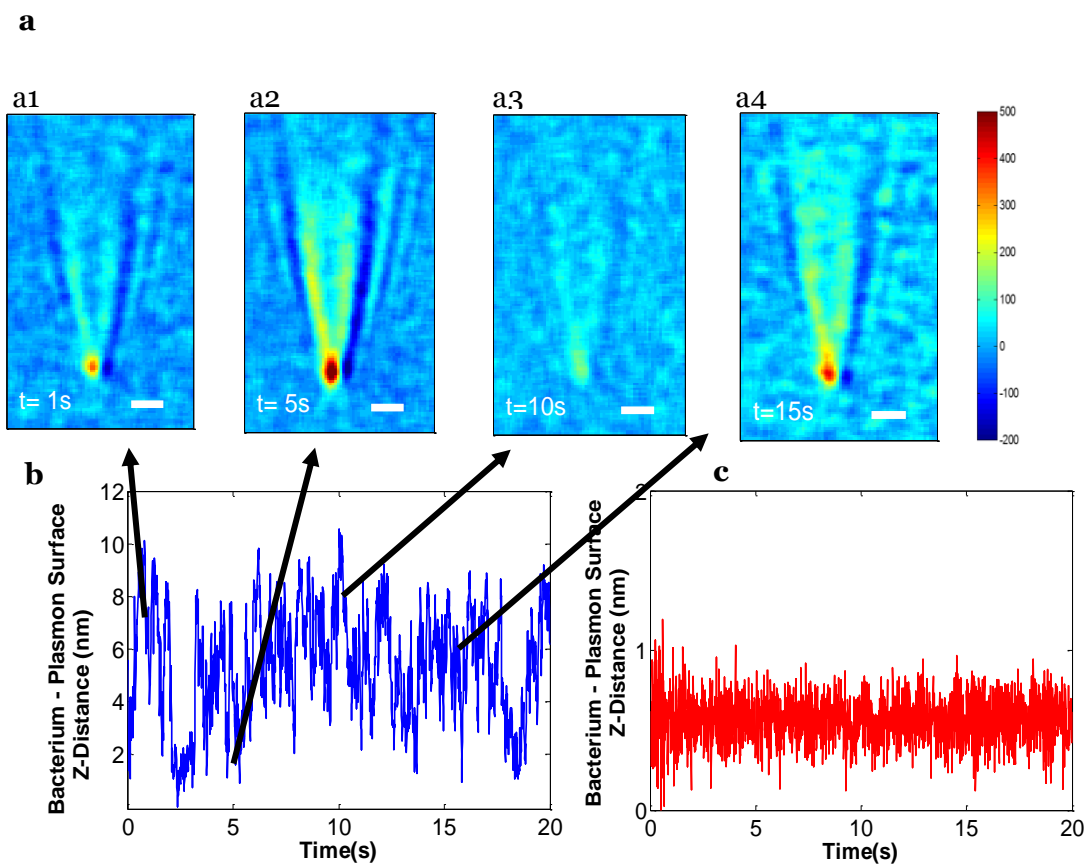
(a) Setup and principle of plasmonic imaging and tracking of bacterial cells tethered to a gold-coated glass sensor chip. *P-polarized* light is directed onto the sensor chip to create surface plasmons on the gold surface, and the reflected light is detected with a CCD to form plasmonic images. Bright field transmission images of the bacterial cells are also simultaneously obtained with the same objective. (b) Bright field image of a tethered bacterial cell. (c) Simultaneously-recorded plasmonic image of the bacterial cell. Scale bar: 2  $\mu\text{m}$ .

## Quantification of Z-Direction Motion

Figure 4-1a shows the PIT setup built on an optical microscope with a high numerical aperture objective.<sup>103,104,110</sup> A sensor chip, made of a glass coverslip coated with 47 nm thick gold film, is placed on the microscope sample stage. Light with a wavelength of 680 nm from a super luminescent diode is directed onto the film *via* the objective. By tuning the incident angle, surface plasmons are excited on the gold surface, and the reflected light is imaged with a CCD imager. The *E. coli* O157:H7 cells, tethered on a sensor chip *via* antibody coupling, scatter the surface plasmonic wave, leading to parabolic-shaped patterns in the plasmonic image.<sup>23</sup> Figures 4-1b and 4-1c show the transmission and plasmonic images of a bacterial cell, where the vertex of the parabolic pattern in the plasmonic image is the location of the cell shown in the simultaneously recorded transmission images.

We have analyzed the motion of the bacterial cells in the transmission and the plasmonic images. The transmission image contrast of the bacterial cells appears to be constant, but the plasmonic image contrast fluctuates significantly. To show the contrast fluctuation of the plasmonic image, we created differential plasmonic images by subtracting the lowest contrast image from all of the images. Figure 4-2a shows a few snapshots of the differential images, which reveal large fluctuations in the plasmonic image contrast of a bacterial cell. This image contrast fluctuation is due to the nano-motion of the bacterial cell normal to the z sensor chip (z direction),<sup>126</sup> which is due to the surface plasmon intense evanescent electric field, which decays exponentially from the surface into the bulk solution. Consequently, the scattering of the plasmonic waves by the bacterial cell decreases exponentially with the distance (z) between the cell and the sensor surface. We have shown previously that the plasmonic image contrast change ( $\Delta I/I$ ) of a particle is related to the distance change (z), by  $\Delta I/I = \exp(-z/95.8 \text{ nm})$ .<sup>125</sup> Using this

relation, we have determined the nano-motion of the bacterial cell in z direction, which is shown in Figure 4-2b. The magnitude of the nano-motion of the bacterial cell above the plasmon surface, is less than 10 nm with an average motion magnitude of  $\sim 6$  nm, which cannot be detected in the traditional transmission optical image. As a control experiment, we tracked the nano-motion of a dead bacterial cell (Figure 4-2c) and observed a much smaller magnitude of nano-motion ( $\sim 0.50$  nm). The data demonstrate the capability of the plasmonic imaging technology for tracking the motion of individual bacterial cells with sub-nm precision.



Figure

4-2. Quantifying Z-direction Nano-motion of Bacterial Cells using Plasmonic Images (a) Snapshots of bacterial z nano-motion revealed by the varying plasmonic image contrast. (b) z-Distance between bacterium and plasmon surface vs. time plot with an average nano-motion magnitude of  $\sim 6$  nm. (c) z-Distance between bacterium and plasmon surface plot of a dead bacterial cell (no motion) showing an average motion magnitude of 0.50 nm. Scale bar ( $2 \mu\text{m}$ ). Reprinted with permission from Syal, K.; Iriya, R.; Yang, Y.; Yu, H.; Wang, S.; Haydel, S. E.; Chen, H.-Y.; Tao, N. Antimicrobial Susceptibility Test with Plasmonic Imaging and Tracking of Single Bacterial Motions on Nanometer Scale. ACS Nano 2015, 10, 845–852. Copyright 2017 American Chemical Society.

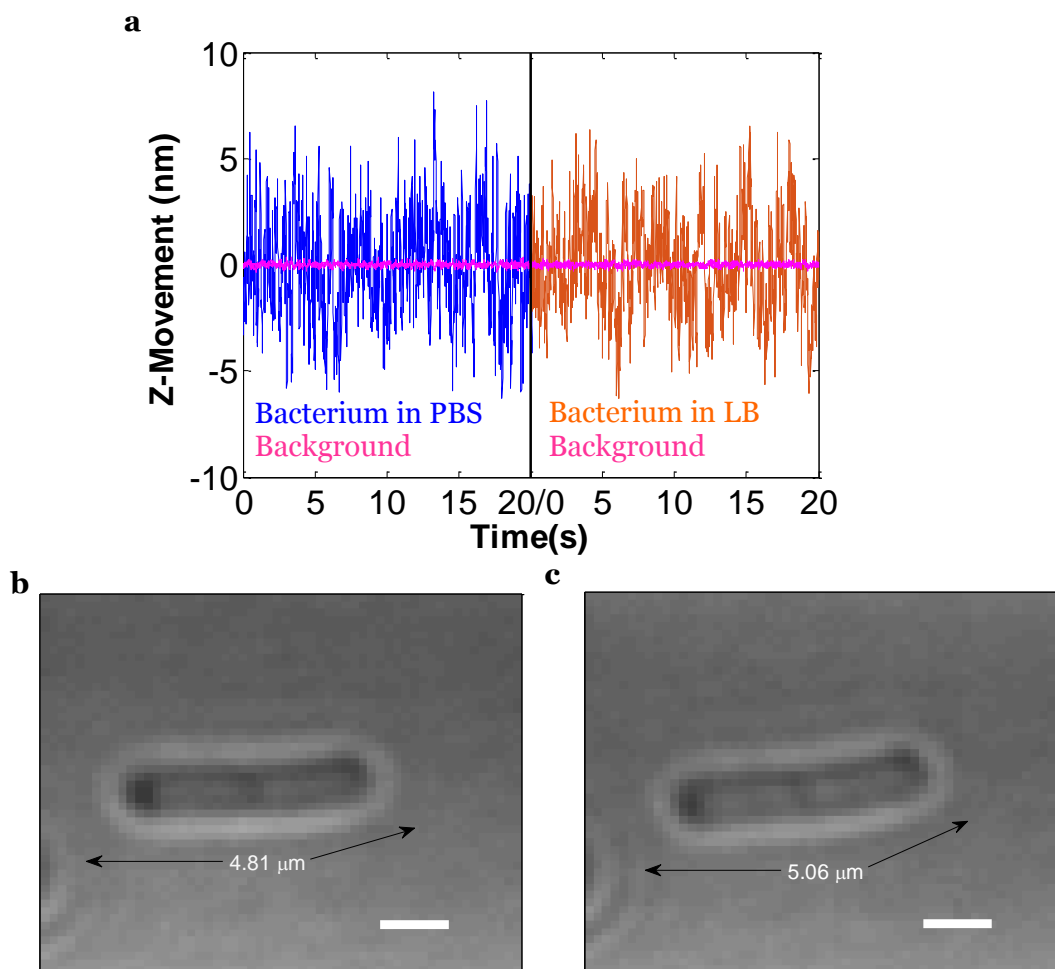
### Correlation Between Nano-motion and Bacterial Metabolism

As supported by further evidence shown below, the bacterial nano-motion is related to the bacterial metabolism. For live cells, bacterial metabolism is associated with

cytoplasmic membrane transport,<sup>44</sup> cytoplasm fluidity,<sup>127</sup> and modifications of membrane lipid composition in response to environmental changes,<sup>128</sup> all of which can cause micro-motion of the cells. In the present system, the bacterial cells are attached to the surface *via* antibodies, involving soft non-covalent bonds that prevent large-scale motions, but allow nano-motion of the bacterial cells.

For better clarity, we define “z-movement” as the relative z-distance, where the mean bacterium-plasmon surface z-distance in a given time duration is subtracted from the z-distance at a given moment. Further “amplitude” is defined as the standard deviation of the z-movement for a given period of time.

The images shown in Figure 4-2 were obtained using 1x PBS as the medium. To ensure that the bacterial cells attached to the surface are metabolically active, we changed the buffer from 1X PBS to Luria Broth (LB) culture medium and incubated the cells for approximately 20 minutes. After incubation in LB, bacterial cells grew, as evident by the elongation of cells detected in the transmission images. Comparisons of the nano-motion of live bacterial cells in 1X PBS and LB revealed similar amplitudes (Figure 4-3).



Figure

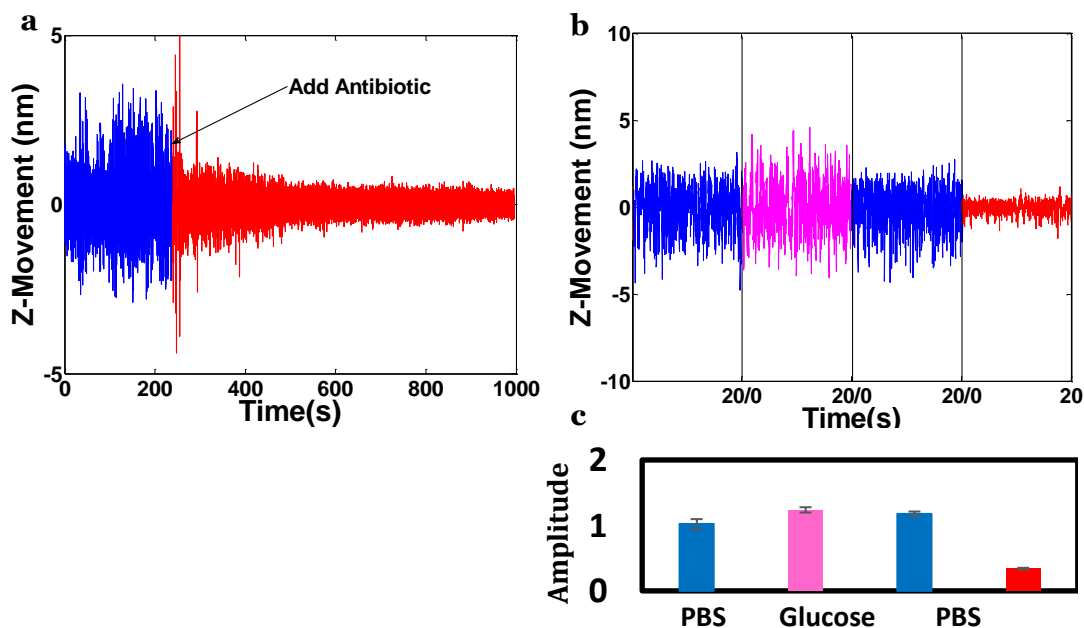
4-3. Z-movement in 1X PBS and LB medium

a) Blue trace shows z-movement of a typical bacterial cell in 1X PBS buffer. Orange trace shows z-movement of a typical bacterial cell incubated in LB medium. The z-movements in both 1X PBS and LB medium are comparable with amplitudes (standard deviation of z-movement) of 2.31 nm and 2.22 nm, respectively. Pink traces show that detectable motion in the bacterial-free area (system noise) are negligible in both cases. B) Transmitted image of a bacterial cell in 1X PBS with a recorded length of 4.81  $\mu\text{m}$ . Scale bar (1  $\mu\text{m}$ ). c) Transmitted image of a bacterial cell in LB medium with a recorded length of 5.06  $\mu\text{m}$ . Scale bar (1  $\mu\text{m}$ ). Reprinted with permission from Syal, K.; Iriya, R.; Yang, Y.; Yu, H.; Wang, S.; Haydel, S. E.; Chen, H.-Y.; Tao, N. Antimicrobial Susceptibility Test with Plasmonic Imaging and Tracking of Single Bacterial Motions on Nanometer Scale. *ACS Nano* 2015, 10, 845–852. Copyright 2017 American Chemical Society.

## **Changes in Nano-motion on Antibiotic Action**

We then studied the effects of antibiotics on the nano-motion of live bacterial cells by adding polymyxin B (PMB) to 1X PBS to reach a final concentration of 500  $\mu\text{g}/\text{ml}$ . PMB is a bactericidal antibiotic which kills Gram-negative bacteria by permeabilizing the outer membrane.<sup>124</sup> At high concentrations, such as 500  $\mu\text{g}/\text{ml}$  used in this study, PMB also depolarizes the cytoplasmic membrane, causing ion-permeable pores in the cell envelope.<sup>124</sup> Within a few seconds after adding the antibiotic, there was a marked decrease in the z-movement of the bacterial cell from about  $\pm 3$  nm to about  $\pm 1$  nm as shown in Figure 4-4a. We further observed that after a few minutes, the bacterial cell z-movement reached a baseline value of  $\pm 0.5$  nm. This decrease in bacterial nano-motion can be attributed to bactericidal activity of PMB, which has been observed at a concentration of 20  $\mu\text{g}/\text{ml}$ .<sup>124</sup> We used 25X the bactericidal concentration in this project to ensure complete loss of cellular viability. Bactericidal activity was also observed by comparing cellular morphology after adding antibiotics, where decreases in bacterial cell length at a high antibiotic concentration were visualized (Figure 4-5). The decrease in bacterial cell length has been previously correlated to cell lysis and cell death after the addition of polypeptide antibiotics.<sup>13</sup> We validated the correlation between the decreases in nano-motion and change of the bacterial metabolic state by replacing the antibiotic-containing PBS with LB medium (lacking PMB) on the sensor chip. We observed no further change in the bacterial nano-motion after incubating in LB medium, indicating irreversible loss of metabolic activity after the treatment with PMB. We subsequently collected a small sample volume from the above sensor chip and subjected it to culturing overnight in LB medium. We observed no growth of bacterial cells after overnight incubation, thus confirming bacterial cell death and bactericidal activity of the PMB antibiotic.

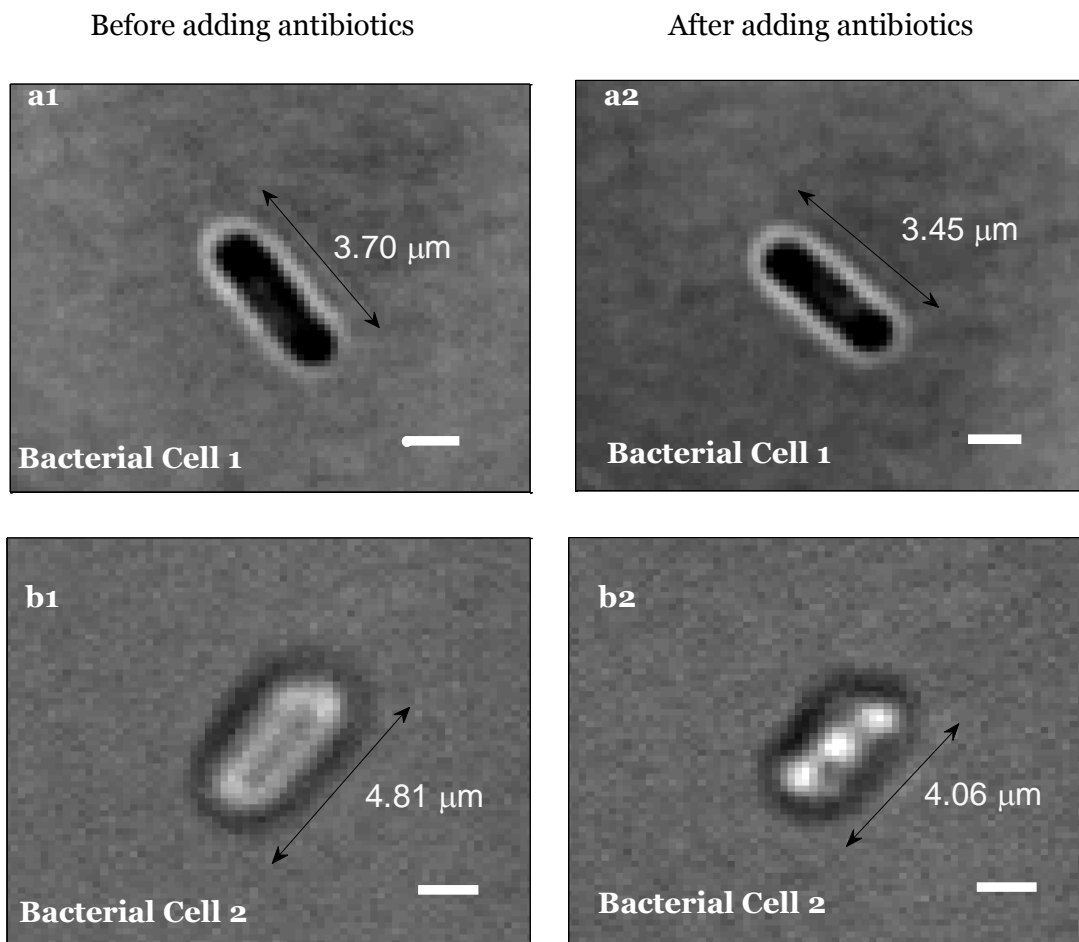




Figure

#### 4-4. Z-movement of a Bacterial Cell in Different Media

(a) Effect of antibiotic polymyxin B at a concentration of 500  $\mu\text{g}/\text{ml}$  on z-movement of a bacterial cell. (b) Control experiments comparing z-movement in PBS (blue) and on injections of 2% glucose (purple), 1X PBS (blue), and antibiotic (red). (c) Amplitude analysis of z-movements in different media. Reprinted with permission from Syal, K.; Iriya, R.; Yang, Y.; Yu, H.; Wang, S.; Haydel, S. E.; Chen, H.-Y.; Tao, N. Antimicrobial Susceptibility Test with Plasmonic Imaging and Tracking of Single Bacterial Motions on Nanometer Scale. *ACS Nano* 2015, 10, 845–852. Copyright 2017 American Chemical Society.

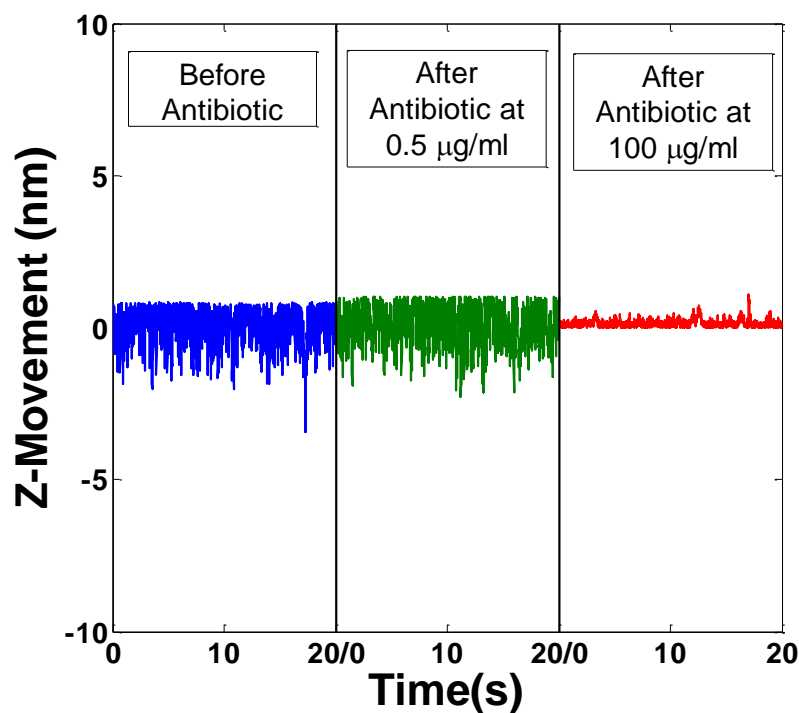


Figure

4-5 Observing Cell Death by Transmitted Images

a) Bacterial cell 1 compared in size before (a1) and after adding antibiotics (a2). The bacterium length shrinks after adding antibiotics, which indicates possible cell death. B) Bacterial cell 2 compared in size before (b1) and after adding antibiotics (b2). The bacterium length shrinks after adding antibiotics, which indicates possible cell death. Subsequent culturing experiments confirmed the death of these cells. Scale bar (1  $\mu\text{m}$ ). Reprinted with permission from Syal, K.; Iriya, R.; Yang, Y.; Yu, H.; Wang, S.; Haydel, S. E.; Chen, H.-Y.; Tao, N. Antimicrobial Susceptibility Test with Plasmonic Imaging and Tracking of Single Bacterial Motions on Nanometer Scale. *ACS Nano* 2015, 10, 845–852. Copyright 2017 American Chemical Society.

Furthermore, we injected antibiotic with a sub-bactericidal concentration (0.5  $\mu\text{g/ml}$ ), followed by a 5x bactericidal concentration injection. At sub-bactericidal concentrations we did not observe changes in the nano-motion after 20 minutes. However, after injecting bactericidal concentrations we observed a significant decrease in nano-motion, which validates the correlation between the decrease in nano-motion and change of the bacterial metabolic state. (Figure 4-6).



Figure

4-6. Z-movement in 1x PBS and Different Concentrations of Antibiotic

Blue trace (left) shows Z-movement of a *E. coli* O157:H7 cell on the sensor chip in 1X PBS buffer. Green trace (middle) show that introducing sub-bactericidal concentrations (0.5  $\mu\text{g/ml}$ ) of antibiotic PMB does not change the Z-movement. However, introducing the antibiotic at 5x bactericidal concentration (100  $\mu\text{g/ml}$ ) leads to a large decrease in Z-movement (red trace). Reprinted with permission from Syal, K.; Iriya, R.; Yang, Y.; Yu, H.; Wang, S.; Haydel, S. E.; Chen, H.-Y.; Tao, N. Antimicrobial Susceptibility Test with Plasmonic Imaging and Tracking of Single Bacterial Motions on Nanometer Scale. *ACS Nano* 2015, 10, 845–852. Copyright 2017 American Chemical Society.

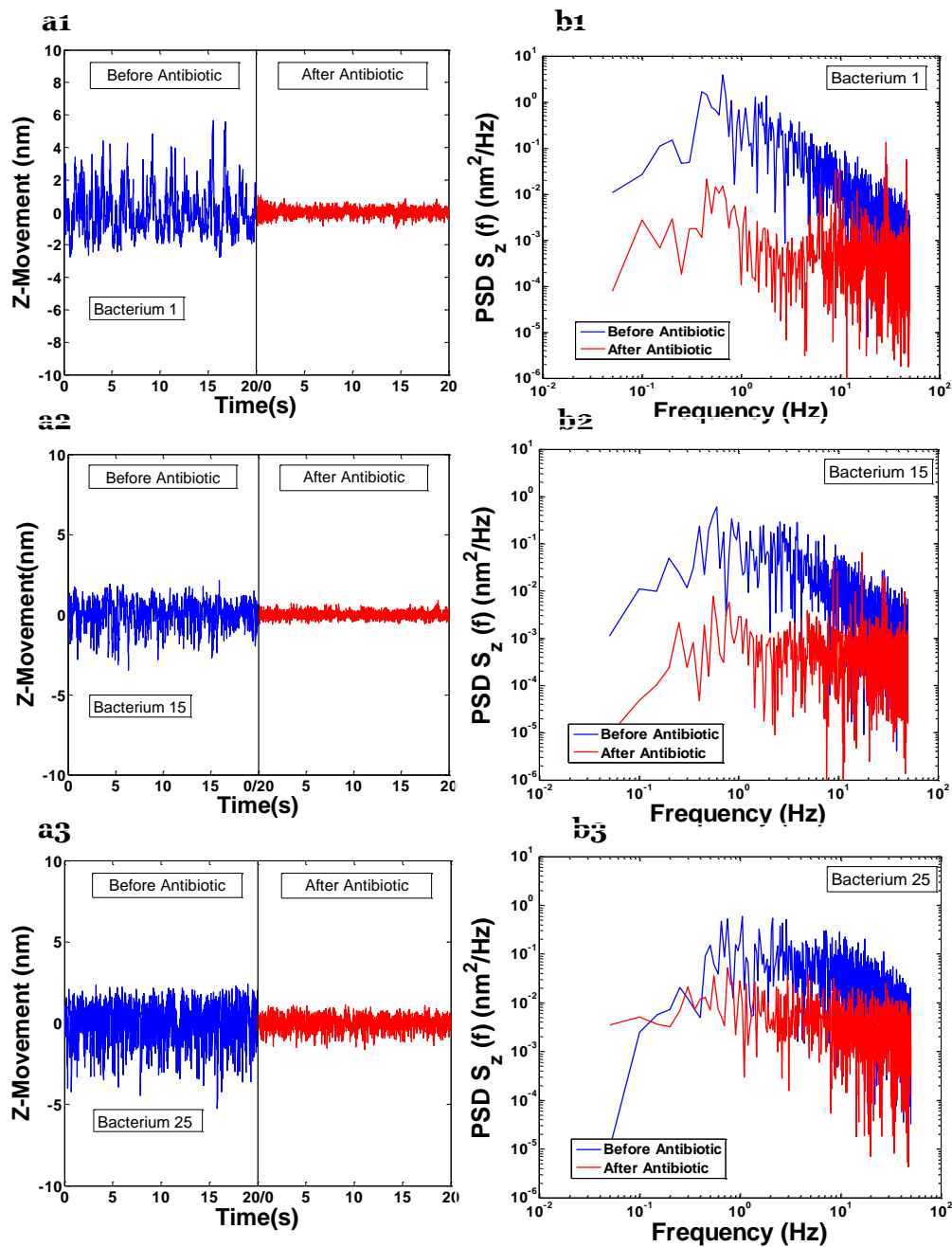
We performed a further control experiment by injecting glucose into the PBS – bacteria mixture. Glucose is a chemoattractant and represents an energy source for the bacteria. As shown in Figure 4-4b, after the injection of 2% glucose, the nano-motion of the bacteria increased slightly. After subsequently eliminating glucose in the 1X PBS medium, the amplitude of the nano-motion, measured over 1s windows for 20s videos, decreased back to the level prior to the injection of glucose (Figure 4-4c). The positive correlation between glucose injection and z-movement strongly supports that bacterial cell nano-motion originates from metabolic activity rather than Brownian motion. Conversely, we observed a decrease in bacterial nano-motion only when PMB was added at the bactericidal concentration of 75  $\mu\text{g}/\text{ml}$ , thus indicating that the decrease in nano-motion is specific to antibiotic action. Antibiotic activity was also observed by the transmitted microscope image, which shows a visible decrease in cell length after the addition of PMB. We subsequently subjected the experimental sample to overnight culturing in LB medium and observed no bacterial growth, thus validating PMB-induced cell death (Figure 4-5).

Figures 4-7 (a1-a3) show additional examples of the nano-motion of several bacterial cells before and after antibiotic injection, revealing similar reductions in the nano-motion caused by PMB. The magnitude of the nano-motion varies from cell to cell, both before and after the antibiotic injection. We attribute these variations to bacterial metabolic activities or interactions of individual bacterial cells with antibodies present on the sensor chip.

### **Power Spectral Analysis of Nano-motion**

We performed power spectral density (PSD) analysis on the nano-motion. For antibiotic-treated bacterial cells where the z-movement is small, the PSD shows weak frequency dependence similar to the background noise (Figure 4-7b, red trace). In contrast,

the PSD of the live bacterial cells is significantly larger and depends on frequency according to  $1/f^\alpha$  frequency with  $1 < \alpha < 2$  for frequencies between 1 to 50 Hz (Figure 4-7b, blue trace). Below 1 Hz, the PSD is not reliable because of the mechanical drift of the optical system, and above 50 Hz, the z-movement decreases to the background noise level. This PSD feature is similar to that of AFM cantilever deflection associated with multiple bacterial cells attached to the cantilever.<sup>78</sup>



Figure

4-7 Power Spectral Analysis and Z-movement Analysis of Different Bacterial Cells

(a) z-movement of individual bacterial cells before and after antibiotic treatment. (b)

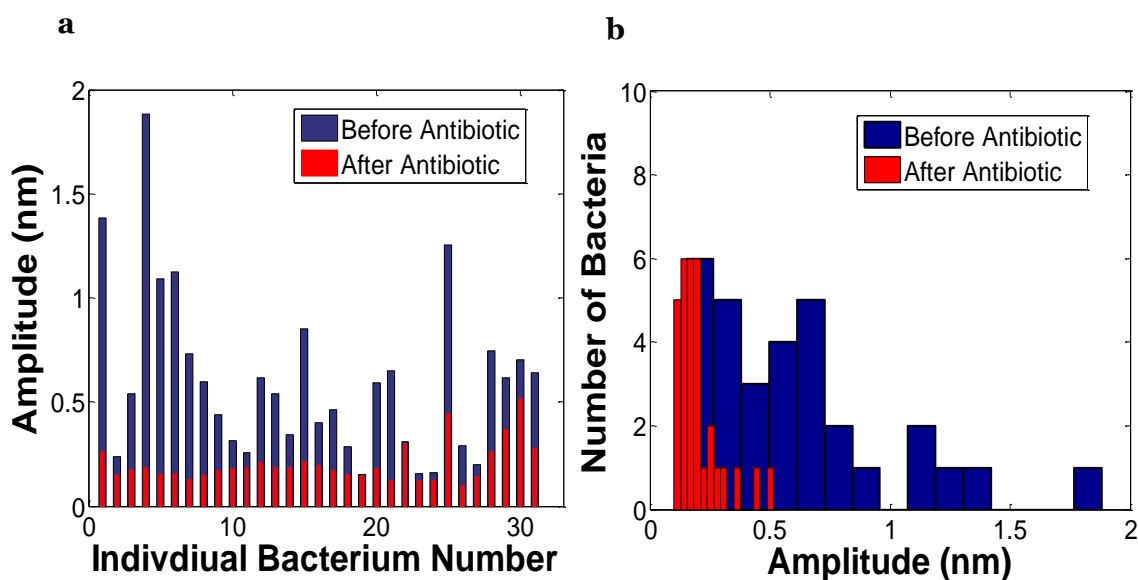
PSD of z-movement of individual bacterial cells before and after antibiotic treatment.

Reprinted with permission from Syal, K.; Iriya, R.; Yang, Y.; Yu, H.; Wang, S.; Haydel, S. E.; Chen, H.-Y.; Tao, N. Antimicrobial Susceptibility Test with Plasmonic Imaging and Tracking of Single Bacterial Motions on Nanometer Scale. ACS Nano 2015, 10, 845–852. Copyright 2017 American Chemical Society.

## Statistics on a Bacterial Population

Figure 4-8 presents the amplitude histograms of 31 individual bacterial cells before and after antibiotic treatment. The amplitude has been calculated as the standard deviation of the z-movement for a period of 20 sec.

Before antibiotic treatment, there was a large variation in the amplitudes of the nano-motion of the bacterial cells. A few cells exhibited low amplitude nano-motion before antibiotic addition and appeared to be tethered strongly to the surface. After antibiotic treatment, the amplitude of nano-motion for almost all of the bacterial cells decreased (Figure 4-8a). However, for those cells with low initial amplitudes, the decreases in nano-motion after antibiotic treatment are small, which are understandable since the strong



Figure

### 4-8. Statistical Analysis of Amplitude Analysis Before and After Antibiotic

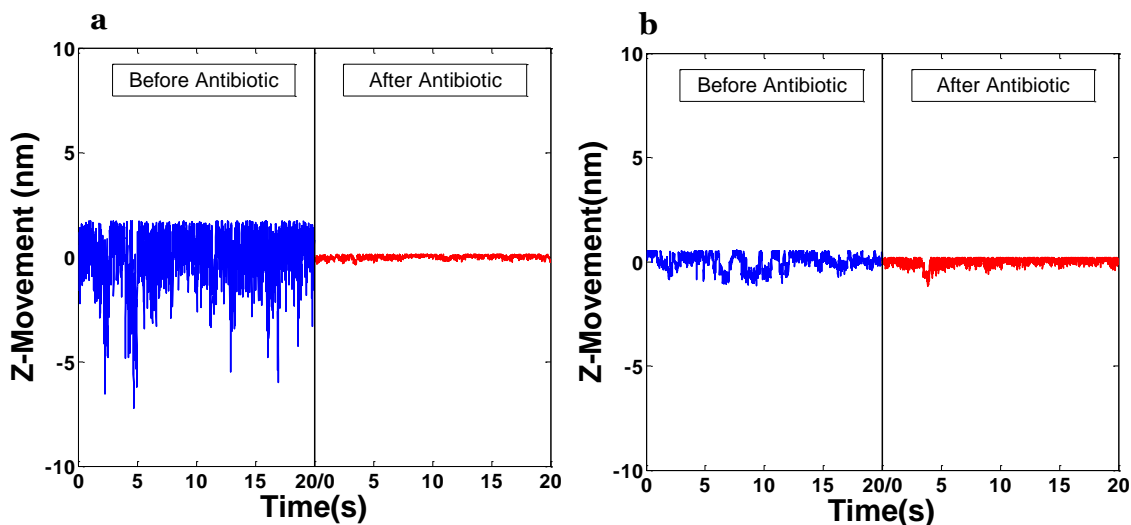
(a) Histograms of amplitude of individual bacterial cell nano-motions before and after antibiotic addition. (b) Distribution of amplitudes before and after the addition of antibiotic. The large difference conveys statistically-significant decreases in bacterial motion after the addition of antibiotics. Reprinted with permission from Syal, K.; Iriya, R.; Yang, Y.; Yu, H.; Wang, S.; Haydel, S. E.; Chen, H.-Y.; Tao, N. Antimicrobial Susceptibility Test with Plasmonic Imaging and Tracking of Single Bacterial Motions on Nanometer Scale. ACS Nano 2015, 10, 845–852. Copyright 2017 American Chemical Society.

tethering restricts motion. Statistical analysis (student t-test) revealed that the mean amplitude value for all bacterial cells is significantly different before and after antibiotic treatment ( $p = 2.66e-06$ ) (Figure 4-8b).

### **Testing Universality of Nano-motion AST**

We further demonstrated the applicability of this technology to UTI infections by extending it to other clinically relevant strains. We immobilized the UPEC strain on the sensor using the (3-Aminopropyl)-triethoxysilane (APTES) linker, rather than using the antibody immobilization for the *Escherichia coli* O157:H7 study described above. We studied the nano-motion changes as antibiotic PMB acted on bacterial cells at a bactericidal concentration of 1 mg/ml (Figure 4-9a). We observed a decrease in bacterial nano-motion when PMB was added indicating that the decrease in nano-motion is specific to antibiotic action. Subsequent overnight culturing of experimental sample in LB medium led to no bacterial growth, thus validating PMB-induced cell death. We also applied the plasmonic tracking and imaging technology to another antibiotic, streptomycin, and observed decrease in the nano-motion in the bacterial cells in PBS supplemented with LB media, after adding streptomycin at a bactericidal concentration of 1mg/ml<sup>122,129</sup> (Figure 4-9b). These experiments indicate that the methods may be used for different bacterial strains and different antibiotics. To fully establish the present method for rapid AST in clinical settings, additional and more comprehensive tests will still be needed in the future.





Figure

#### 4-9. Z-movement Changes in Different Conditions

a) 1x PBS and Antibiotic for UPEC strain. Blue trace (left) shows Z-movement of a bacterial cell of UPEC strain immobilized with APTES on a sensor chip in 1X PBS buffer. Red trace shows Z-movement after injecting 1 mg/ml polymyxin B antibiotic. The large decrease in the nano-motion is due to bactericidal action of antibiotic and subsequent over-night culturing experiments confirmed the death of the bacteria. b) Z-movement for antibiotic Streptomycin for *E. coli* O157:H7 Blue trace (left) shows Z-movement of a bacterial cell in 0.4x LB media. Red trace shows Z-movement after injecting 1mg/ml streptomycin antibiotic. The decrease in in nano-motion (Z-movement) correlates to bactericidal action of antibiotic and subsequent over-night culturing experiments confirmed the death of the bacteria. Reprinted with permission from Syal, K.; Iriya, R.; Yang, Y.; Yu, H.; Wang, S.; Haydel, S. E.; Chen, H.-Y.; Tao, N. Antimicrobial Susceptibility Test with Plasmonic Imaging and Tracking of Single Bacterial Motions on Nanometer Scale. ACS Nano 2015, 10, 845–852. Copyright 2017 American Chemical Society.

## **Conclusions**

In summary, we have demonstrated a plasmonic imaging technique to track the real-time motion of bacterial cells attached to a sensor surface with sub-nanometer detection limits. The detected nanometer-scaled motion of bacterial cells is a signature of metabolic activity and is correlated with viability. Upon exposure of the bacteria to high bactericidal concentrations of the PMB antibiotic, the nano-motion decreases substantially, thus revealing lethality. Despite the large variability among different cells, antibiotic-induced reduction of bacterial nano-motion is a robust and statistically significant phenomenon. These results promise development of a rapid antibiotic susceptibility testing method that does not require culturing and associates resistance detection with phenotypic measurements. The PIT tracking-based AST is capable of label-free detection of antibiotic activity in real time and offers a quick, simple, and low cost comparison to the current clinical microbiology approaches. Moreover, this method offers single cell analysis capabilities that will be especially useful for quantifying susceptibility patterns of individual cells in polymicrobial clinical infections.

RAPID ANTIBIOTIC SUSCEPTIBILITY TESTING OF UROPATHOGENIC *E. COLI* IN  
URINE SAMPLES BY TRACKING SUB-MICRON SCALE MOTION OF SINGLE  
BACTERIAL CELLS

Antibiotic resistance infections are challenging to be treated at point-of-care due to the lack of a rapid antibiotic susceptibility testing (AST) technology to identify resistant infections at disease onset. Current clinical AST technologies take 1-3 days because of the slow culturing steps. Here, we demonstrate a rapid culture-free AST method by tracking sub- $\mu\text{m}$  scale bacterial motion with bright field optical imaging. Clinically relevant bacterial pathogens *E. coli* O157:H7 and Uropathogenic *E. coli* (UPEC) are partially tethered to glass surface. Alive bacterial cells have on an average sub- $\mu\text{m}$  motion above 200 nm and dead bacterial cells killed by lethal dose of antibiotic polymyxin have a reduced motion below 100 nm. While the motion of dead bacteria is mainly from Brownian motion, we believe the larger sub- $\mu\text{m}$  motion of alive bacteria is contributed from metabolism related activity. By analyzing dose dependent sub- $\mu\text{m}$  motion changes of a population of bacterial cells in a multiplexed assay, we obtained minimum bactericidal concentration of polymyxin on the UPEC pathogens within 2 hours. We also applied the method directly to human urine samples spiked with bacteria and demonstrated rapid AST within 2 hours. The results are validated with the standard culture based AST method.

## Introduction

Antibiotic susceptibility testing (AST) is used clinically to diagnose antibiotic resistant strains and prescribe appropriate antibiotics.<sup>10,130</sup> However, current AST technologies take 1-3 days due to their dependence on bacterial culturing.<sup>4,130</sup> In the absence of rapid AST, physicians rely on community susceptible patterns and experience to often prescribe broad-spectrum antibiotics.<sup>3,33</sup> This practice has contributed to the acceleration of bacterial resistance.<sup>3,29</sup> A faster AST technique will empower physicians to prescribe effective narrow-spectrum antibiotics, preferably within 1-2 hour or shorter.<sup>4,92</sup>

Emerging AST technologies based on detecting bacterial growth rate via measuring cell numbers<sup>48,54,61</sup>, cell size<sup>46,91</sup>, and biochemical markers (RNA,<sup>50,67</sup> DNA,<sup>68</sup> or redox molecules<sup>51,75,76,131</sup>) have been developed (Chapter 2). Several culture-free AST technologies measuring bacterial metabolism such as bacterial nano-motion,<sup>26,44,122</sup> heat-signature,<sup>84,85</sup> and biochemical profiles<sup>132</sup> have also been pursued for real time AST (Chapter 2). While these technologies offer potential solutions, a simple and robust AST technology that can deliver accurate results within 2 hours requires further works. I introduces a rapid AST based on quantitating the sub- $\mu\text{m}$  motion of bacterial cells captured with standard brightfield microscopy.

The hydrodynamic<sup>133,134</sup> and motility-induced long-range motions<sup>133,135</sup> of live bacterial cells in the range of several  $\mu\text{m}$  near a surface have been studied using particle image velocimetry algorithms<sup>136</sup> and digital holographic imaging technologies.<sup>134</sup> However, short-range motion (a few nm) of surface-attached bacterial cells and their correlation to bacterial metabolism have only been recently studied using highly sensitive tools, such as atomic force microscopy<sup>44,77</sup>, and plasmonic imaging and tracking.<sup>23,26</sup> In this work, by using simple brightfield imaging and automated image processing algorithms, we measured sub- $\mu\text{m}$  motion of surface-tethered bacterial cells. We studied correlation of

sub- $\mu\text{m}$  motion with bacterial viability and performed AST on clinically important strains, *E. coli* O157:H7<sup>24</sup> and Uropathogenic *E. coli* (UPEC), with antibiotic polymyxin.<sup>27</sup> UPEC accounts for ~75% of all Urinary tract infections (UTIs), which affect over 10 million people,<sup>27</sup> and often result in sepsis.<sup>27</sup> Polymyxin is important because it is a last-line antibiotic for septic patients, and polymyxin-resistance strains have been found in UTI patients<sup>137,138,139</sup>

To accomplish the goal of performing rapid AST within 2 hours on clinical urine samples, we performed multiple experiments. We first tethered bacterial cells onto the surface, and tested our algorithms to quantitate the sub- $\mu\text{m}$  motion of tethered cells. Next, we measured the antibiotic induced sub- $\mu\text{m}$  motion changes of individual cells with population-based statistical analysis. Then, we studied dose dependency of antibiotic induced motion changes in a multiplexed assay to determine the clinically relevant minimum bactericidal concentration of the antibiotic. Finally we demonstrated 2-hour AST on human-urine samples spiked with UPEC cells.

## **Materials and Methods**

### **Materials**

Lyophilized pellets of bacteria *E. coli* O157:H7 (ATCC 43888) were purchased from Fisher Scientific and UPEC *E. coli* strain CFT073 was purchased from ATCC. Human urine samples, pooled from 20 healthy patients, was purchased from Bioreclamation IVT (WestBurry, New York) and stored at -80 °C. (3-Aminopropyl)triethoxysilane (APTES) was purchased from Sigma Aldrich, aliquoted to smaller volumes under vacuum and stored at 4°C in a desiccator. Affinity-purified goat anti-*E. coli* O157:H7 IgG polyclonal antibodies were purchased from Kirkegaard and Perry Laboratory Inc. (Gaithersburg, MD). Antibodies were further suspended in 1 ml PBS (1X), and stored in aliquots at -20°C. 1-Mercapto-11-undecyl hexa(ethylene glycol) (PEG) and carboxyl-terminated

hexa(ethylene glycol) undecane thiol (PEG-COOH) were purchased from Nanoscience Instruments (Phoenix, AZ). Antibiotic Polymyxin B (PMB) was purchased from Sigma-Aldrich, dissolved in 1x PBS at a stock concentration of 10 mg/ml and further stored in dark at 2-8°C according to manufacturer's instruction. Other reagents were purchased from Sigma-Aldrich.

### **Preparation and Growth of Bacteria**

The lyophilized *E. coli* O157:H7 bacteria were suspended in PBS, centrifuged at the speed of 50 x g for 1 min to pellet the charcoal. The supernatant containing bacteria was collected and centrifuged at 2000 x g for 15 min to pellet the bacteria. The bacterial pellet was re-suspended in 1 ml 1X PBS and mixed thoroughly. After 3 rounds of purification, the final 1 ml of bacteria in PBS solution was added with 5% glycerol, aliquoted into smaller volumes of 20 µl and stored at -80°C. Similarly, *E. coli* strain CFT073 strain was cultured on solid LB agar media, suspended in 1x PBS containing 5% glycerol and frozen in smaller aliquots at -80°C.

An aliquot of frozen *E. coli* O157:H7 or *E. coli* CFT073 strain was thawed and used to inoculate 3 ml of LB medium one day prior to the experiments. Both strains were prepared before the experiment by diluting the overnight culture (grown at 37°C) into LB medium to a concentration of 10<sup>7</sup> colony forming units (CFU)/ml and continuing growth at 37°C with gentle rotary mixing until the cultures reached an OD<sub>600</sub> of 0.56 which is the mid-logarithmic phase of growth. The corresponding concentration of the bacteria was 4.67x10<sup>8</sup> CFU/ml. Bacterial cells were collected by centrifugation at 2000 x g for 15 min and re-suspended in 1 ml PBS (1X) to an OD of 0.56. For urine experiments, pooled urine samples were first filtered using a 0.2 µm filter, followed by spiking urine with freshly cultured bacterial cells to a desired concentration.

## Surface Functionalization

Clean BK7 glass cover slips were coated with 1.5 nm chromium and 48 nm gold and used as PIT sensing chips. The chips were cleaned with deionized water, ethanol multiple times followed by drying with nitrogen gas and then cleaned by hydrogen flame. For antibody surface, the cleaned chips were submerged in 1 mM PEG/PEG-COOH ethanol solution and left in the dark for 24 h to coat a PEG/PEG-COOH self-assembled monolayer (SAM) on each chip. To attach antibodies next, the PEG/PEG-COOH SAM-coated chips were activated with 500  $\mu$ l of a freshly prepared mixture of 0.1 M NHS and 0.4M EDC in 1:1 ratio to produce NHS ester receptors, which react with the primary amine groups on the antibodies *via* an amide bond. Chips with activated PEG/PEG-COOH SAM were cleaned with deionized water and blown dry with nitrogen gas. Polyclonal anti-*E. Coli* O157:H7 IgG antibodies dissolved in 20 mM sodium acetate (NaOAc), pH 5.5 at a concentration of 30  $\mu$ g/ml were immediately applied to the NHS/EDC-activated surfaces and incubated for 30 mins. The antibody-coated chips were again cleaned with deionized water and dried with nitrogen gas prior bacterial cell capture on the imaging setups.

For APTES surface, we used BK7 glass slides from VRW (Radnor, Pennsylvania) which were 22x60 mm. Further, the glass slides were thoroughly cleaned with deionized water and ethanol, followed by drying with nitrogen gas. To attach the APTES linker to the sensor surface, the glass slide was activated with freshly prepared 1% APTES in ethanol (with 5% water) for 15 seconds. The APTES linked sensor chips were again cleaned with ethanol, dried with nitrogen gas prior bacterial cell capture on the imaging setup.

## Imaging and Flow Setups

The imaging setup consisted of an inverted microscope (Olympus IX-81) (Fig. 1).<sup>103,104,110</sup> A 60x oil immersion objective with numerical aperture (NA) of 1.49 or a 40x air objective (NA 0.75) was used to perform experiments. The APTES or antibody coated

slides were placed on the objective lens. Further, brightfield light was illuminated from top and a CCD camera (Pike-032B, Allied Vision Technologies, Newburyport, MA, USA and GS3-U3-23S6M-C, PointGrey, Richmond, BC, Canada) was used to record images.

For APTES coated glass slides, a black marker spot was placed beneath the coated surface, followed by placing a multi-well FlexiPerm (SARSTEDT) reusable well atop. The assembled glass coated chips was then mounted on top of the imaging setup. The brightfield light intensity was adjusted to an appropriate contrast without saturating the image.

### **Bacterial Immobilization**

Bacterial cells of the strain *E. coli* O157:H7 (20  $\mu$ l) were added to the sensor chip coated with antibodies, with a FlexiPerm well atop containing 500  $\mu$ l PBS (1x). The cells tethered onto the sensor surface and after 10-15 min incubation at room temperature, sufficient bacterial cells were sufficiently attached to the surface. PBS buffer was subsequently flowed over the chip to remove unattached bacterial cells. Bacterial cells were elongated in length on the chip by culturing in Luria Broth media to validate that cells are metabolically alive and healthy, prior to performing experiments.

UPEC cells in Urine or 1x PBS were added to the APTES coated surface with a FlexiPerm multi-well atop. Cells were incubated for 10-15 mins for cells to tether on the surface. If needed, 1-2 washes of 1x PBS using manual pipetting removed unattached bacterial cells.

### **Image Collection and Processing**

All *E. coli* O157:H7 experiment image sequences were collected at 106 fps at a pixel resolution of 640x480 using pike camera. Images were recorded in either transmitted or plasmonic imaging mode for various time durations. All UPEC experiment image



sequences were collected at 26.6 fps at a pixel resolution of 1920x1200 using transmitted images via PointGrey camera. Further, we recorded images for 5s for each Well near the marker spot, followed by semi-automatically translating the stage to next marker spot below another well This was repeated every 15 mins for all wells across multiple time points. We chose an appropriate exposure time to maximize image intensity, avoid over exposure. The focus of the cell was appropriately chosen to image bright bacterial cells with darker backgrounds. All images from the videos were processed using custom-written MATLAB programs and ImageJ scripts.

### **Sample Addition**

For, *E.coli* O157:H7, multiple sample solutions, such as LB medium, PBS were added to the bacterial cells *via* a gravity-based multichannel drug perfusion system (Warner Instrument, Hamden, CT). The drug perfusion system flew sample solutions at a flow rate of 330  $\mu\text{l}/\text{min}$  with the transition time between different solutions in the range of 1-2 sec. The flow system was stopped and stabilized for 5 min before recording videos. To deliver antibiotics for both *E.coli* O157:H7 and UPEC experiments, we pipetted small volumes of antibiotics into the Flexiperm well mounted on the microscope.

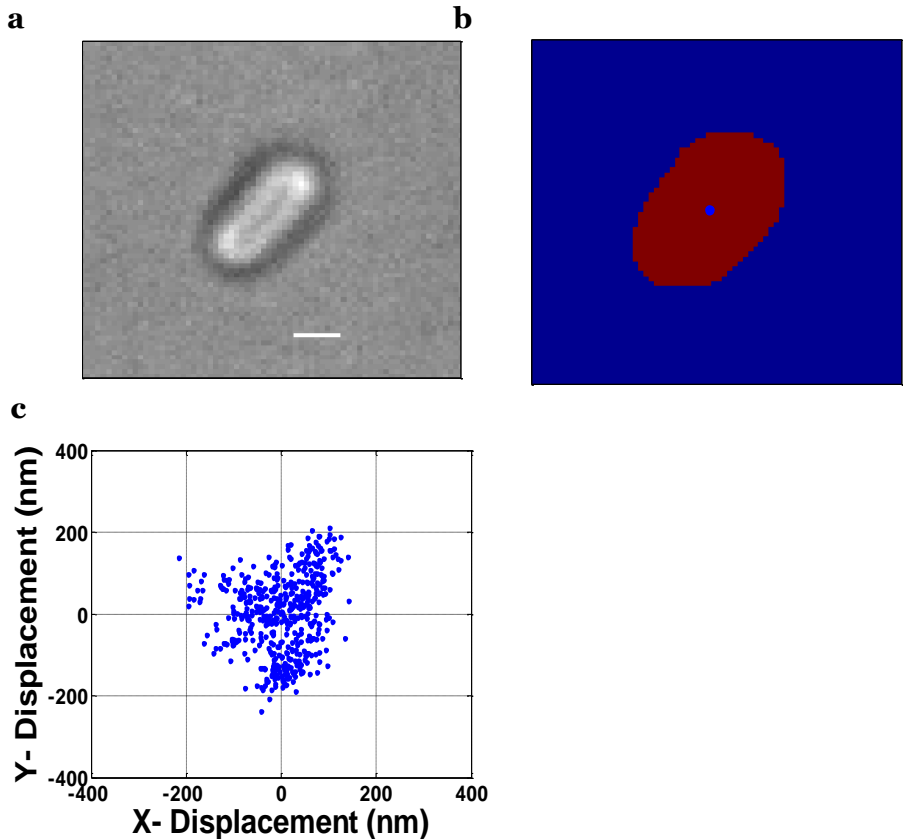
### **Data Analyses from Images**

#### **Image Segmentation and Cell Tracking Algorithm**

Greyscale images were converted into binary images using custom MATLAB scripts. For every greyscale image, we plotted a histogram of pixel intensities, which is unimodal.<sup>140</sup> We computed a threshold value (T), at the point of drop in the intensity histogram towards the higher pixel intensity tail. All, pixel intensities higher than the threshold value T, were given a new intensity 1, while all the pixel intensities lower than the threshold were given a 0. This gave us binary images with segmented cells from the background. Once segmented cells were obtained by the thresholding algorithm, standard

morphological operations such as removing spur points, breaking H-connected sections, filling holes were performed to improve segmentation. The greyscale image of a bacterial cell is thus converted into a binary image with segmented bacterial cells from the background (Figure 5-1). Using *regionprops* MATLAB command, we further obtained a “Centroid” for each segmented cell (blue dot in Figure 5-1b) in the binary image. Centroid signifies the X and Y coordinates of the bacterial cell center and is calculated as the mean of all non-zero pixels which the bacterial cell occupies. We next tracked cell motion over a period of video. Each segmented cell in image  $I_n$  is matched to the previous frame  $I_{n-1}$  if the centers are closest and within 1 cell length. This produces the motion of the center of the bacterial cell over a video. The X and Y displacement of the center (Figure S1c) was calculated by subtracting the X and Y coordinates of an individual cell from the cell’s mean position over the length of the video.

The X and Y displacement of the center was calculated by subtracting the X and Y coordinates of an individual cell from the cell’s mean position over the length of the video. The “Distance” moved by the center of a bacterial cell was calculated by using the formula  $\text{Distance} = \sqrt{\sigma_x^2 + \sigma_y^2}$  where  $\sigma_x$  and  $\sigma_y$  represents the standard deviation of X and Y displacement respectively. Further,  $D_{\text{AVG}}$  for a population of cells was calculated by taking the average of distances of individual cells.



Figure

5-1. Image Processing of Bacterial Cells to Quantitate X and Y Displacement.

(a) Snapshot of a bacterial cell captured using our imaging setup as a greyscale image.

(b) The greyscale image of a bacterial cell is converted into a binary image with the superimposed center of the cell (Blue dot in Figure 5-1b)

(c) The center of the cell is plotted over 20s of video to obtain the displacement of every cell. Scale Bar – 1  $\mu\text{m}$

### Broth Micro-Dilution Assay

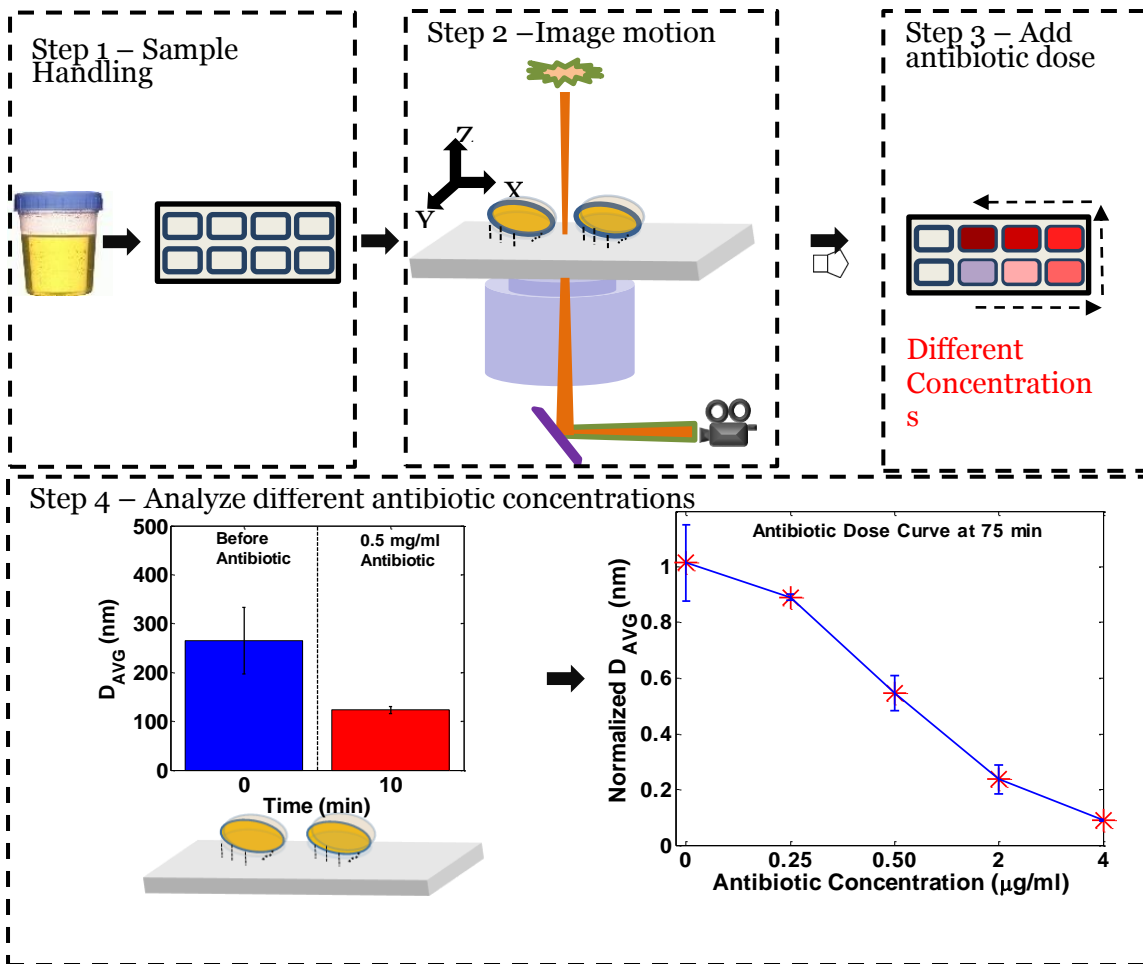
Broth microdilution assay was used to determine the minimum inhibitory concentration from a previously described protocol.<sup>32</sup> Frozen aliquots of CFT073 were thawed and cultured overnight. We prepared a bacterial suspension of  $1 \times 10^8$  colony-forming units (cfu)/ml of UPEC cells from overnight culturing. Further, antibiotic dilutions ranging from 0.125  $\mu\text{g}/\text{ml}$  to 8  $\mu\text{g}/\text{ml}$  were prepared in sterile Mueller Hinton

(MH) broth. 50  $\mu$ l of antibiotic solutions were added to the 7 antibiotic wells, control well and sterility well in triplicate. Further, the bacterial suspension was diluted 1:100 before adding 50  $\mu$ l to each of the wells above to a final concentration of  $5 \times 10^5$  cfu/ml. The 96 well plate was incubated at 37 °C for 16 hours. The optical density measurements of the 96 well plate were measured using a spectrophotometer.

Further, a 5  $\mu$ l suspension after overnight culturing was spot plated on LB agar plates to measure the minimum bactericidal concentration of polymyxin for UPEC cells. We estimated MBC to be the concentration which failed to yield any positive bacterial cultures.

## **Results and Discussion**

The experimental setup consisted of an inverted optical microscope attached with a CCD camera to record brightfield image sequences of bacterial cells (Figure 5-2). These images were analyzed using motion-tracking algorithms to perform rapid AST. Samples containing bacterial cells were added to a multi-well sample holder mounted on a glass slide. The bacterial cells were tethered to the slide surface via antibody specific to bacterial surface antigens or a linker molecule, (3-Aminopropyl) triethoxysilane (APTES). The surface chemistry was optimized to make a large portion of the bacterial cells partially tethered to the surface, so that they still have sub-micron scale motions. Antibiotics at different concentrations were then added to different wells, and the bacterial cells tethered on the glass slide were imaged at different time points. The captured image sequences were processed to determine changes in the bacterial motion before and after the addition of antibiotic. Clinically relevant minimum bactericidal concentration (MBC) was determined by analyzing the motion of a population bacteria cells exposed to different antibiotic doses.



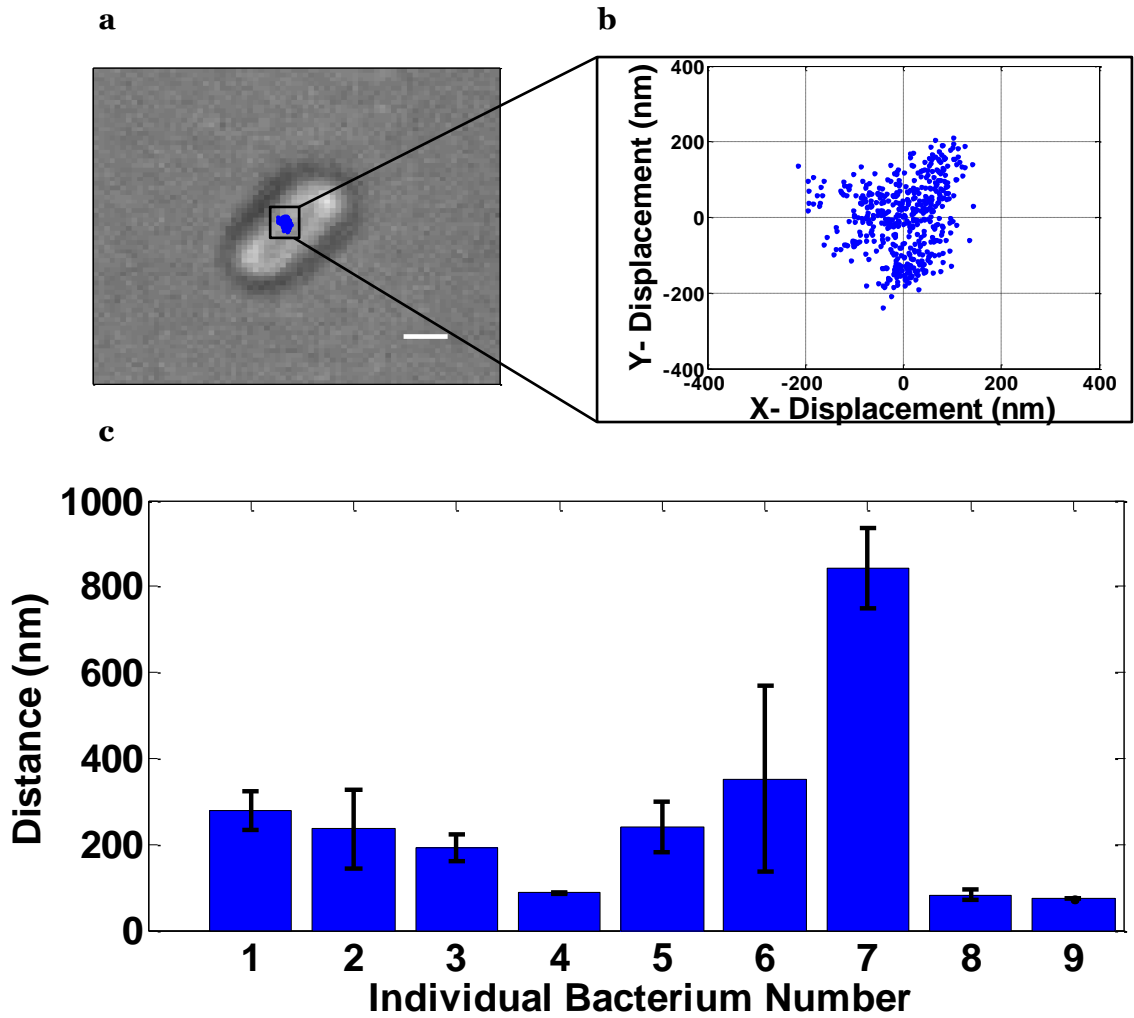
Figure

5-2. Schematic of the Experimental Setup to Image and Track Bacterial Cell Sub- $\mu\text{m}$  Motions

Step 1 – Live bacteria spiked human urine samples are added to a multi-well glass slide allowing bacterial cells to tether onto the glass surface. Step 2 – Individual wells of the slide are imaged by the microscope, and the motions of tethered bacterial cells are quantitated via image analysis. Step 3 – Different doses of antibiotics are added to the wells on the slides, and the changes in bacterial cell motions are recorded. Step 4 – Image analysis reveals that the bacterial cells show a decrease in motion after exposure to antibiotics (blue bar – motion before antibiotic, red bar – motion after antibiotic). Statistical analysis on a population of cells for each antibiotic dose is performed, and an antibiotic dose curve is obtained.

## Quantification of the Bacterial Motion

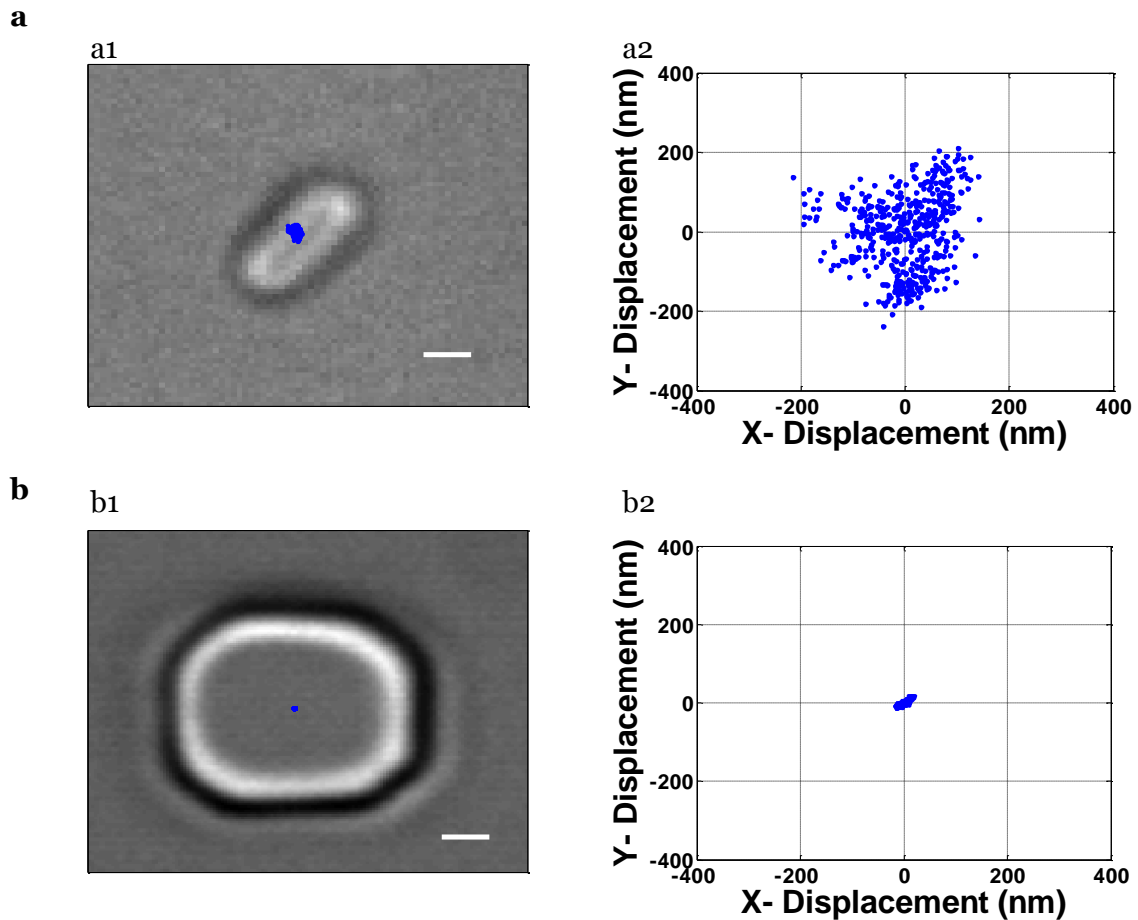
Alive *E. coli* O157:H7 bacterial cells were tethered to the glass slide by an antibody specific to the cell-surface glycan antigen and imaged by an optical setup (Figure 5-2a).<sup>20</sup> The centroid (center) of each bacterial cell was extracted in each image frame using the procedure described in the materials section (Figure 5-1). Blue dots superimposed over the bacterial cell in Figure 5-3a are the center positions of the cell at different moments over a 20-second period. The displacements of the bacterial cell are more clearly shown in the zoomed-in plot in Figure 5-3b, revealing sub- $\mu\text{m}$  scale motion of the cell tethered to the surface. For quantitative analysis of the sub- $\mu\text{m}$  motion of the bacterial cell, we defined “Distance” derived as the root-mean-square of the displacement, over 20s. The distance for different bacterial cells varies from 75 nm to 842 nm (Figure 5-3c), with an average of 265 nm. The error in extracting the center positions of the bacterial cells was determined to be 25 nm, by calculating the distance of a fixed marker spot (pillars attached within a microfluidic cassette)<sup>141</sup> (Figure 5-4). This error was much smaller than the average distance (278 nm) of the typical bacterial cell shown in Figure 5-3a. This result validates the ability of our method to quantitate the sub- $\mu\text{m}$  motion of the bacteria cell. A population of bacterial cells tethered to the surface has both partially bound and tightly bound cells (e.g Cell 4,8 and 9 in Figure 5-3c). The tightly bound alive cells have been previously exhibited to show z-direction motion using plasmonic imaging.<sup>26</sup>



Figure

5-3. Bacterial Cells Tethered on a Surface with Sub- $\mu\text{m}$  Motion

(a) A snapshot of a bacterial cell with superimposed motion of the cell center over 20s shown via blue dots. (b) Displacement of the cell center over 20s, reflecting the sub- $\mu\text{m}$  motion of the cell (c) Distance, defined as the root-mean-square of the displacement of cell center over 20s, of 9 different bacterial cells. Scale Bar – 1  $\mu\text{m}$ .



Figure

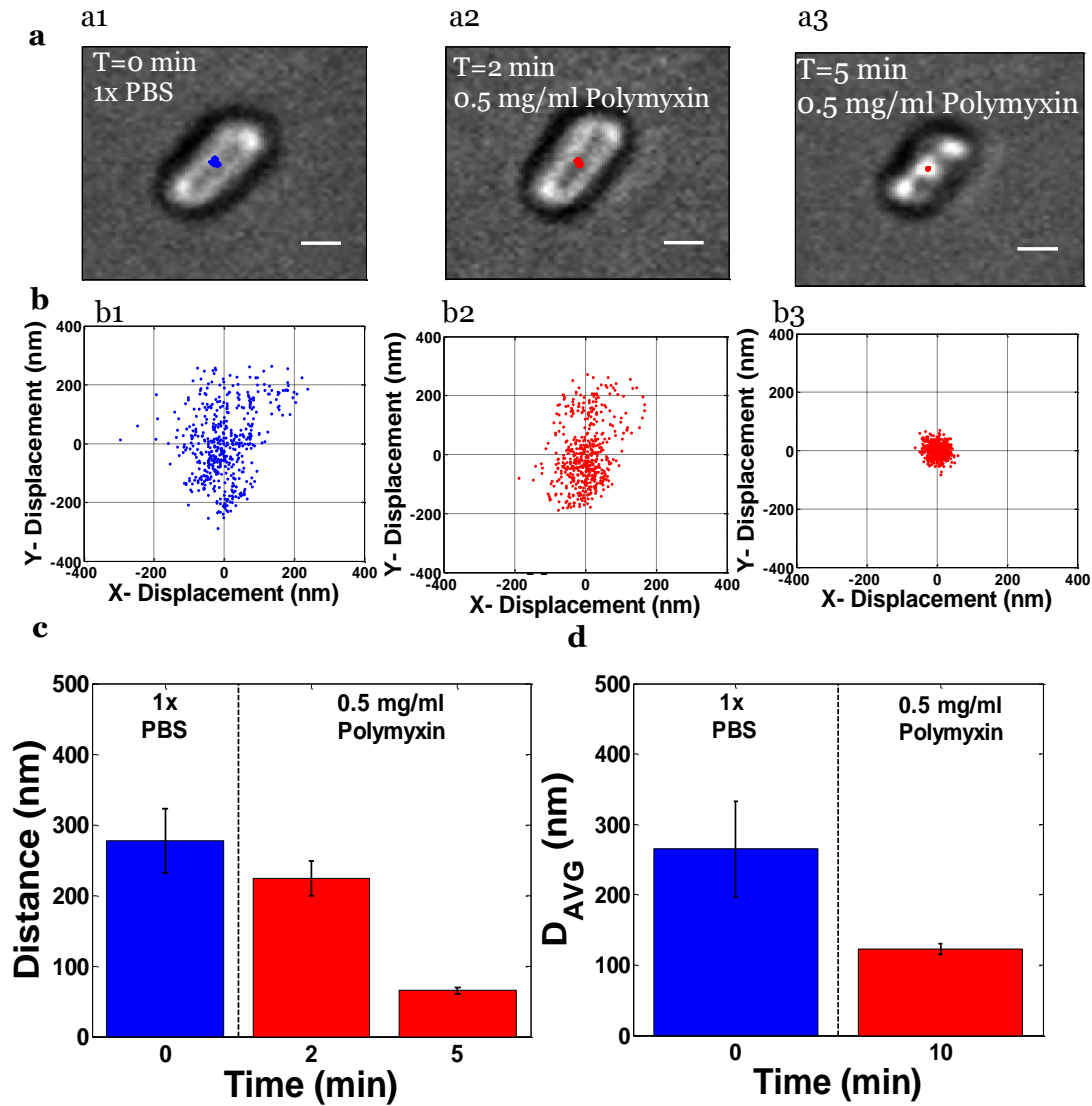
5-4. X and Y Displacement of a Bacterial Cell Compared to a Fixed Spot

(a1) Snapshot of a bacterial cell captured using our imaging setup with superimposed displacement of the center shown via blue dots (a2) Enlarged displacement of the center of the cell over 20s. (b1) Snapshot of a fixed marker captured using our imaging setup with superimposed displacement of center shown via blue dots (b2) Enlarged displacement of the center of the marker over 20s shown. The error of our imaging algorithm was found to be 25nm. Scale Bar – 1  $\mu$ m



### **Effect of Antibiotic on the Sub- $\mu\text{m}$ Motion**

To correlate bacterial metabolism and sub- $\mu\text{m}$  motion exhibited by surface tethered bacterial cells, we added the antibiotic polymyxin. After imaging bacterial cells in 1x PBS, polymyxin at a bactericidal concentration of 0.5 mg/ml was added, and the concurrent change in the bacterial motion was monitored (Figure 5-5). Figures 5-5a1 – 5-5a3 show the brightfield images of the alive bacterial cell partially tethered to the surface, where blue and red dots are the sub- $\mu\text{m}$  motion of the bacteria before adding the antibiotic, 2 mins and 5 mins after adding the antibiotic. Zooming-in of the displacements reveals more clearly the sub- $\mu\text{m}$  motion and decrease in motion associated with the addition of antibiotics (Figure 5-5b1-5-5b3). For a bacterial cell before adding the antibiotic, the distance over 20s is 278 nm (Figure 5-5c - blue bar). 2 mins after adding the antibiotic, the motion of bacterial cell decreases as observed in the scatter plot (Figure 5-5b2) with a decreased distance of 225 nm (Figure 5-5c – red bar). This decrease in sub- $\mu\text{m}$  motion is due to the action of antibiotic. 5 mins after adding the antibiotic, the distance of the bacterial cell reduces to 65 nm (Figure 5-5b3 and Figure 5-5c) along with a visible decrease in bacterial cell size. The decrease in cell size is due to cell lysis, which is known attribute of bactericidal action of antibiotics.<sup>13</sup> The metabolically dead state of the cells post the addition of antibiotics was also validated by overnight culturing, which failed to yield any alive cells. Thus, the sub- $\mu\text{m}$  motion exhibited by single bacterial cells is a signature of a bacterial cell's metabolism state. Further, adding antibiotics led to a decrease in the motion, which can be quantified to perform antibiotic susceptibility analysis of antibiotics to individual cells.



Figure

5-5. Sub- $\mu\text{m}$  Motion Before and After Adding Antibiotic for Single Cells as Well as a Population

Snapshots of cells before the antibiotic in 1xPBS and after adding the antibiotic polymyxin B at a bactericidal concentration of 0.5 mg/ml. (a) Snapshots of a bacterial cell with superimposed displacement of center of cells at different time points in 1x PBS and after adding the antibiotic. (b) Displacement of the center of the bacterial cell over 20s at various time points (c) Distance of the cell at various time points (d)  $D_{AVG}$  of a population of cells before and 10 mins after the addition of 0.5 mg/ml of the antibiotic polymyxin. Scale bar –  $1\mu\text{m}$ .

### **Population Level Bacteria Motion Changes on Antibiotic Action**

While partially tethered cells showed a decrease in the sub- $\mu\text{m}$  motion upon exposure to the antibiotic, tightly bound cells didn't show any changes. To successfully use brightfield imaging for AST, it's important to obtain measurable changes in the sub- $\mu\text{m}$  motion on antibiotic action for a population of bacterial cells on a chip, containing a mixture of partially and tightly bound cells. We studied the effect of antibiotic on "Average Distance", denoted by  $D_{\text{AVG}}$  for a sample of bacterial cells.  $D_{\text{AVG}}$  is measured by averaging distances of individual cells, including tightly bound and partially bound cells. The  $D_{\text{AVG}}$  due to sub- $\mu\text{m}$  motion for a sample of cells before adding the antibiotic is 265 nm (Figure 5-5b) which reduces to 123 nm within 10 mins after adding bactericidal concentration of antibiotic polymyxin. This indicates that we can carry susceptibility testing based on calculating sub- $\mu\text{m}$  motion holistically to a population of cells on a given chip, without filtering for only the partially tethered cells.

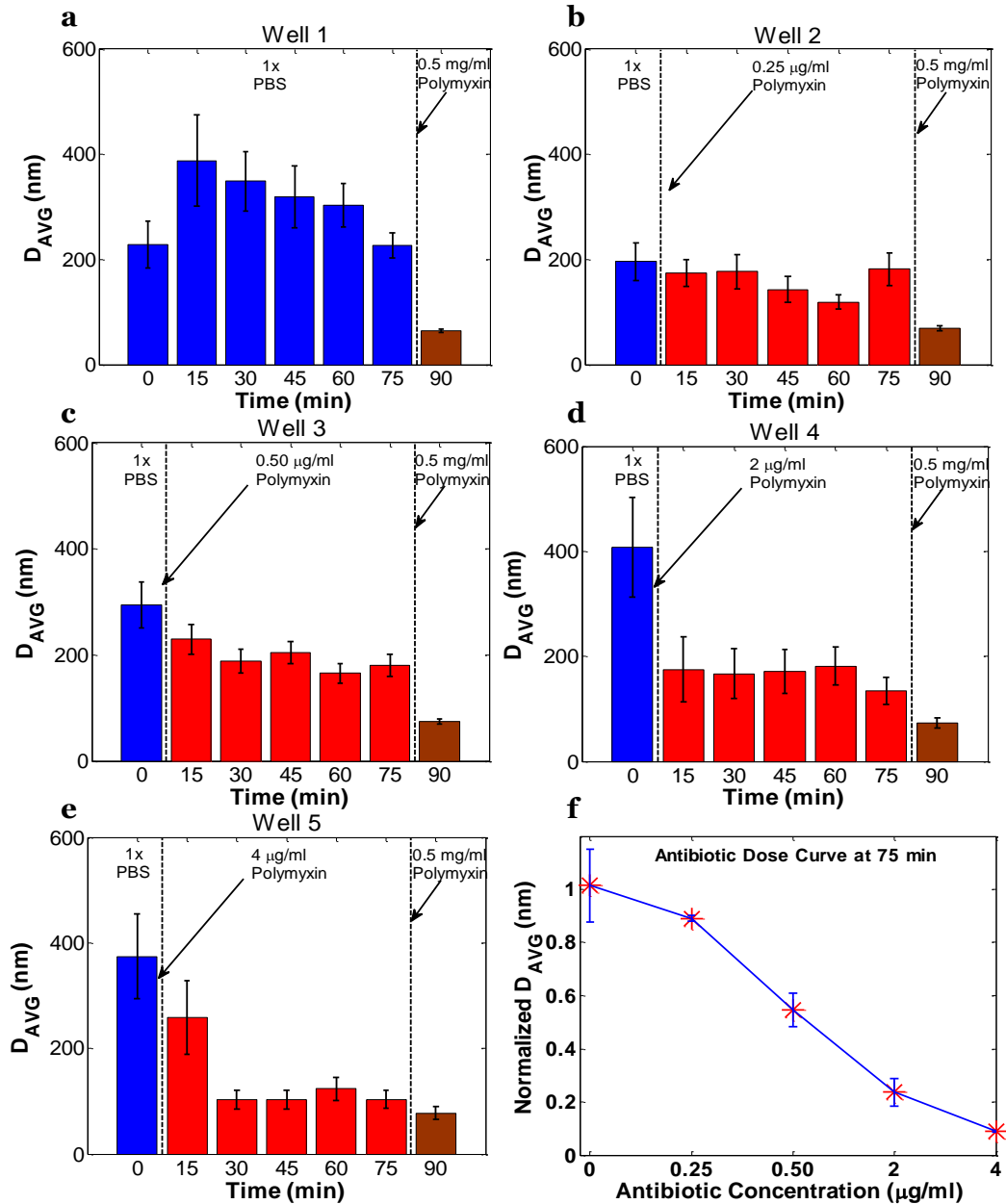
### **Application to UPEC with Multiple Antibiotic Doses**

We next tested the applicability of our approach to the clinically relevant UPEC strain. UPEC cells were tethered to glass surface with a more general linker using APTES surface chemistry, which conjugates to the amine group of the bacterial surface protein. Also, the antibiotic dose dependent experiments were performed in a multiplexed format using a multi-well slides and a 40x air objective so that rapid imaging amongst the wells is feasible. We incubated bacterial cells in 5 different wells (Well 1 to Well5), and recorded an initial baseline image sequences at 0 min for each of the wells. Further, we added a clinical relevant dosage of antibiotic in increasing concentrations from 0 to 4  $\mu\text{g}/\text{ml}$  across different wells and recorded image sequences at 15 min interval for all wells. After 75 mins, we added 0.5mg/ml antibiotic polymyxin (positive control dose that is supposed to kill all

bacteria) across all wells and recorded again after 15 mins (at 90 min) of lethal dose addition.

### **Control Well**

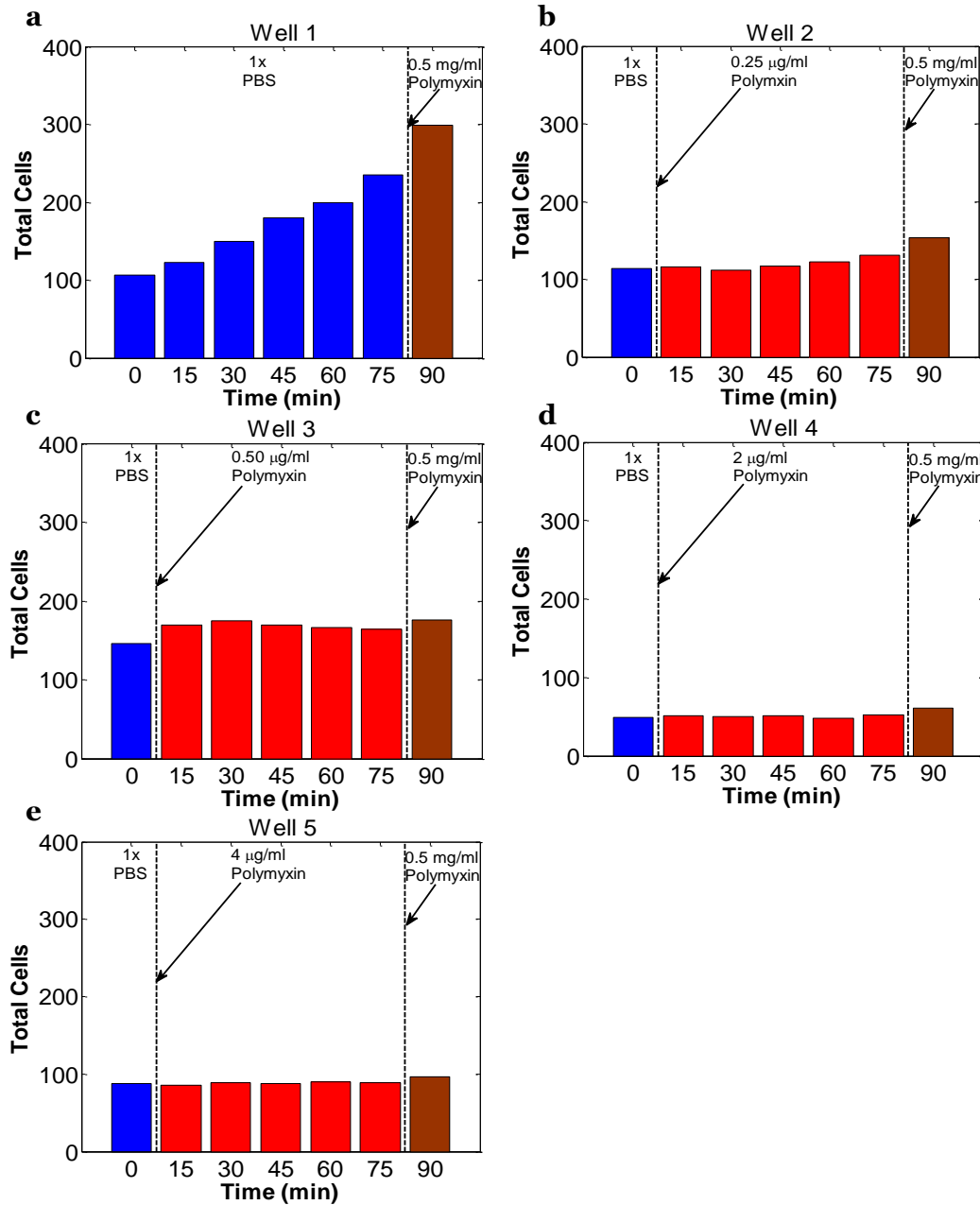
Well1, which has no antibiotic for the first 75 mins, has an initial  $D_{AVG}$  of 228nm (Figure 5-6a) with 100 cells (Figure 5-7a) tethered to the surface initially. Over time, the number on cells on the surface gradually increases (Figure 5-7a) on account of active replication of surface tethered cells (Figure 5-8 and Figure 5-9). The  $D_{AVG}$  of the population increases from 228nm to 388nm from 0 min to 15 mins, followed by a gradual decrease from 388 nm to 227 nm over 75 mins (Figure 5-6a). The decrease in  $D_{AVG}$  can be due to depleted nutrients per cell over time. On adding the positive control dose of antibiotic after 75 mins, we observed (Figure 5-6a) a huge decrease in the  $D_{AVG}$  of cells from 227 nm to 64 nm. This result validated that the sub- $\mu\text{m}$  motion of surface tethered UPEC cells with APTES chemistry is correlated with its metabolism and can be used to perform susceptibility testing.



Figure

5-6.  $D_{AVG}$  of a population of cells in different wells at various time points.

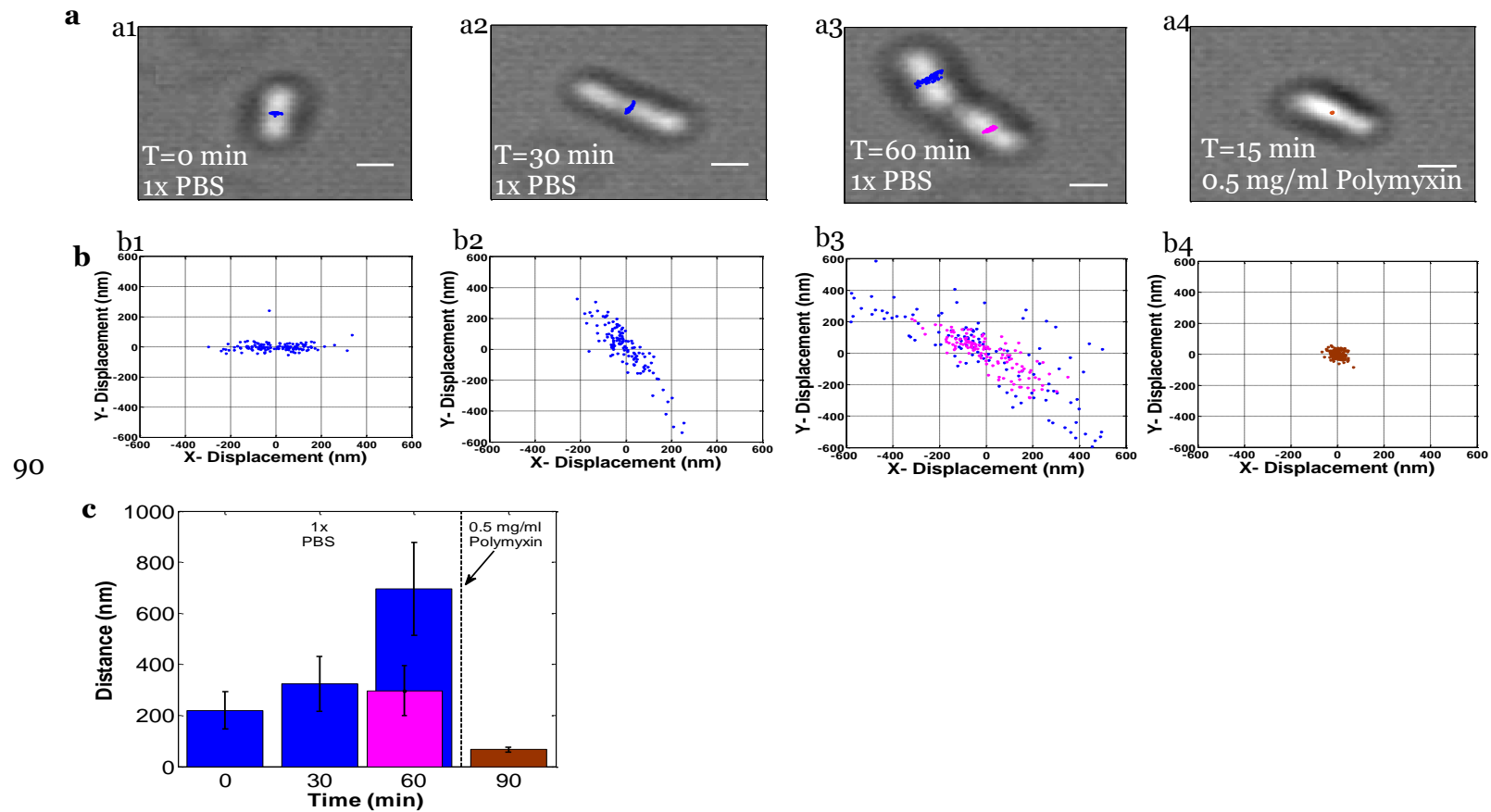
Wells are sequentially exposed to 1xPBS (blue bar, the base line measurement), different clinically relevant doses of antibiotics (red bars, antibiotics added immediately after the baseline measurement), and a lethal dose of antibiotic (brown bar, 0.5 mg/ml added after the 75 min measurement) a)-e)  $D_{AVG}$  of cells in Well1-Well5 with 0 µg/ml – 4 µg/ml of antibiotic respectively. f) Antibiotic dose curve of normalized  $D_{AVG}$  at 75 mins.



Figure

5-7. Number of UPEC Cells in Different Wells over Time.

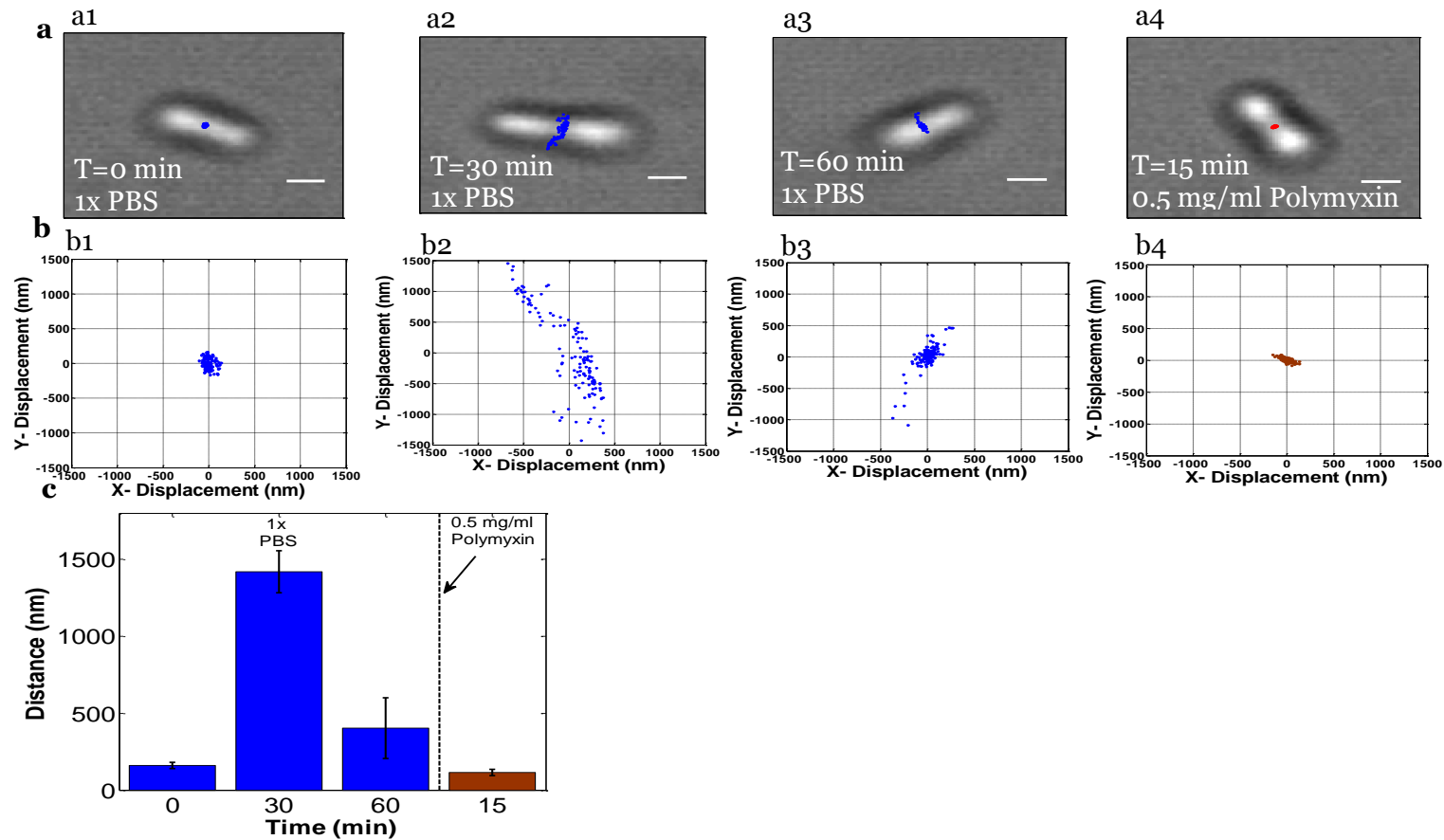
Total number of bacterial cells in different wells at different time points, where they are sequentially exposed to 1xPBS (blue bar, the base line measurement), different clinically relevant doses of antibiotics (red bars, antibiotics added immediately after the baseline measurement), and a lethal dose of antibiotic (brown bar, 0.5 mg/ml added after the 75 min measurement) a)-e) Total cells in Well1-Well5 with 0  $\mu$ g/ml – 4  $\mu$ g/ml of antibiotic respectively.



Figure

5-8. Changes in Sub- $\mu\text{m}$  Motion of a UPEC Cell Replicating on the Surface.

a1-a4 Snapshots of a UPEC cell with superimposed displacement of the center over time in 1x PBS followed by addition of 0.5mg/ml antibiotic. b1-b4 Scatter plot of displacement over time in 1xPBS followed by adding 0.5mg/ml antibiotic. c) Bar graph showing changes in distance

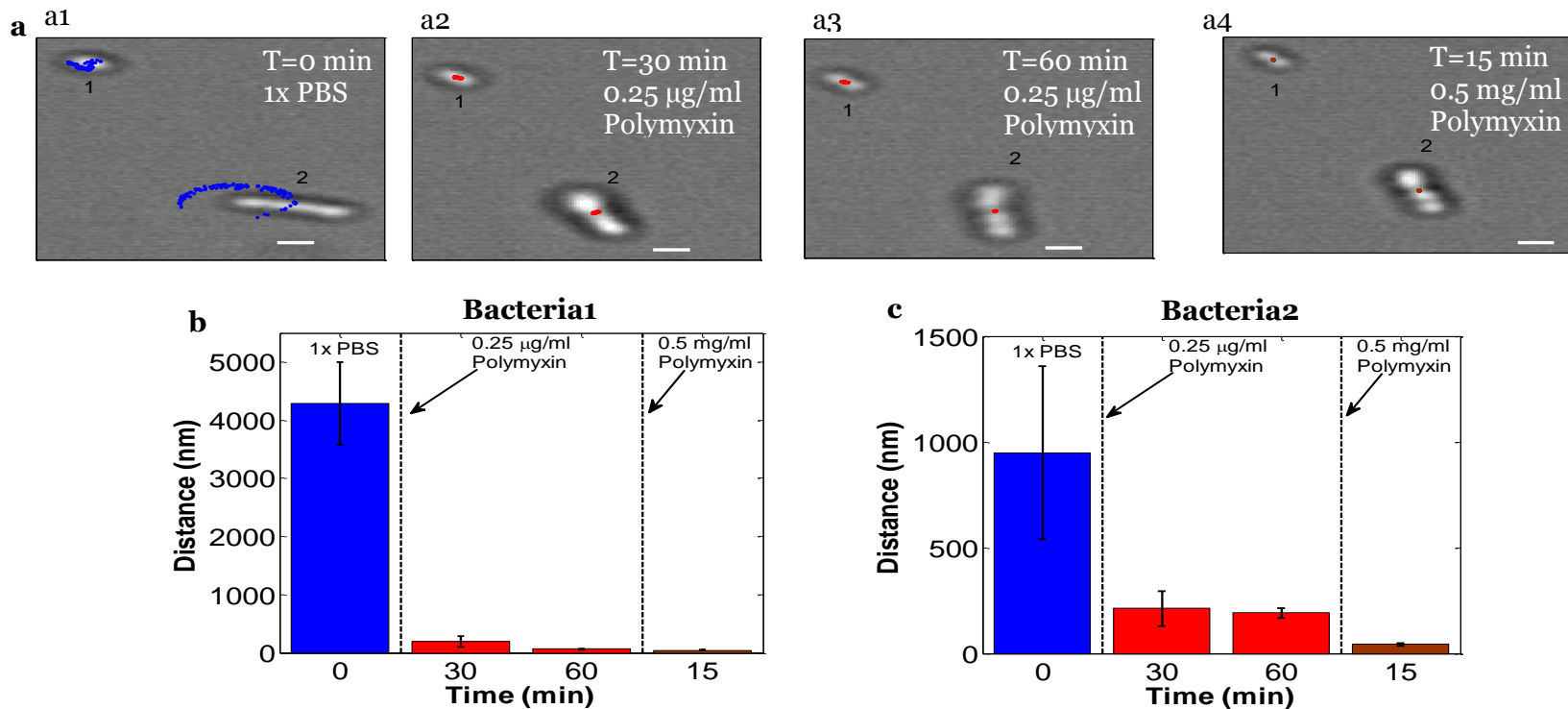


Figure

5-9. Changes in Sub- $\mu\text{m}$  Motion of a UPEC Cell Replicating on the Surface

a1-a4 Snapshots of a UPEC bacterial cell with superimposed displacement in 1x PBS followed by addition of 0.5mg/ml antibiotic. b1-b4 Scatter plot of displacement over time in 1xPBS followed by 0.5mg/ml antibiotic. c) Bar graph showing increase in distance



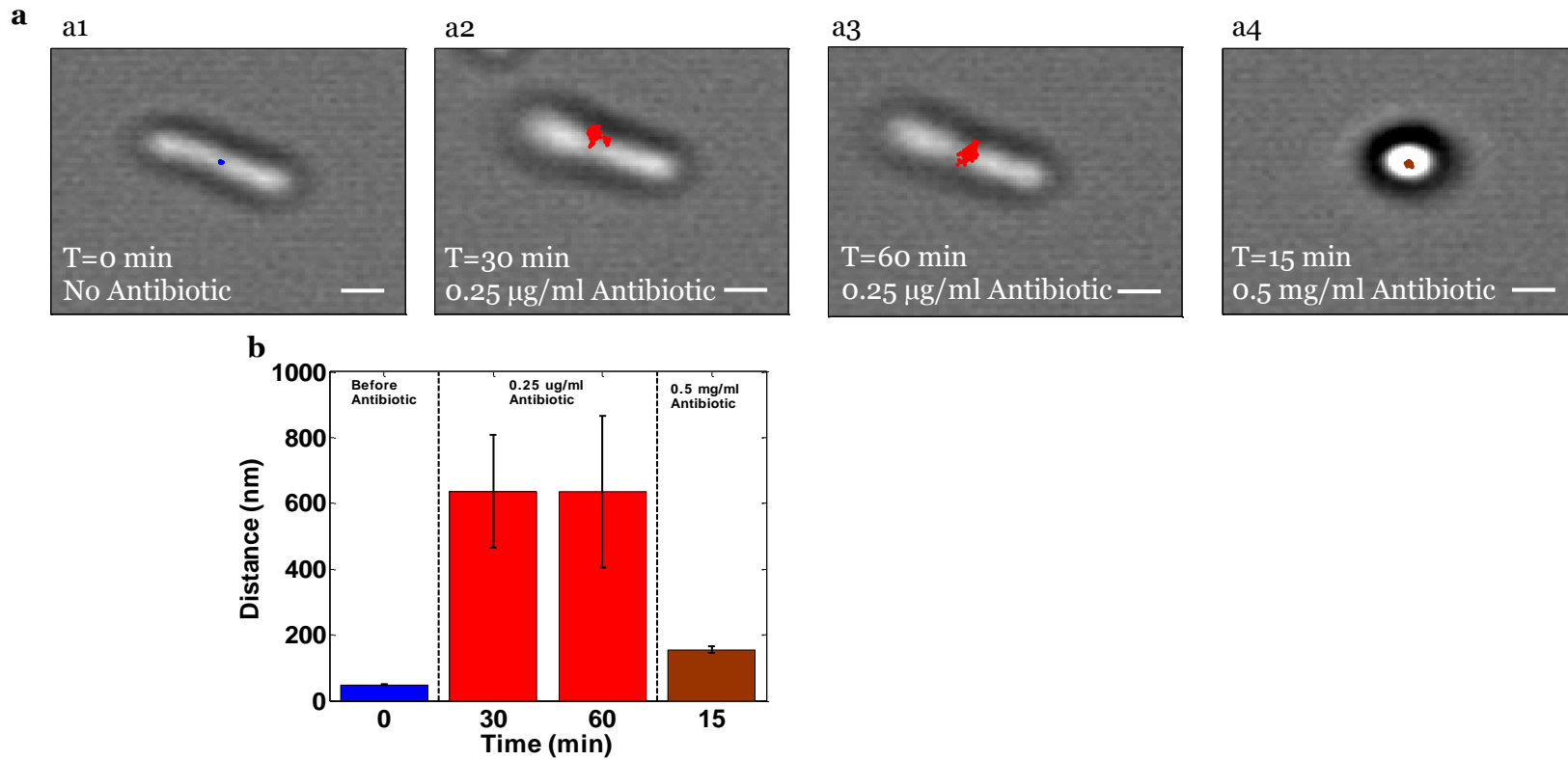


92

Figure

5-10. Decrease in Sub-µm Motion of a UPEC Cell on the Surface in 0.25 µg/ml of Antibiotic

a1-a4 Snapshots of two individual UPEC bacterial cell with superimposed displacement in 1x PBS followed by addition of 0.25 µg/ml antibiotic. b) - c) Show distance at different time points. Both the cells show a decrease in distance at 30mins and 60mins on adding a low dosage of 0.25µg/ml of antibiotic (red bars). These cells are representative of sub-population1 on which low dosage of antibiotic acts immediately and which dominates the initial decrease in  $D_{AVG}$  of the population.

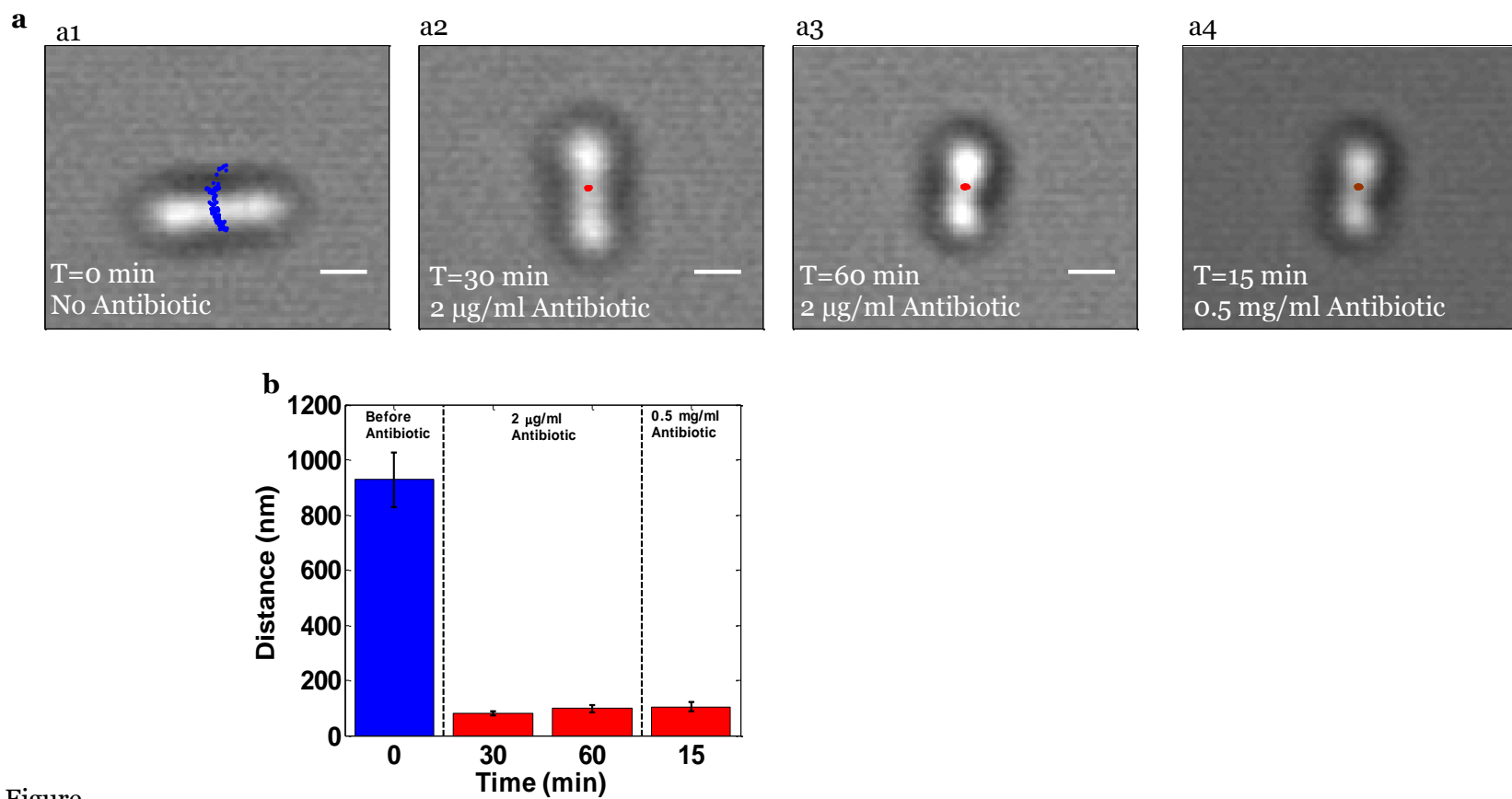


93

Figure

5-11. Increase in Sub-µm Motion of a UPEC cell on the Surface in a 0.25 µg/ml of Antibiotic

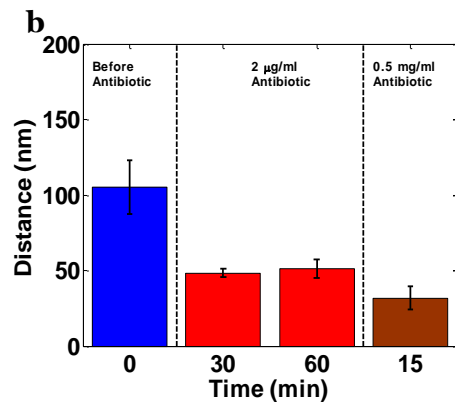
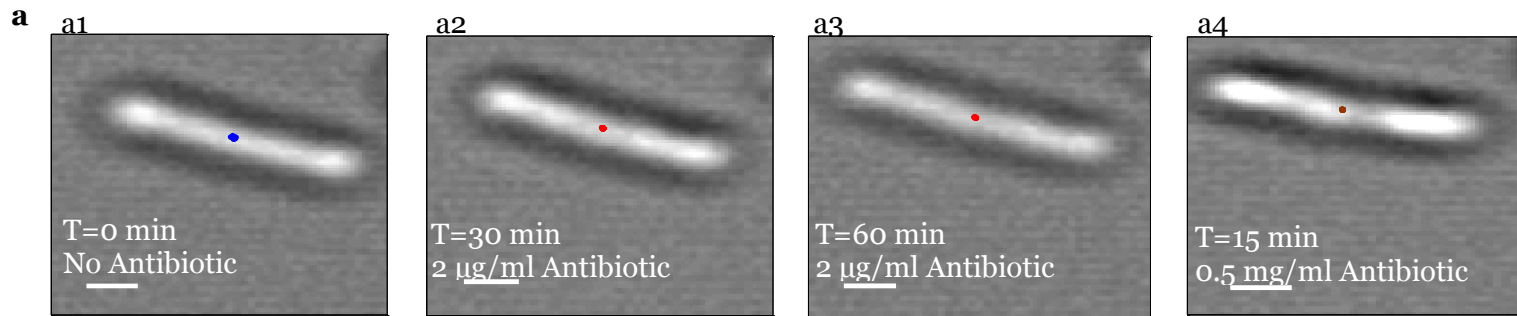
a1-a4 Snapshots of an individual UPEC bacterial cell with superimposed motion over time in 1x PBS followed by addition of 0.25 µg/ml antibiotic. b) Bar graphs of motion at different time points. The cells show an increase in distance at 30mins and 60mins, on adding a low dosage of antibiotic as evident in bar graph (red bars). These cells are representative of sub-population2 on which low dosage of antibiotic doesn't act and which dominates the later increase in  $D_{AVG}$  of the population.



Figure

5-12. Decrease in Sub- $\mu\text{m}$  Motion of a UPEC Cell on the Surface in a 2  $\mu\text{g}/\text{ml}$  of Antibiotic

a1-a4 Snapshots of an individual UPEC bacterial cell with superimposed motion over time in 1x PBS followed by addition of 2  $\mu\text{g}/\text{ml}$  antibiotic and 0.5 mg/ml antibiotic. b) Bar graphs of motion at different time points. The cells show a decrease in motion at 30mins and 60mins, on adding a low dosage of antibiotic (red bars). The decreased motion is equal to the decrease observed after adding the bactericidal concentration of 0.5 mg/ml, indicating cell-death on adding 2  $\mu\text{g}/\text{ml}$  antibiotic.



95

Figure

5-13. Decrease in Sub- $\mu\text{m}$  Motion of a UPEC Cell on the Surface in a 2  $\mu\text{g/ml}$  of Antibiotic

a1-a4 Snapshots of an individual UPEC bacterial cell with superimposed motion over time in 1x PBS followed by addition of 2  $\mu\text{g/ml}$  antibiotic and 0.5  $\text{mg/ml}$  antibiotic. b) Bar graphs of motion at different time points. The cells show a decrease in distance at 30mins and 60mins, on adding a low dosage of antibiotic (red bars). There is a further decrease observed after adding the bactericidal concentration of 0.5  $\text{mg/ml}$ , indicating that this individual cell might not be dead on adding 2  $\mu\text{g/ml}$ .

## **Bacteria Motion Responses to Clinically Relevant Antibiotic Doses**

For wells 2-5 with different antibiotic dosages, we observe immediate decreases in the  $D_{AVG}$  (Figure 5-6b to 5-6e) of the cell-population at 15 mins compared to initial values at 0 min in each well. Over 75 mins, all antibiotic wells except Well2 (explained later) showed a gradual decrease in  $D_{AVG}$ , indicating decrease in sub- $\mu$ m motion over time. The number of cells across in wells with 0.5-4  $\mu$ g/ml antibiotic doses remains steady over 75 mins (Figure 5-7), indicating cessation of bacterial replication in the presence of antibiotics. After adding the lethal dose across all wells at 75 mins, we observed a further decrease in  $D_{AVG}$  of the cell-population in all antibiotic wells except Well5, in which the  $D_{AVG}$  remains similar. Different decreases in  $D_{AVG}$  in various wells, signifies that the sub- $\mu$ m motion changes are scaled with the concentration of the antibiotics, providing a strong evidence that this method can be used to measure dose dependence antibiotic action.

### **Single Cells Analysis and Cell to Cell Variations in Motion Responses to Antibiotics**

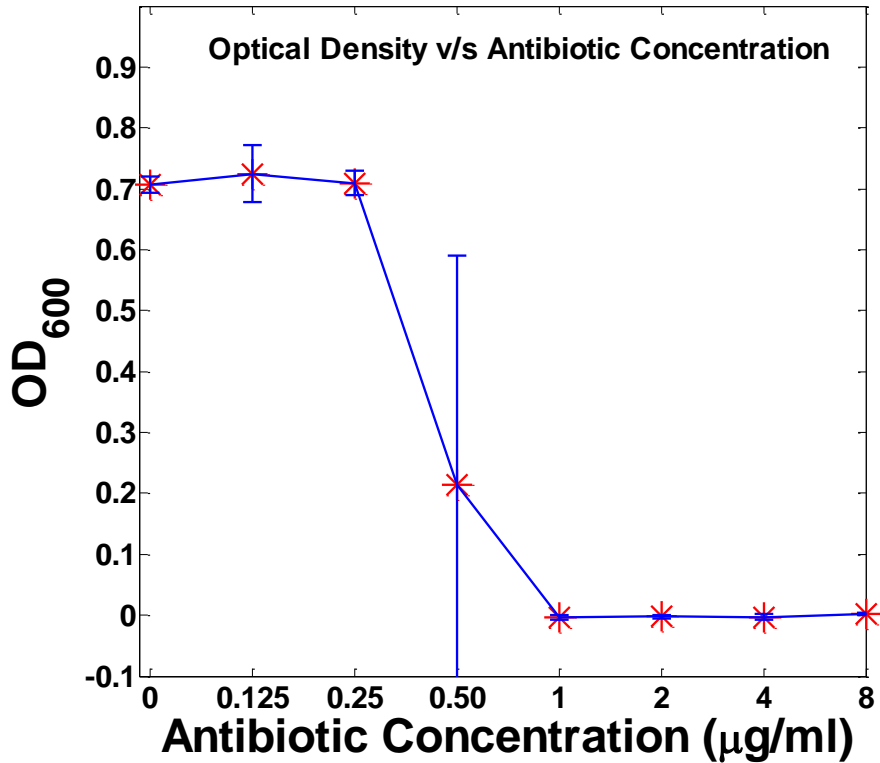
Observing single cells in different wells gives us interesting insights into the sub- $\mu$ m behavior of cells at low dosages of antibiotic. In Well1, individual cell (Figures 5-8 and 5-9) at different time points show clearly that the distance of actively replicating cells generally increases as cells replicate followed by a decrease on adding antibiotics. This further validates that sub- $\mu$ m motion is correlated with bacterial metabolism. However establishing a more precise relationship between bacterial metabolism and the sub- $\mu$ m motion of surface tethered cells will need additional research going forward. In Well2, for the entire sample of cells, there is a steady decrease in  $D_{AVG}$  from 0 min to 60 mins followed by an increase at 75 mins, which is due to two distinct subpopulations (sub-population 1 and sub-population 2) of cells. In sub-population1 (Figure 5-10), there is an immediate decrease in distance of individual cells on adding a low dose antibiotic, whereas in sub-

population 2, there is an increase in distance as the bacterial cells continue to divide in the presence of low dosage of antibiotic (Figure 5-11). Towards 75 mins sub-population 2 dominates leading to an overall increase in  $D_{AVG}$  for the complete well. Both sub-populations show a decrease in distance on adding the lethal antibiotic dose after 75 mins. These results mean that sub-population 2 is more resistant to the antibiotic than sub-population 1, indicating the heterogeneous responses to antibiotic treatment among the bacteria population, and the power of single cell sub- $\mu$ m motion analysis for finding sub-population of resistant strains in a sample. In Well4, all individual cells (Figure 5-12 and 5-13), decrease their distance immediately post the addition of 2  $\mu$ g/ml antibiotics. However, for some cells (Figure 5-12) the distance doesn't recover over time and is comparable to the distance obtained after subsequent addition of the lethal dose. This result means that the particular cells are killed at 2  $\mu$ g/ml of antibiotic.

### **Dose-curve and Defining MBC for Sub- $\mu$ m Motion**

To obtain the antibiotic dose dependent changes on the motions, we normalized the  $D_{AVG}$  at 75 min from each well, to the  $D_{AVG}$  values between a particular Well's control measurement at 0 min and positive control measurement at the lethal 0.5mg/ml antibiotic dose. Figure 5-6 is the dose curve obtained at 75 mins, which shows a steady decrease in the normalized  $D_{AVG}$  as the antibiotic dosage is increased. At 4  $\mu$ g/ml antibiotic concentration (Figure 5-6f), the normalized  $D_{AVG}$  value (0.08) is close to 0, indicating 4  $\mu$ g/ml to be the minimum bactericidal concentration, defined for our particular assay as the minimum antibiotic concentration where the  $D_{AVG}$  is close to the average motion distance at a known bactericidal concentration. We further compared our MBC value to the gold standard culture based method, which gives a MIC value of 1  $\mu$ g/ml (Figure 5-14) and MBC value of 2  $\mu$ g/ml (data not shown). Our MBC value obtained within 2 hours is close to the reference techniques which require 24-72 hours to obtain the MIC and MBC

values. Our MBC is within the QC range of Clinical & Laboratory Standards Institute (CLSI), indicating our technology can provide clinically significant MBC values and perform rapid AST within 2 hours.



Figure

#### 5-14. Comparison with Reference Techniques

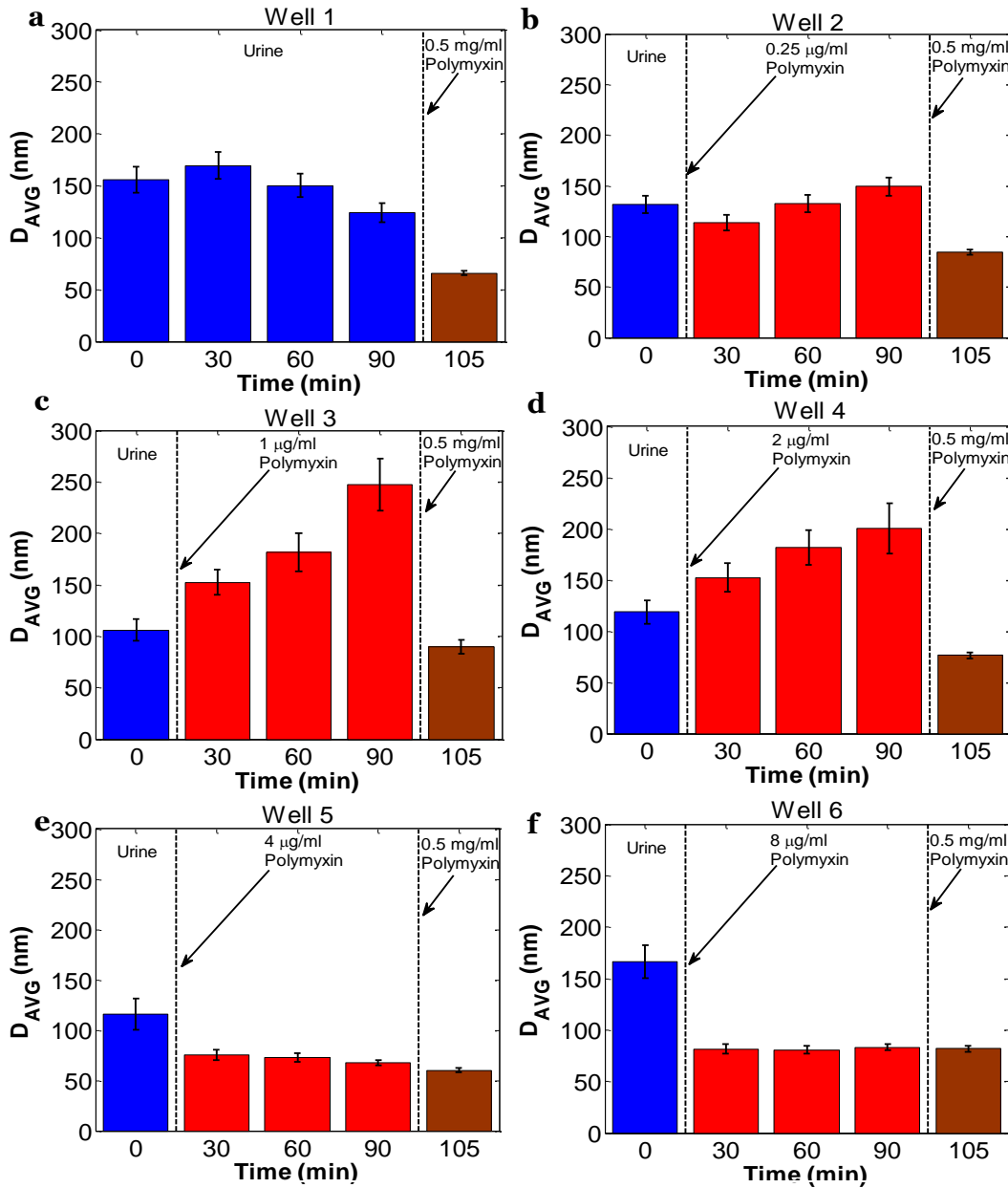
Using optical density measurement, we measured the minimum inhibitory concentration (MIC) of polymyxin against UPEC strain is 1µg/ml. The Minimum Bactericidal Concentration (MBC) was obtained by spot plating individual concentrations. The MBC is found to be 2µg/ml

### Urine Samples

To test the feasibility of our method to work directly on clinical samples, we spiked UPEC bacterial cells in urine samples collected from healthy patients. Following surface tethering, we recorded image sequences from 6 different wells with antibiotic doses

between 0  $\mu\text{g/ml}$  to 8  $\mu\text{g/ml}$ . From 0  $\mu\text{g/ml}$  to 2  $\mu\text{g/ml}$ , the  $D_{\text{AVG}}$  is steady or increases over time (Figure 5-15a to 5-15c). The increase in sub- $\mu\text{m}$  motion between 0 min and 90 mins in Well1 to Well4 should be due to sufficient nutrients in urine that promote bacterial cells divide. This is in contrast to measurements in 1x PBS, where the bacteria sub- $\mu\text{m}$  motion decreases over time due to depleted nutrients. After adding the lethal dose, Well1 to Well4 show a sharp drop in  $D_{\text{AVG}}$  within 15 minutes (Figure 5-15a-5d). Well 5 and Well 6 (4  $\mu\text{g/ml}$  and 8  $\mu\text{g/ml}$ ) show immediate drop in  $D_{\text{AVG}}$  (Figure 5-15e and 5-15f), and negligible drops in  $D_{\text{AVG}}$  upon adding the lethal dose (Figure 5-15e and 5-15f). In well 6, with 8  $\mu\text{g/ml}$  antibiotic, the  $D_{\text{AVG}}$  at 90 minutes is indifferent from the positive control at a lethal dosage. We estimate 8  $\mu\text{g/ml}$  to be the MBC of polymyxin against UPEC strain in Urine samples.





Figure

5-15.  $D_{AVG}$  of a Population of Bacterial Cells Spiked in Urine to a Concentration of  $5 \times 10^6$  cfu/ml.

Different wells at different time points are sequentially in Urine (blue bar, the base line measurement), different clinically relevant doses of antibiotics (red bars, antibiotics added immediately after the baseline measurement), and a lethal dose of antibiotic (brown bar, 0.5 mg/ml added after the 90 min measurement) a)-e)  $D_{AVG}$  of cells in Well1-Well6 with 0 µg/ml – 8 µg/ml of antibiotic respectively.

On repeating this experiment for different concentrations of spiked bacterial cells in urine samples, we predict a range of MBC between 4-8 µg/ml for polymyxin B using our method. This number is in close agreement with previous experiments and gold standard techniques which take 24-48 hours to obtain the clinical MBC. This validates the ability of our technique to perform rapid AST within 2 hours, directly on urine samples.

Table

5-1. MBC of the Antibiotic at Different Concentrations of UPEC cells Spiked into Urine

<b>Bacteria Concentration in Urine</b>	<b>Estimated MBC</b>
$5 \times 10^6$ cfu/ml	8 µg/ml
$10^7$ cfu/ml	4 µg/ml
$10^8$ cfu/ml	4 µg/ml

## Conclusion

The motility-induced motion of bacterial cells close to the surface or swimming in the solution has been previously studied using multiple optical techniques.<sup>134,142</sup> Bacterial cells have also been studied by attaching them firmly to the surface to enable imaging within the field of focus.<sup>13</sup> However, none of the previous approaches quantify the sub- $\mu\text{m}$  motion of surface tethered bacterial cells and apply it for AST. Our approach has been made possible by optimizing the surface chemistry which enables capture of sufficient number of partially tethered cells close to the surface. For the antibody surface chemistry, we optimized the time of incubation of antibody on the surface while for APTES surface chemistry, we optimized both the time of incubation and APTES concentration. As we have shown these partially tethered cells show a decrease in the sub- $\mu\text{m}$  motion on antibiotic action, while strongly tethered cells don't show any visible changes in sub- $\mu\text{m}$  motion using brightfield imaging. To quantify the motion changes of free cells in solution post antibiotic action is challenging, because of the Brownian-motion of these cells, which superimposes on the metabolic motion of such cells.

We demonstrated rapid (within 2 hours) AST of clinically important strains, *E. coli* O157:H7<sup>24</sup> and UPEC, by quantifying the sub- $\mu\text{m}$  motion of single bacterial cells with optical tracking. Compared to culture based methods that measure increases in cell size or numbers, our approach is faster. Compared to AFM, which measure bacterial nano-motion in z-direction, our present bright-field based optical tracking method can simultaneously imaging multiple bacterial cells in parallel and provide single-cell resolution that can be used for poly-microbial analysis as well as finding resistant sub-populations. Compared to plasmonic imaging and tracking (PIT) reported by us in a previously publication, the present optical tracking is simpler in both instrumentation and sensor chip preparation. One limitation of the present method compare to PIT is the lack

of resolution in Z direction. However, our results show that tracking of x/y sub- $\mu\text{m}$  motion is sufficient for the purpose of AST. While we were able to obtain clinically relevant MBC values within 2 hours in urine samples, possible limitations of our method include the inability to perform this analysis at lower concentrations of bacteria in Urine. However, this limitation can be potentially overcome by pre-concentrating bacterial cells from patient samples with filtration/centrifuge or microfluidic captures, and by improving surface chemistry to enable uniform partial tethering across all cells. While we showed a direct correlation between the sub- $\mu\text{m}$  motion and bacterial viability, the applicability of our technique to a wider set of bacteriostatic antibiotics needs further study. However, since previous studies have shown the applicability of using nano-motion to other antibiotics such as ampicillin, streptomycin and other bacterial strains,<sup>26,44,122</sup>, we have confidence that our method will work for other cases as well.

We have demonstrated a rapid AST using sub- $\mu\text{m}$  bacterial motion with a turnaround time of 2 hours and capable of working directly with urine samples. The sub- $\mu\text{m}$  bacterial motion is a signature of its metabolism and is also dependent upon the degree of a cell's surface attachment. The sub- $\mu\text{m}$  motion decreases on antibiotic action for partially tethered cells, while no such changes happen in tightly tethered cells. Despite variability amongst cells, we can use sub- $\mu\text{m}$  motion to perform susceptibility testing for a population of cells. By analyzing dose dependent sub- $\mu\text{m}$  motion changes in a multiplexed assay, we obtained within 2 hours minimum bactericidal concentration of polymyxin against UPEC. We plan to conduct more research to validate our method for a broader set of antibiotics, pathogens and clinical conditions. We anticipate that clinical labs with brightfield imaging would be able to incorporate our methodology in parallel to already existing microscopic urinalysis protocols. This will greatly ease the adaptation challenges which other AST tools might face. Further, with the advent of paper

microfluidics,<sup>143,144</sup> low-cost microscopy such as Foldoscope<sup>145</sup> and smart-phone based diagnostics,<sup>146,147</sup> we anticipate our tool to be coupled with such techniques to perform point-of-care rapid AST, to reach a much broader audience in the developing world, which face a humanitarian crisis of resistant bugs.

## CONCLUSION AND FUTURE WORK

### **Conclusions**

I developed a culture-independent AST, based on quantifying the motion of surface-tethered bacterial cells using two separate imaging techniques. I also developed plasmonic imaging technique to quantify cell-to-cell heterogeneity with potential applications in antibiotic drug development. In Chapter 3, I measured kinetic constants of antibody interactions with single cells and found out that these interactions are “noisy” due to small-micromotion of alive bacterial cells. The distribution of kinetic constants is unimodal and spread over four orders of magnitude which reflects cell-to-cell heterogeneity in bacterial surfaces present within a population. The center of the unimodal distribution, is similar to the value found in the literature by techniques measuring interactions of antibody with bulk populations. This validated the use of the plasmonic technique to quantify bacterial heterogeneity and gain more information about evolutionary microbial diversity while developing new antimicrobials and humanized antibodies as future therapeutic drugs against bacterial surfaces.

In Chapter 4, I correlated small-micromotion present in surface tethered cells to z-direction vibration of alive bacterial cells. Using PIT, we tracked z-direction motion with sub-nm precision and found out that alive bacterial cells vibrate in the z-direction with nano-meter scale amplitude (nano-motion) of 5-10 nm. We discovered nano-motion as an effective signature of bacterial metabolism, which changes in different nutrient and culture conditions. Nano-motion increases in the presence of active metabolic substances such as glucose and decreases on giving antibiotics, which we used to perform antibiotic susceptibility testing. We showed that the principle of AST based on quantifying nano-motion can be universally applied to multiple strains (UPEC, E. coli O157), multiple

antibiotics (polymyxin, streptomycin) and different surface tethering molecules (antibodies, APTES).

In Chapter 5, I enabled simple brightfield microscopes, present commonly in clinical labs across the healthcare world, to perform rapid AST within 2 hours on UPEC strains directly in urine samples. I demonstrated that via an optimal combination of surface chemistry, hardware changes and automated image processing algorithms, we can perform susceptibility testing by quantitating the sub-um motion of bacterial cells. Partially tethered bacterial cells show sub-um motion with an average of 260nm, tightly tethered bacterial cells show decreased sub-um motion of about 75nm. The sub-um motion decreases on antibiotic action of partially tethered cells and no such changes happen in tightly tethered cells. For a population of cells, containing a mixture of cells with different degrees of surface attachment, we observe a decrease in average motion ( $D_{AVG}$ ) on antibiotic action at a lethal dose. We performed multi-dose experiments in a multi-well format at clinically relevant concentrations and estimated minimum bactericidal concentration (MBC) of polymyxin against UPEC strains within 2 hours. We also estimated MBC directly in urine samples spiked with different bacterial concentrations. Our MBC estimate was in good agreement with current gold standard culturing techniques which take 3 days, thus enabling point-of-care use.

### **Future Work**

To achieve long term impact both in the pharmaceutical and clinical microbiology, I discuss future projects which can be built on the current work.

1. Study AST application of 3D motion of surface tethered UPEC bacteria for different classes of antibiotics. To investigate broad applicability of our method and for a faster clinical adaptation, it is important to quantify 3D movement of UPEC in the presence of different classes of antibiotics: ampicillin ( $\beta$ -lactam),

kanamycin (aminoglycoside), tetracycline, ciprofloxacin (quinolone). We anticipate that the antibiotics, which affect cell wall synthesis, protein synthesis, or DNA replication, will have an effect on active cellular motion. Monitoring 3D cellular movement and comparing inhibitory and killing effects of bacteriostatic and bactericidal antibiotics, respectively, will help establish a rapid AST. Action of antibiotics can be orthogonally validated using previously well characterized strategies such as engineering *E. coli* with protein fluorescent tags, culturing in media to check for cell growth. While it's possible that motion changes due to bactericidal antibiotics within 2 hours are minimal, we expect a dose dependent response which should be helpful to estimate MIC/MBC.

2. Correlate cellular metabolism and motility with 3D cellular movement. To investigate the metabolic causes behind 3D motion of surface tethered bacteria, it's important to perform this study. Measuring the 3D movement of UPEC in various culture media, with and without supplements and metabolites (i.e., tryptophan, cas-amino acids, maltose, glucose, different carbon sources), and at various temperatures will change cellular growth and metabolism along with giving a better understanding of underlying phenomenon. To differentiate cellular metabolism and motility effects on the cellular movement, we can also study UPEC *E. coli* CFT073 (Gram negative, rod-shaped, motile) and *E. coli* CFT073  $\Delta$ fliC mutant (non-motile mutant without flagella). These experiments will allow us to differentiate metabolism and motility-related 3D movements and correlate the movements of viable bacteria to physiological processes. Another strategy is to monitor the effect of stimuli on motility in normal and abnormal cells. For example, after the addition of L-serine (attractant) to



induce continuous running and block tumbling or sodium benzoate (repellent) to induce continuous tumbling, UPEC chemotactic responses can be monitored by light microscopy and then assessed for 3D movement. This study will examine the potential interdependence of 3D movement and *E. coli* flagella and changes in 3D movement with differentially induced motility phenotypes. Further, this aim will also help understand the applicability of this principle to UPEC strains with repressed motility.

3. Studying bacterial strains directly in clinical urine samples to enable rapid, point-of-care AST for application in clinical samples. It's important to test the feasibility of this approach for a wider range of real-patient conditions. Urine samples must be tested containing UPEC pathogens from diverse patients accounting for diversity in gender, age, past-surgical procedures, catheter related UTIs, past resistant history. This study will be useful in developing a protocol to enrich bacterial cells from urine, separation of eukaryotic material from bacterial cells, testing upper and lower limits of detection for different bacterial concentrations in clinical samples as well as establishing healthy nutrient conditions to enable sub- $\mu\text{m}$  motion for AST testing. This will eventually be useful in carrying out a multi-center comparative study closer to regulatory approval.
4. Studying combined kinetic interactions and nano-motion changes of antibiotic action on bacterial cells. In the pharmaceutical industry, kinetics of antibiotic interaction with bacterial surface and MIC testing of an antibiotic against a bacterial cell is carried out in two separate diverse assays. However, both these phenomenon are fundamentally similar in nature and can lead into interesting insights into resistant mechanisms. We propose a single step assay, using PIT,

capable of studying kinetic interactions and nano-motion changes together for single bacterial cells. We hypothesize that resistant and susceptible strains, which have resistant markers on the surface, will have different kinetic interactions with antibiotics. This will help elucidate binding potential of new antibiotics and quantitate bacterial heterogeneity. We also expect differential changes in 3D motion varying with antibiotic dosage which can give insights into single cell behavior. Potential pitfalls might be that antibiotics are small molecules and they might not lead to measurable kinetics. Also, at low dosage of antibiotics, the longer time scales might not be amenable to perform kinetic studies.

## REFERENCES

- (1) Fleming, A. On the Antibacterial Action of Cultures of a *Penicillium*, with Special Reference to Their Use in the Isolation of *B. Influenzae*. *Br. J. Exp. Pathol.* **1929**, *10*, 226–336.
- (2) Laxminarayan, R.; Duse, A.; Wattal, C.; Zaidi, A. K. M.; Wertheim, H. F. L.; Sumpradit, N.; Vlieghe, E.; Hara, G. L.; Gould, I. M.; Goossens, H.; *et al.* Antibiotic Resistance – the Need for Global Solutions. *Lancet Infect. Dis.* **2013**, *3099*, 1057–1098.
- (3) Van Boeckel, T. P.; Gandra, S.; Ashok, A.; Caudron, Q.; Grenfell, B. T.; Levin, S. A.; Laxminarayan, R. Global Antibiotic Consumption 2000 to 2010: An Analysis of National Pharmaceutical Sales Data. *Lancet Infect. Dis.* **2014**, *14*, 742–750.
- (4) Bauer, K. A.; Perez, K. K.; Forrest, G. N.; Goff, D. A. Review of Rapid Diagnostic Tests Used by Antimicrobial Stewardship Programs. *Clin. Infect. Dis.* **2014**, *59*, S134–S145.
- (5) Bartlett, J. G.; Gilbert, D. N.; Spellberg, B. Seven Ways to Preserve the Miracle of Antibiotics. *Clin. Infect. Dis.* **2013**, *56*, 1445–1450.
- (6) Hancock, R. E. W. The End of an Era? *Nat. Rev. Drug Discov.* **2006**, *6*, 28–28.
- (7) Daniels, R. Surviving the First Hours in Sepsis : Getting the Basics Right ( an Intensivist ' S Perspective ). *J Antimicrob Chemother.* **2011**, *66*, 11–23.
- (8) Syal, K.; Mo, M.; Yu, H.; Iriya, R.; Jing, W.; Guodong, S.; Wang, S.; Gryns, T. E.; Haydel, S. E.; Tao, N. Current and Emerging Techniques for Antibiotic Susceptibility Tests. *Theranostics* **2017**, *7*, 1795–1805.
- (9) Jorgensen, J. H.; Ferraro, M. J. Antimicrobial Susceptibility Testing: A Review of General Principles and Contemporary Practices. *Clin. Infect. Dis.* **2009**, *49*, 1749–1755.
- (10) Barenfanger, J.; Drake, C.; Kacich, G. Clinical and Financial Benefits of Rapid Bacterial Identification and Antimicrobial Susceptibility Testing. *J. Clin. Microbiol.* **1999**, *37*, 1415–1418.
- (11) Delcour, A. H. Outer Membrane Permeability and Antibiotic Resistance. *Biochim. Biophys. Acta* **2009**, *1794*, 808–816.
- (12) Fantner, G. E.; Barbero, R. J.; Gray, D. S.; Belcher, A. M. Kinetics of Antimicrobial Peptide Activity Measured on Individual Bacterial Cells Using High-Speed Atomic Force Microscopy. *Nat. Nanotechnol.* **2010**, *5*, 280–285.
- (13) Sochacki, K. a; Barns, K. J.; Bucki, R.; Weisshaar, J. C. Real-Time Attack on Single *Escherichia Coli* Cells by the Human Antimicrobial Peptide LL-37. *Proc. Natl. Acad. Sci. U. S. A.* **2011**, *108*, E77–81.
- (14) Van Houdt, R.; Michiels, C. W. Role of Bacterial Cell Surface Structures in *Escherichia*

- Coli Biofilm Formation. *Res. Microbiol.* **2005**, *156*, 626–633.
- (15) Lower, S. K.; Lamlerthton, S.; Casillas-Ituarte, N. N.; Lins, R. D.; Yongsunthon, R.; Taylor, E. S.; DiBartola, A. C.; Edmonson, C.; McIntyre, L. M.; Reller, L. B.; *et al.* Polymorphisms in Fibronectin Binding Protein A of Staphylococcus Aureus Are Associated with Infection of Cardiovascular Devices. *Proc. Natl. Acad. Sci. U. S. A.* **2011**, *108*, 18372–18377.
  - (16) Carnes, E. C.; Lopez, D. M.; Donegan, N. P.; Cheung, A.; Gresham, H.; Timmins, G. S.; Brinker, C. J. Confinement-Induced Quorum Sensing of Individual Staphylococcus Aureus Bacteria. *Nat. Chem. Biol.* **2010**, *6*, 41–45.
  - (17) van der Mei, H. C.; Busscher, H. J. Bacterial Cell Surface Heterogeneity: A Pathogen's Disguise. *PLoS Pathog.* **2012**, *8*, e1002821.
  - (18) Chiang, Y.-L.; Lin, C.-H.; Yen, M.-Y.; Su, Y.-D.; Chen, S.-J.; Chen, H.-F. Innovative Antimicrobial Susceptibility Testing Method Using Surface Plasmon Resonance. *Biosens. Bioelectron.* **2009**, *24*, 1905–1910.
  - (19) Medina, M. B.; Houten, L. Van; Cooke, P. H.; Tu, S. I. Real-Time Analysis of Antibody Binding Interactions with Immobilized E. Coli O157 : H7 Cells Using the BIAcore. *Biotechnol. Tech.* **1997**, *11*, 173–176.
  - (20) Subramanian, A.; Irudayaraj, J.; Ryan, T. A Mixed Self-Assembled Monolayer-Based Surface Plasmon Immunosensor for Detection of E. Coli O157:H7. *Biosens. Bioelectron.* **2006**, *21*, 998–1006.
  - (21) Cywes-Bentley, C.; Skurnik, D.; Zaidi, T.; Roux, D.; Deoliveira, R. B.; Garrett, W. S.; Lu, X.; O'Malley, J.; Kinzel, K.; Zaidi, T.; *et al.* Antibody to a Conserved Antigenic Target Is Protective against Diverse Prokaryotic and Eukaryotic Pathogens. *Proc. Natl. Acad. Sci. U. S. A.* **2013**, *110*, E2209-18.
  - (22) Chang, P. V; Bertozzi, C. R. Imaging beyond the Proteome. *Chem. Commun. (Camb).* **2012**, *48*, 8864–8879.
  - (23) Syal, K.; Wang, W.; Shan, X.; Wang, S.; Chen, H. Y.; Tao, N. Plasmonic Imaging of Protein Interactions with Single Bacterial Cells. *Biosens. Bioelectron.* **2015**, *63*, 131–137.
  - (24) Besser, R. E.; Griffin, P. M.; Slutsker, L. Escherichia Coli O157:H7 Gastroenteritis and the Hemolytic Uremic Syndrome: An Emerging Infectious Disease. *Annu. Rev. Med.* **1999**, *50*, 355–367.
  - (25) Saylor, C.; Dadachova, E.; Casadevall, A. Monoclonal Antibody-Based Therapies for Microbial Diseases. *Vaccine* **2009**, *27 Suppl 6*, G38-46.
  - (26) Syal, K.; Iriya, R.; Yang, Y.; Yu, H.; Wang, S.; Haydel, S. E.; Chen, H.-Y.; Tao, N. Antimicrobial Susceptibility Test with Plasmonic Imaging and Tracking of Single Bacterial Motions on Nanometer Scale. *ACS Nano* **2015**, *10*, 845–852.

- (27) Flores-Mireles, A. L.; Walker, J. N.; Caparon, M.; Hultgren, S. J. Urinary Tract Infections: Epidemiology, Mechanisms of Infection and Treatment Options. *Nat. Rev. Microbiol.* **2015**, *13*, 269–284.
- (28) States, U. Antibiotic Resistance Threats. *CDC* **2013**.
- (29) Zurek, L.; Ghosh, A. Insects Represent a Link between Food Animal Farms and the Urban Environment for Antibiotic Resistance Traits. *Appl. Environ. Microbiol.* **2014**, *80*, 3562–3567.
- (30) Daniels, R. Surviving the First Hours in Sepsis: Getting the Basics Right (an Intensivist’s Perspective). *J. Antimicrob. Chemother.* **2011**, *66*, 11–23.
- (31) Jorgensen, J. H.; Ferraro, M. J. Antimicrobial Susceptibility Testing: A Review of General Principles and Contemporary Practices. *Clin. Infect. Dis.* **2009**, *49*, 1749–1755.
- (32) Wiegand, I.; Hilpert, K.; Hancock, R. E. W. Agar and Broth Dilution Methods to Determine the Minimal Inhibitory Concentration (MIC) of Antimicrobial Substances. *Nat. Protoc.* **2008**, *3*, 163–175.
- (33) Humphries, R. M.; Hindler, J. A. Emerging Resistance, New Antimicrobial Agents . . . but No Tests! The Challenge of Antimicrobial Susceptibility Testing in the Current Us Regulatory Landscape. *Clin. Infect. Dis.* **2016**, *63*, 83–88.
- (34) Martínez, J. L.; Coque, T. M.; Baquero, F. What Is a Resistance Gene ? Ranking Risk in Resistomes. *Nat. Publ. Gr.* **2014**, *13*, 116–123.
- (35) Balouiri, M.; Sadiki, M.; Ibsouda, S. K. Methods for in Vitro Evaluating Antimicrobial Activity: A Review. *J. Pharm. Anal.* **2016**, *6*, 71–79.
- (36) Fluit, A. D. C.; Visser, M. R.; Schmitz, F. Molecular Detection of Antimicrobial Resistance. *Clin. Microbiol. Rev.* **2001**, *14*, 836–871.
- (37) Chotinantakul, K.; Suginta, W.; Schulte, A. Advanced Amperometric Respiration Assay for Antimicrobial Susceptibility Testing. *Anal. Chem.* **2014**, *86*, 10315–10322.
- (38) McGregor, A.; Schio, F.; Beaton, S.; Boulton, V.; Perman, M.; Gilbert, G. The MicroScan WalkAway Diagnostic Microbiology System--an Evaluation. *Pathology* **1995**, *27*, 172–176.
- (39) Winstanley, T.; Courvalin, P. Expert Systems in Clinical Microbiology. *Clin. Microbiol. Rev.* **2011**, *24*, 515–556.
- (40) Choi, J.; Yoo, J.; Lee, M.; Kim, E.; Lee, J. S.; Lee, S.; Joo, S.; Song, S. H.; Kim, E.; Lee, J. C.; *et al.* A Rapid Antimicrobial Susceptibility Test Based on Single-Cell Morphological Analysis. *Sci. Transl. Med.* **2014**, *6*, 267ra174.
- (41) Metzger, S.; Frobel, R. a.; Dunne, W. M. Rapid Simultaneous Identification and Quantitation of *Staphylococcus Aureus* and *Pseudomonas Aeruginosa* Directly from

- Bronchoalveolar Lavage Specimens Using Automated Microscopy. *Diagn. Microbiol. Infect. Dis.* **2014**, *79*, 160–165.
- (42) Mohan, R.; Mukherjee, A.; Sevgen, S. E.; Sanpitakseree, C.; Lee, J.; Schroeder, C. M.; Kenis, P. J. a. A Multiplexed Microfluidic Platform for Rapid Antibiotic Susceptibility Testing. *Biosens. Bioelectron.* **2013**, *49*, 118–125.
- (43) Godin, M.; Delgado, F. F.; Son, S.; Grover, W. H.; Bryan, A. K.; Tzur, A.; Jorgensen, P.; Payer, K.; Grossman, A. D.; Kirschner, M. W.; *et al.* Using Buoyant Mass to Measure the Growth of Single Cells. *Nat. Methods* **2010**, *7*, 387–390.
- (44) Longo, G.; Alonso-Sarduy, L.; Rio, L. M.; Bizzini, a; Trampuz, a; Notz, J.; Dietler, G.; Kasas, S. Rapid Detection of Bacterial Resistance to Antibiotics Using AFM Cantilevers as Nanomechanical Sensors. *Nat. Nanotechnol.* **2013**, *8*, 522–526.
- (45) Etayash, H.; Khan, M. F.; Kaur, K.; Thundat, T.; Farahi, R. H.; Passian, A.; Tetard, L.; Thundat, T.; Fournier, P. E.; Wildt, R. M. T. de; *et al.* Microfluidic Cantilever Detects Bacteria and Measures Their Susceptibility to Antibiotics in Small Confined Volumes. *Nat. Commun.* **2016**, *7*, 12947.
- (46) Sinn, I.; Albertson, T.; Kinnunen, P.; Breslauer, D. N.; McNaughton, B. H.; Burns, M. a; Kopelman, R. Asynchronous Magnetic Bead Rotation Microviscometer for Rapid, Sensitive, and Label-Free Studies of Bacterial Growth and Drug Sensitivity. *Anal. Chem.* **2012**, *84*, 5250–5256.
- (47) Hayden, R. T.; Clinton, L. K.; Hewitt, C.; Koyamatsu, T.; Sun, Y.; Jamison, G.; Perkins, R.; Tang, L.; Pounds, S.; Bankowski, M. J. Rapid Antimicrobial Susceptibility Testing Using Forward Laser Light Scatter Technology. *J. Clin. Microbiol.* **2016**, *54*, 2701–2706.
- (48) Price, C. S.; Kon, S. E.; Metzger, S. Rapid Antibiotic Susceptibility Phenotypic Characterization of Staphylococcus Aureus Using Automated Microscopy of Small Numbers of Cells. *J. Microbiol. Methods* **2014**, *98*, 50–58.
- (49) Kinnunen, P.; Sinn, I.; McNaughton, B. H.; Newton, D. W.; Burns, M. a; Kopelman, R. Monitoring the Growth and Drug Susceptibility of Individual Bacteria Using Asynchronous Magnetic Bead Rotation Sensors. *Biosens. Bioelectron.* **2011**, *26*, 2751–2755.
- (50) MacH, K. E.; Mohan, R.; Baron, E. J.; Shih, M. C.; Gau, V.; Wong, P. K.; Liao, J. C. A Biosensor Platform for Rapid Antimicrobial Susceptibility Testing Directly from Clinical Samples. *J. Urol.* **2011**, *185*, 148–153.
- (51) Ivančić, V.; Mastali, M.; Percy, N.; Gornbein, J.; Babbitt, J. T.; Li, Y.; Landaw, E. M.; Bruckner, D. a.; Churchill, B. M.; Haake, D. a. Rapid Antimicrobial Susceptibility Determination of Uropathogens in Clinical Urine Specimens by Use of ATP Bioluminescence. *J. Clin. Microbiol.* **2008**, *46*, 1213–1219.
- (52) Listed], [No Author]. Roche Gobbles Smarticles. *Nat. Biotechnol.* **2015**, *33*, 1012–1012.

- (53) Chantell, C. Multiplexed Automated Digital Microscopy for Rapid Identification and Antimicrobial Susceptibility Testing of Bacteria and Yeast Directly from Clinical Samples. *Clin. Microbiol. Newsl.* **2015**, *37*, 161–167.
- (54) Choi, J.; Jung, Y.-G.; Kim, J.; Kim, S.; Jung, U.; Na, H.; Kwon, S. Rapid Antibiotic Susceptibility Testing by Tracking Single Cell Growth in a Microfluidic Agarose Channel System. *Lab Chip* **2012**, *13*, 280–287.
- (55) Fredborg, M.; Andersen, K. R.; Jørgensen, E.; Droce, A.; Olesen, T.; Jensen, B. B.; Rosenvinge, F. S.; Sondergaard, T. E. Real-Time Optical Antimicrobial Susceptibility Testing. *J. Clin. Microbiol.* **2013**, *51*, 2047–2053.
- (56) Fredborg, M.; Rosenvinge, F. S.; Spillum, E.; Kroghsbo, S.; Wang, M.; Sondergaard, T. E. Rapid Antimicrobial Susceptibility Testing of Clinical Isolates by Digital Time-Lapse Microscopy. *Eur. J. Clin. Microbiol. Infect. Dis.* **2015**, *34*, 2385–2394.
- (57) Kim, S.; Cestellos-Blanco, S.; Inoue, K.; Zare, R. Miniaturized Antimicrobial Susceptibility Test by Combining Concentration Gradient Generation and Rapid Cell Culturing. *Antibiotics* **2015**, *4*, 455–466.
- (58) Lu, Y.; Gao, J.; Zhang, D. D.; Gau, V.; Liao, J. C.; Wong, P. K. Single Cell Antimicrobial Susceptibility Testing by Confined Microchannels and Electrokinetic Loading. *Anal. Chem.* **2013**, *85*, 3971–3976.
- (59) Boedicker, J. Q.; Li, L.; Kline, T. R.; Ismagilov, R. F. Detecting Bacteria and Determining Their Susceptibility to Antibiotics by Stochastic Confinement in Nanoliter Droplets Using Plug-Based Microfluidics. *Lab Chip* **2008**, *8*, 1265–1272.
- (60) Chen, C. H.; Lu, Y.; Sin, M. L. Y.; Mach, K. E.; Zhang, D. D.; Gau, V.; Liao, J. C.; Wong, P. K. Antimicrobial Susceptibility Testing Using High Surface-to-Volume Ratio Microchannels. *Anal. Chem.* **2010**, *82*, 1012–1019.
- (61) Mohan, R.; Sanpitakseree, C.; Desai, A. V.; Sevgen, S. E.; Schroeder, C. M.; Kenis, P. J. A. A Microfluidic Approach to Study the Effect of Bacterial Interactions on Antimicrobial Susceptibility in Polymicrobial Cultures. *RSC Adv.* **2015**, *5*, 35211–35223.
- (62) Quach, D. T.; Sakoulas, G.; Nizet, V.; Pogliano, J.; Pogliano, K. Bacterial Cytological Profiling (BCP) as a Rapid and Accurate Antimicrobial Susceptibility Testing Method for *Staphylococcus Aureus*. *EBIOM* **2016**, *4*, 95–103.
- (63) Kadlec, M. W.; You, D.; Liao, J. C.; Wong, P. K. A Cell Phone-Based Microphotometric System for Rapid Antimicrobial Susceptibility Testing. *J. Lab. Autom.* **2013**, *19*, 258–266.
- (64) Kinnunen, P.; McNaughton, B. H.; Albertson, T.; Sinn, I.; Mofakham, S.; Elbez, R.; Newton, D. W.; Hunt, A.; Kopelman, R. Self-Assembled Magnetic Bead Biosensor for Measuring Bacterial Growth and Antimicrobial Susceptibility Testing. *Small* **2012**, *8*, 2477–2482.

- (65) Bugrysheva, J. V.; Lascols, C.; Sue, D.; Weigel, L. M. Rapid Antimicrobial Susceptibility Testing of *Bacillus Anthracis*, *Yersinia Pestis*, and *Burkholderia Pseudomallei* Using Laser Light Scattering Technology. *J. Clin. Microbiol.* **2016**, *5*, 1462–1471.
- (66) Burg, T. P.; Godin, M.; Knudsen, S. M.; Shen, W.; Carlson, G.; Foster, J. S.; Babcock, K.; Manalis, S. R. Weighing of Biomolecules, Single Cells and Single Nanoparticles in Fluid. *Nature* **2007**, *446*, 1066–1069.
- (67) Mohan, R.; Mach, K. E.; Bercovici, M.; Pan, Y.; Dhulipala, L.; Wong, P. K.; Liao, J. C. Clinical Validation of Integrated Nucleic Acid and Protein Detection on an Electrochemical Biosensor Array for Urinary Tract Infection Diagnosis. *PLoS One* **2011**, *6*, e26846.
- (68) Rolain, J. M.; Mallet, M. N.; Fournier, P. E.; Raoult, D. Real-Time PCR for Universal Antibiotic Susceptibility Testing. *J Antimicrob Chemother.* **2004**, *54*, 538–541.
- (69) Schoepp, N. G.; Khorosheva, E. M.; Schlappi, T. S.; Curtis, M. S.; Humphries, R. M.; Hindler, J. A.; Ismagilov, R. F. Digital Quantification of DNA Replication and Chromosome Segregation Enables Determination of Antimicrobial Susceptibility after Only 15 Minutes of Antibiotic Exposure. *Angew. Chem. Int. Ed. Engl.* **2016**, *128*, 9709–9713.
- (70) Buchan, B. W.; Ledebor, N. A. Emerging Technologies for the Clinical Microbiology Laboratory. *Clin. Microbiol. Rev.* **2014**, *27*, 783–822.
- (71) Rogers, G. B.; Marsh, P.; Stressmann, A. F.; Allen, C. E. The Exclusion of Dead Bacterial Cells Is Essential for Accurate Molecular Analysis of Clinical Samples. *Eur. Soc. Clin. Infect. Dis.* **2010**, *16*, 1656–1658.
- (72) Clarridge, J. E. Impact of 16S rRNA Gene Sequence Analysis for Identification of Bacteria on Clinical Microbiology and Infectious Diseases. *Clin. Microbiol. Rev.* **2004**, *17*, 840–862.
- (73) Martineau, F.; Picard, O. I. S. J.; Lansac, N.; Me, C.; Roy, P. H.; Ouellette, M.; Bergeron, M. G.; Hemother, A. N. A. G. C. Correlation between the Resistance Genotype Determined by Multiplex PCR Assays and the Antibiotic Susceptibility Patterns of *Staphylococcus Aureus* and *Staphylococcus Epidermidis*. *Antimicrob Agents Chemother* **2000**, *44*, 231–238.
- (74) Besant, J. D.; Sargent, E. H.; Kelley, S. O. Rapid Electrochemical Phenotypic Profiling of Antibiotic-Resistant Bacteria. *Lab Chip* **2015**, *15*, 2799–2807.
- (75) Ertl, P.; Robello, E.; Battaglini, F.; Mikkelsen, S. R. Rapid Antibiotic Susceptibility Testing via Electrochemical Measurement of Ferricyanide Reduction by *Escherichia Coli* and *Clostridium Sporogenes*. *Anal. Chem.* **2000**, *72*, 4957–4964.
- (76) Mann, T. S.; Mikkelsen, S. R. Antibiotic Susceptibility Testing at a Screen-Printed Carbon Electrode Array. *Anal. Chem.* **2008**, *80*, 843–848.



- (77) Aghayee, S.; Benadiba, C.; Notz, J.; Kasas, S.; Dietler, G.; Longo, G. Combination of Fluorescence Microscopy and Nanomotion Detection to Characterize Bacteria. *J. Mol. Recognit.* **2013**, *26*, 590–595.
- (78) Lissandrello, C.; Inci, F.; Francom, M.; Paul, M. R.; Demirci, U.; Ekinici, K. L. Nanomechanical Motion of Escherichia Coli Adhered to a Surface. *Appl. Phys. Lett.* **2014**, *113701*, 113701–113705.
- (79) Kasas, S.; Simone, F.; Benadiba, C.; Maillard, C.; Stupar, P.; Tournu, H. Detecting Nanoscale Vibrations as Signature of Life. *Proc. Natl. Acad. Sci. U. S. A.* **2014**, *112*, 378–381.
- (80) Álvarez-Barrientos, A.; Arroyo, J.; Cantón, R.; Nombela, C.; Sánchez-Pérez, M. Applications of Flow Cytometry to Clinical Microbiology. *Clin. Microbiol. Rev.* **2000**, *13*, 167–195.
- (81) Jepras, R. I.; Paul, F. E.; Pearson, S. C.; Wilkinson, M. J. Rapid Assessment of Antibiotic Effects on Escherichia Coli by Bis-(1,3- Dibutylbarbituric Acid) Trimethine Oxonol and Flow Cytometry. *Antimicrob. Agents Chemother.* **1997**, *41*, 2001–2005.
- (82) Fredricks, B. A.; DeCoster, D. J.; Kim, Y.; Sparks, N.; Callister, S. M.; Schell, R. F. Rapid Pyrazinamide Susceptibility Testing of Mycobacterium Tuberculosis by Flow Cytometry. *J. Microbiol. Methods* **2006**, *67*, 266–272.
- (83) Van Belkum, A.; Dunne, W. M. Next-Generation Antimicrobial Susceptibility Testing. *J. Clin. Microbiol.* **2013**, *51*, 2018–2024.
- (84) von Ah, U.; Wirz, D.; Daniels, A. U. Isothermal Micro Calorimetry--a New Method for MIC Determinations: Results for 12 Antibiotics and Reference Strains of E. Coli and S. Aureus. *BMC Microbiol.* **2009**, *9*, 106.
- (85) Bonkat, G.; Braissant, O.; Widmer, A. F.; Frei, R.; Rieken, M.; Wyler, S.; Gasser, T. C.; Wirz, D.; Daniels, A. U.; Bachmann, A. Rapid Detection of Urinary Tract Pathogens Using Microcalorimetry: Principle, Technique and First Results. *BJU Int.* **2012**, *110*, 892–897.
- (86) Howell, M.; Wirz, D.; Daniels, A. U.; Braissant, O. Application of a Microcalorimetric Method for Determining Drug Susceptibility in Mycobacterium Species. *J. Clin. Microbiol.* **2012**, *50*, 16–20.
- (87) Eigner, U.; Schmid, A.; Wild, U.; Bertsch, D.; Fahr, A. Analysis of the Comparative Workflow and Performance Characteristics of the VITEK 2 and Phoenix Systems Analysis of the Comparative Workflow and Performance Characteristics of the VITEK 2 and Phoenix Systems. *J. Clin. Microbiol.* **2005**, *43*, 3829–3834.
- (88) Wanger, A.; Cole, K. E.; Schaeffer, F. Evaluation of the BD Phoenix System for Identification and Susceptibility Testing of Gram-Positive and Negative Clinical Isolates ABSTRACT BD Phoenix Was Compared to Pasco for Identification and Antibiotic Susceptibility of Gram-Negative and Susceptibilit. *Am. Soc. Microbiol.* **2005**.

- (89) Price, C. S.; Kon, S. E.; Metzger, S. Rapid Antibiotic Susceptibility Phenotypic Characterization of *Staphylococcus Aureus* Using Automated Microscopy of Small Numbers of Cells. *J. Microbiol. Methods* **2014**, *98*, 50–58.
- (90) Douglas, I. S.; Price, C. S.; Overdier, K. H.; Wolken, R. F.; Metzger, S. W.; Hance, K. R.; Howson, D. C. Rapid Automated Microscopy for Microbiological Surveillance of Ventilator-Associated Pneumonia. *Am. J. Respir. Crit. Care Med.* **2015**, *191*, 566–573.
- (91) Choi, J.; Yoo, J.; Lee, M.; Kim, E.-G.; Lee, J. S.; Lee, S.; Joo, S.; Song, S. H.; Kim, E.-C.; Lee, J. C.; *et al.* A Rapid Antimicrobial Susceptibility Test Based on Single-Cell Morphological Analysis. *Sci. Transl. Med.* **2014**, *6*, 267ra174.
- (92) Sin, M. L. Y.; Mach, K. E.; Wong, P. K.; Liao, J. C. Advances and Challenges in Biosensor-Based Diagnosis of Infectious Diseases. *Expert Rev. Mol. Diagn.* **2014**, *14*, 225–244.
- (93) Woude, M. W. Van Der; Bäumlner, A. J. Phase and Antigenic Variation in Bacteria Phase and Antigenic Variation in Bacteria. *Clin. Microbiol. Rev.* **2004**, *17*, 581–611.
- (94) Shen, Z.; Huang, M.; Xiao, C.; Zhang, Y.; Zeng, X.; Wang, P. G. Non-Labeled QCM Biosensor for Bacterial Detection Using Carbohydrate and Lectin Recognitions. *Anal. Chem.* **2007**, *79*, 2312–2319.
- (95) Früh, V.; IJzerman, A. P.; Siegal, G. How to Catch a Membrane Protein in Action: A Review of Functional Membrane Protein Immobilization Strategies and Their Applications. *Chem. Rev.* **2011**, *111*, 640–656.
- (96) Hirst, D. J.; Lee, T.-H.; Swann, M. J.; Aguilar, M.-I. Combined Mass and Structural Kinetic Analysis of Multistate Antimicrobial Peptide-Membrane Interactions. *Anal. Chem.* **2013**, *85*, 9296–9304.
- (97) Liu, Q.; Boyd, B. J. Liposomes in Biosensors. *Analyst* **2013**, *138*, 391–409.
- (98) Holden, M. a; Jayasinghe, L.; Daltrop, O.; Mason, A.; Bayley, H. Direct Transfer of Membrane Proteins from Bacteria to Planar Bilayers for Rapid Screening by Single-Channel Recording. *Nat. Chem. Biol.* **2006**, *2*, 314–318.
- (99) Grant, C. F.; Kanda, V.; Yu, H.; Bundle, D. R.; McDermott, M. T. Optimization of Immobilized Bacterial Disaccharides for Surface Plasmon Resonance Imaging Measurements of Antibody Binding. *Langmuir* **2008**, *24*, 14125–14132.
- (100) Lee, A. G. How Lipids Affect the Activities of Integral Membrane Proteins. *Biochim. Biophys. Acta* **2004**, *1666*, 62–87.
- (101) Tracy, B. P.; Gaida, S. M.; Papoutsakis, E. T. Flow Cytometry for Bacteria: Enabling Metabolic Engineering, Synthetic Biology and the Elucidation of Complex Phenotypes. *Curr. Opin. Biotechnol.* **2010**, *21*, 85–99.
- (102) Huang, B.; Yu, F.; Zare, R. N. Surface Plasmon Resonance Imaging Using a High Numerical Aperture Microscope Objective. *Anal. Chem.* **2007**, *79*, 2979–2983.

- (103) Wang, W.; Yang, Y.; Wang, S.; Nagaraj, V. J.; Liu, Q.; Wu, J.; Tao, N. Label-Free Measuring and Mapping of Binding Kinetics of Membrane Proteins in Single Living Cells. *Nat. Chem.* **2012**, *4*, 846–873.
- (104) Wang, S.; Shan, X.; Patel, U.; Huang, X.; Lu, J.; Li, J.; Tao, N. Label-Free Imaging, Detection, and Mass Measurement of Single Viruses by Surface Plasmon Resonance. *Proc. Natl. Acad. Sci. U. S. A.* **2010**, *107*, 16028–16032.
- (105) Waswa, J.; Irudayaraj, J.; DebRoy, C. Direct Detection of E. Coli O157:H7 in Selected Food Systems by a Surface Plasmon Resonance Biosensor. *LWT - Food Sci. Technol.* **2007**, *40*, 187–192.
- (106) Torun, O.; Hakkı Boyacı, I.; Temür, E.; Tamer, U. Comparison of Sensing Strategies in SPR Biosensor for Rapid and Sensitive Enumeration of Bacteria. *Biosens. Bioelectron.* **2012**, *37*, 53–60.
- (107) Tawil, N.; Sacher, E.; Mandeville, R.; Meunier, M. Surface Plasmon Resonance Detection of E. Coli and Methicillin-Resistant S. Aureus Using Bacteriophages. *Biosens. Bioelectron.* **2012**, *37*, 24–29.
- (108) Zordan, M. D.; Grafton, M. M. G.; Acharya, G.; Reece, L. M.; Cooper, C. L.; Aronson, A. I.; Park, K.; Leary, J. F. Detection of Pathogenic E. Coli O157:H7 by a Hybrid Microfluidic SPR and Molecular Imaging Cytometry Device. *Cytometry. A* **2009**, *75*, 155–162.
- (109) Casadevall, A.; Dadachova, E.; Pirofski, L. Passive Antibody Therapy for Infectious Diseases. *Nat. Rev. Microbiol.* **2004**, *2*, 695–703.
- (110) Shan, X.; Díez-Pérez, I.; Wang, L.; Wiktor, P.; Gu, Y.; Zhang, L.; Wang, W.; Lu, J.; Wang, S.; Gong, Q.; *et al.* Imaging the Electrocatalytic Activity of Single Nanoparticles. *Nat. Nanotechnol.* **2012**, *7*, 668–672.
- (111) Wang, W.; Foley, K.; Shan, X.; Wang, S.; Eaton, S.; Nagaraj, V. J.; Wiktor, P.; Patel, U.; Tao, N. Single Cells and Intracellular Processes Studied by a Plasmonic-Based Electrochemical Impedance Microscopy. *Nat. Chem.* **2011**, *3*, 249–255.
- (112) Park, C. H.; Martin, E. a; White, E. L. Isolation of a Nonpathogenic Strain of Citrobacter Sedlakii Which Expresses Escherichia Coli O157 Antigen. *J. Clin. Microbiol.* **1998**, *36*, 1408–1409.
- (113) Reyes, R. E.; González, C. R.; Jiménez, R. C.; Herrera, M. O.; Andrade, A. A. Mechanisms of O-Antigen Structural Variation of Bacterial Lipopolysaccharide ( LPS ). **2012**.
- (114) Woodward, R.; Yi, W.; Li, L.; Zhao, G.; Eguchi, H.; Sridhar, P. R.; Guo, H.; Song, J. K.; Motari, E.; Cai, L.; *et al.* In Vitro Bacterial Polysaccharide Biosynthesis: Defining the Functions of Wzy and Wzz. *Nat. Chem. Biol.* **2010**, *6*, 418–423.
- (115) Whitfield, C.; Larue, K. Stop and Go: Regulation of Chain Length in the Biosynthesis of Bacterial Polysaccharides. *Nat. Struct. Mol. Biol.* **2008**, *15*, 121–123.

- (116) Lidstrom, M. E.; Konopka, M. C. The Role of Physiological Heterogeneity in Microbial Population Behavior. *Nat. Chem. Biol.* **2010**, *6*, 705–712.
- (117) Wood, K. a.; Angus, D. C. Pharmacoeconomic Implications of New Therapies in Sepsis. *Pharmacoeconomics* **2004**, *22*, 895–906.
- (118) Sivanandan, S.; Soraisham, A. S.; Swarnam, K. Choice and Duration of Antimicrobial Therapy for Neonatal Sepsis and Meningitis. *Int. J. Pediatr.* **2011**, *2011*, 1–9.
- (119) Dalgaard, P.; Ross, T.; Kamperman, L.; Neumeyer, K.; McMeekin, T. a. Estimation of Bacterial Growth Rates from Turbidimetric and Viable Count Data. *Int. J. Food Microbiol.* **1994**, *23*, 391–404.
- (120) Wang, X.; Meier, R. J.; Wolfbeis, O. S. Fluorescent pH-Sensitive Nanoparticles in an Agarose Matrix for Imaging of Bacterial Growth and Metabolism. *Angew. Chem. Int. Ed. Engl.* **2013**, *52*, 406–409.
- (121) King, A.; King, A. Those Requiring Special Handling. *J. Antimicrob. Chemother.* **2001**, *48*, 77–80.
- (122) Lissandrello, C.; Inci, F.; Francom, M.; Paul, M. R.; Demirci, U.; Ekinici, K. L. Nanomechanical Motion of Escherichia Coli Adhered to a Surface. *Appl. Phys. Lett.* **2014**, *113701*, 113701–113704.
- (123) Song, L.; Sjollem, J.; Sharma, P. K.; Kaper, H. J.; van der Mei, H. C.; Busscher, H. J. Nanoscopic Vibrations of Bacteria with Different Cell-Wall Properties Adhering to Surfaces under Flow and Static Conditions. *ACS Nano* **2014**, 8457–8467.
- (124) Daugelavičius, R.; Bakienė, E.; Bamford, D. H. Stages of Polymyxin B Interaction with the Escherichia Coli Cell Envelope. *Antimicrob. Agents Chemother.* **2000**, *44*, 2969–2978.
- (125) Shan, X.; Fang, Y.; Wang, S.; Guan, Y.; Chen, H. Y.; Tao, N. Detection of Charges and Molecules with Self-Assembled Nano-Oscillators. *Nano Lett.* **2014**, *14*, 4151–4157.
- (126) Yang, Y.; Yu, H.; Shan, X.; Wang, W.; Liu, X.; Wang, S.; Tao, N. Label-Free Tracking of Single Organelle Transportation in Cells with Nanometer Precision Using a Plasmonic Imaging Technique. *Small* **2015**, *11*, 2878–2884.
- (127) Parry, B. R.; Surovtsev, I. V.; Cabeen, M. T.; O’Hern, C. S.; Dufresne, E. R.; Jacobs-Wagner, C. The Bacterial Cytoplasm Has Glass-like Properties and Is Fluidized by Metabolic Activity. *Cell* **2014**, *156*, 183–194.
- (128) Zhang, Y.; Rock, C. O. Membrane Lipid Homeostasis in Bacteria. *Nat. Rev. Microbiol.* **2008**, *6*, 222–233.
- (129) Ocampo, P. S.; Lázár, V.; Papp, B.; Arnoldini, M.; Zur Wiesch, P. A.; Busa-Fekete, R.; Fekete, G.; Pál, C.; Ackermann, M.; Bonhoeffer, S. Antagonism between Bacteriostatic and Bactericidal Antibiotics Is Prevalent. *Antimicrob. Agents Chemother.* **2014**, *58*, 4573–4582.

- (130) Jorgensen, J. H.; Ferraro, M. J. Antimicrobial Susceptibility Testing : A Review of General Principles and Contemporary Practices. *Clin. Infect. Dis.* **2009**, *7750*, 1749–1755.
- (131) Besant, J. D.; Sargent, E. H.; Kelley, S. O. Rapid Electrochemical Phenotypic Profiling of Antibiotic-Resistant Bacteria. *Lab Chip* **2015**, *15*, 2799–2807.
- (132) Barczak, a. K.; Gomez, J. E.; Kaufmann, B. B.; Hinson, E. R.; Cosimi, L.; Borowsky, M. L.; Onderdonk, a. B.; Stanley, S. a.; Kaur, D.; Bryant, K. F.; *et al.* RNA Signatures Allow Rapid Identification of Pathogens and Antibiotic Susceptibilities. *Proc. Natl. Acad. Sci.* **2012**, *109*, 6217–6222.
- (133) Berke, A. P.; Turner, L.; Berg, H. C.; Lauga, E. Hydrodynamic Attraction of Swimming Microorganisms by Surfaces. *Phys. Rev. Lett.* **2008**, *101*, 1–4.
- (134) Molaie, M.; Barry, M.; Stocker, R.; Sheng, J. Failed Escape: Solid Surfaces Prevent Tumbling of Escherichia Coli. *Phys. Rev. Lett.* **2014**, *113*, 1–6.
- (135) Frymier, P. D.; Ford, R. M.; Berg, H. C.; Cummings, P. T. Three-Dimensional Tracking of Motile Bacteria near a Solid Planar Surface. *Proc. Natl. Acad. Sci. U. S. A.* **1995**, *92*, 6195–6199.
- (136) Sokolov, A.; Aranson, I. S. Reduction of Viscosity in Suspension of Swimming Bacteria. *Phys. Rev. Lett.* **2009**, *103*, 2–5.
- (137) Lim, L. M.; Pharm, D.; Ly, N.; Anderson, D.; Pharm, D.; Yang, J. C.; Pharm, D.; Macander, L.; Pharm, D.; Iii, A. J.; *et al.* Resurgence of Colistin: A Review of Resistance, Toxicity, Pharmacodynamics, and Dosing. **2015**, *30*, 1279–1291.
- (138) Mcgann, P.; Snesrud, E.; Maybank, R.; Corey, B.; Ong, A. C.; Clifford, R.; Hinkle, M.; Whitman, T. Escherichia Coli Harboring Mcr-1 and Bla CTX-M on a Novel IncF Plasmid : First Report of Mcr-1 in the United States. *Antimicrob Agents Chemother* **2016**, *60*, 4420–4421.
- (139) Liu, Y.; Wang, Y.; Walsh, T. R.; Yi, L.; Zhang, R.; Spencer, J.; Doi, Y.; Tian, G.; Dong, B.; Huang, X.; *et al.* Emergence of Plasmid-Mediated Colistin Resistance Mechanism MCR-1 in Animals and Human Beings in China : A Microbiological and Molecular Biological Study. *Lancet Infect. Dis.* **2016**, *16*, 161–168.
- (140) Shen, S.; Syal, K.; Tao, N.; Wang, S. Note: An Automated Image Analysis Method for High-Throughput Classification of Surface-Bound Bacterial Cell Motions. *Rev. Sci. Instrum.* **2015**, *86*, 1–4.
- (141) Liu, J.; Prindle, A.; Humphries, J.; Gabalda-sagarra, M.; Asally, M.; Lee, D. D. Metabolic Co-Dependence Gives Rise to Collective Oscillations within Biofilms. *Nature* **2015**, *523*, 550–554.
- (142) Sheng, J.; Malkiel, E.; Katz, J. Digital Holographic Microscope for Measuring Three-Dimensional Particle Distributions and Motions. *Appl. Opt.* **2006**, *45*, 3893.

- (143) Yetisen, A. K.; Akram, M. S.; Lowe, C. R. Paper-Based Microfluidic Point-of-Care Diagnostic Devices. *Lab Chip* **2013**, *13*, 2210–2251.
- (144) Park, T. S.; Li, W.; Mccracken, K. E.; Yoon, J. Lab on a Chip Smartphone Quantifies Salmonella from Paper. *Lab Chip* **2013**, *13*, 4832–4840.
- (145) Cybulski, J. S.; Clements, J.; Prakash, M. Foldscope : Origami-Based Paper Microscope. *PLoS One* **2014**, *9*, e98781.
- (146) Bates, M.; Zumla, A. Rapid Infectious Diseases Diagnostics Using Smartphones. *Ann Transl Med* **2015**, *3*, 3–7.
- (147) D'Ambrosio, M. V; Bakalar, M.; Bennuru, S.; Reber, C.; Skandarajah, A.; Nilsson, L.; Switz, N.; Kamgno, J.; Pion, S.; Boussinesq, M.; *et al.* Point-of-Care Quantification of Blood-Borne Filarial Parasites with a Mobile Phone Microscope. *Sci. Transl. Med.* **2015**, *7*, 286re4.

APPENDIX A  
COPYRIGHT PERMISSIONS CHAPTER 2

**THE AMERICAN ASSOCIATION FOR THE ADVANCEMENT OF SCIENCE LICENSE  
TERMS AND CONDITIONS**

Apr 18, 2017


This Agreement between Karan Syal ("You") and The American Association for the Advancement of Science ("The American Association for the Advancement of Science") consists of your license details and the terms and conditions provided by The American Association for the Advancement of Science and Copyright Clearance Center.

License Number	4092060684700
License date	Apr 18, 2017
Licensed Content Publisher	The American Association for the Advancement of Science
Licensed Content Publication	Science Translational Medicine
Licensed Content Title	A rapid antimicrobial susceptibility test based on single-cell morphological analysis
Licensed Content Author	Jungil Choi, Jungheon Yoo, Mincheol Lee, Eun-Geun Kim, Ji Soo Lee, Seungok Lee, Seik Joo, Sang Hoon Song, Eui-Chong Kim, Jung Chan Lee, Hee Chan Kim, Yong-Gyun Jung, Sunghoon Kwon
Licensed Content Date	Dec 17, 2014
Licensed Content Volume	6
Licensed Content Issue	267
Volume number	6
Issue number	267
Type of Use	Thesis / Dissertation
Requestor type	Scientist/individual at a research institution
Format	Print and electronic
Portion	Figure
Number of figures/tables	1
Order reference number	
Title of your thesis / dissertation	Rapid Antimicrobial Susceptibility Testing Based On Motion Tracking
Expected completion date	May 2017
Estimated size(pages)	130
Requestor Location	Karan Syal Biodesign Institute 727 E. Tyler St. Tempe,  TEMPE, AZ 85281 United States Attn: Karan Syal
Billing Type	Invoice
Billing Address	Karan Syal Biodesign Institute 727 E. Tyler St. Tempe,





## Current and emerging techniques for antibiotic susceptibility tests

Karan Syal<sup>1</sup>, Manni Mo<sup>1, 3</sup>, Hui Yu<sup>1</sup>, Rafael Iriya<sup>1, 3</sup>, Wenwen Jing<sup>1</sup>, Sui Guodong<sup>4</sup>, Shaopeng Wang<sup>1, 2</sup>, Thomas E. Grys<sup>5</sup>, Shelley E. Haydel<sup>6, 7</sup>, Nongjian Tao<sup>1,2,3</sup> 

1. Center for Biosensors and Bioelectronics, The Biodesign Institute, Arizona State University, Tempe, Arizona 85287, USA;
2. State Key Laboratory of Analytical Chemistry for Life Science, School of Chemistry and Chemical Engineering, Nanjing University, Nanjing 210093, China;
3. School of Electrical, Computer and Energy Engineering, Arizona State University, Tempe, Arizona 85287, USA;
4. Institute of Biomedical Science, Fudan University, Shanghai, China;
5. Department of Laboratory Medicine and Pathology, Mayo Clinic, Phoenix, Arizona 85054, USA;
6. Center for Immunotherapy, Vaccines, and Virotherapy, The Biodesign Institute, Arizona State University, Tempe, Arizona 85287, USA;
7. School of Life Sciences, Arizona State University, Tempe, Arizona 85287, USA.

This is an open access article distributed under the terms of the [Creative Commons Attribution \(CC BY-NC\) License](http://creativecommons.org/licenses/by-nc/4.0/). See <http://ivyspring.com/terms> for full terms and conditions.

### How to cite this article:

Syal K, Mo M, Yu H, Iriya R, Jing W, Guodong S, Wang S, Grys TE, Haydel SE, Tao N. Current and emerging techniques for antibiotic susceptibility tests. *Theranostics* 2017; 7(7):1795-1805. doi:10.7150/thno.19217. Available from <http://www.thno.org/v07p1795.htm>

APPENDIX B  
COPYRIGHT PERMISSIONS CHAPTER 3

**ELSEVIER LICENSE  
TERMS AND CONDITIONS**

Apr 18, 2017

---

This Agreement between Karan Syal ("You") and Elsevier ("Elsevier") consists of your license details and the terms and conditions provided by Elsevier and Copyright Clearance Center.

License Number	4092061371108
License date	Apr 18, 2017
Licensed Content Publisher	Elsevier
Licensed Content Publication	Biosensors and Bioelectronics
Licensed Content Title	Plasmonic imaging of protein interactions with single bacterial cells
Licensed Content Author	Karan Syal,Wei Wang,Xiaonan Shan,Shaopeng Wang,Hong-Yuan Chen,Nongjian Tao
Licensed Content Date	15 January 2015
Licensed Content Volume	63
Licensed Content Issue	n/a
Licensed Content Pages	7
Start Page	131
End Page	137
Type of Use	reuse in a thesis/dissertation
Intended publisher of new work	other
Portion	full article
Format	both print and electronic
Are you the author of this Elsevier article?	Yes
Will you be translating?	No
Order reference number	
Title of your thesis/dissertation	Rapid Antimicrobial Susceptibility Testing Based On Motion Tracking
Expected completion date	May 2017
Estimated size (number of pages)	130
Elsevier VAT number	GB 494 6272 12
Requestor Location	Karan Syal Biodesign Institute 727 E. Tyler St. Tempe,  TEMPE, AZ 85281 United States Attn: Karan Syal

APPENDIX C  
COPYRIGHT PERMISSIONS CHAPTER 4



RightsLink®

[Home](#)

[Account Info](#)

[Help](#)



ACS Publications  
Most Trusted. Most Cited. Most Read.

**Title:** Antimicrobial Susceptibility Test with Plasmonic Imaging and Tracking of Single Bacterial Motions on Nanometer Scale

Logged in as:

Karan Syal

Account #:

3001110538

**Author:** Karan Syal, Rafael Iriya, Yunze Yang, et al

[LOGOUT](#)

**Publication:** ACS Nano

**Publisher:** American Chemical Society

**Date:** Jan 1, 2016

Copyright © 2016, American Chemical Society

### PERMISSION/LICENSE IS GRANTED FOR YOUR ORDER AT NO CHARGE

This type of permission/license, instead of the standard Terms & Conditions, is sent to you because no fee is being charged for your order. Please note the following:

- Permission is granted for your request in both print and electronic formats, and translations.
- If figures and/or tables were requested, they may be adapted or used in part.
- Please print this page for your records and send a copy of it to your publisher/graduate school.
- Appropriate credit for the requested material should be given as follows: "Reprinted (adapted) with permission from (COMPLETE REFERENCE CITATION). Copyright (YEAR) American Chemical Society." Insert appropriate information in place of the capitalized words.
- One-time permission is granted only for the use specified in your request. No additional uses are granted (such as derivative works or other editions). For any other uses, please submit a new request.